Design and Analysis of Optimal Braided Composite Lattice Structures

by

Austin Russell Gurley

A thesis submitted to the Graduate Faculty of
Auburn University
in partial fulfillment of the
requirements for the Degree of
Master of Science

Auburn, Alabama
August 2, 2014

Keywords: open-architecture composite structures, braided lattice
MATLAB, topological optimization, finite element analysis

Approved by

David Beale, Chair, Professor of Mechanical Engineering
Royall Broughton, Jr., Co-chair, Professor Emeritus of Polymer and Fiber Engineering
David Branscomb, R&D Specialist - Braids and Engineered Composites - Takata Highland

Abstract

This work applies to structural optimization within geometric constraints of braided truss structures. Prototypes of the newly developed open-structures have proven useful for their high specific stiffness and rapid manufacturing. Current prototype development has principally been based on trial-and-error and has yielded great improvements. The properties of the structures continue to improve with design changes. To date, no rigorous design tools have been able to predict the structure properties or to suggest advances in the design of optimal structures within the constraints of the braiding process. The results of this thesis provide tools for both those objectives and implement them in software.

The computational tools carry the analysis of Open-Architecture Composites Structures (referred to equivalently as O-ACS, open-structures, or simply 'structures') from concept and initial constraints, to optimal design. Beginning with the specification of a braiding machine, a geometry model is constructed which can replicate any O-ACS tube the specified machine can manufacture. The geometry model is discretized into finite elements, where the nature of composite yarns is leveraged using beam elements to create an efficient mechanics model of the geometry. The Finite Element (FE) model is validated against a wide range of O-ACS specimens, and is capable of predicting the stiffness of the tubes in bending and torsion to within 5.7% and 8.4%, respectively, across the range tested. For various reasons including manufacturing and testing imprecision, the model cannot accurately predict axial stiffness (60% error across the range tested). Open-structure tubes were found to be significantly more rigid

than equal weight composite and aluminum thin-walled tubes in asymmetric loading scenarios such as bending and torsion. Particularly the ability to increase diameter of O-ACS without significant change in mass allows it to exceed the specific stiffness of commercially available, equal weight, competitors. The FE model is wrapped in an optimization routine, in which it can be used to predict the highest specific stiffness structure, given a target weight and known applied loads. The optimized O-ACS tubes' specific stiffness is predicted to be seven times that of a commercial filament-wound competitor in bending stiffness, and four times in torsional stiffness. All these tools, programmed in MATLAB, have been combined into an accessible Graphic User Interface (GUI) which allows any engineer easy access to the geometry simulation, finite element analysis, and optimization abilities of this work.

Acknowledgments

Thanks to my family and friends for being patient with my isolation and lack of contact, and for understanding my commitment to my work.

Thanks to David for getting me started with braiding, I would never have touched on any of this work without his encouragement and his foundational research. Thanks to Drs. Beale, Broughton, Branscomb, and Maggie for assisting me in reading and editing this document. Thanks to the O-ACS research team for what information they have supplied to this work.

Table of Contents

List of Tables

List of Illustrations

xi

List of Abbreviations

GUI   Graphical User Interface

FE   Finite Element

FEA   Finite Element Analysis

O-ACS Open-Architecture Composite Structure

RMS   square Root of Mean of Square

Summary and Outline

Open-Structures as Lattice Reinforcement

Open-Architecture Composite Structures are a new and novel use of composites for minimal weight component design. Historically, trusses and lattices have been proven to yield higher specific stiffness and strength than continuous materials. Even before the first well-documented attempt at structural optimization (Michell, 1904),

Figure 1 - O-ACS tube during manufacturing

engineers have known strength can be gained from geometry more efficiently than by simple addition of raw material and mass. These concepts can be deduced from sources as loose as intuition, observations of nature, or rigorously from first principles such as general relativity (Vasiliev & Gurdal, 1999). While large structures like bridges and buildings can be made of trusses easily, there are few building materials (tubes, beams, sheets) which utilize truss or lattice reinforcement design. This is mostly an economic issue, as smooth shapes lend themselves to the faster manufacturing processes and tighter quality controls. A few exceptions exist, for instance; NASA has developed grid reinforcement for spacecraft (McDonnell Douglas Astronautics Company, 1973), the results of which is still used in rocket design. Some manufactured truss structures have been designed, but are not currently economically feasible due to complicated manufacturing involved (Jensen, Jensen, & Howcraft, 2010). O-ACS has the benefit of truss geometry, while utilizing the conventional maypole braiding process for speed. The details of initial development of the O-ACS can be found in the work of David Branscomb (Branscomb, Minimal Weight Composites Utilizing Advanced Manufacturing Techniques, 2012). The technology is patent pending, covered by US 20130291476 A1 *Minimal Weight Composites Using Open-Structure*. An example of a typical O-ACS tube is shown in Figure 2.

Figure 2 – Example of an open-structure composite beam

Design Tool Development Process

Casual observation shows that the open-structure concept is that of an 'optimized beam' problem. The structures are long compared to their width, and are usually tubular in form. They will be typically loaded by forces applied to their axial end-points, and likewise constrained by them. The objective then is to design *ideal* open-structure tubes based on known loading conditions. Because the objective of O-ACS is minimal weight composites, 'Ideal' will generally take the form of 'highest specific stiffness' within design constraints such as loading conditions, manufacturing, and strength requirements. The objective of this research is to create a complete computer toolset, named *fell_point*, which will allow the design of O-ACS structures. To ensure the accuracy of the computational models, a thorough test of a sampling of structure geometries in a sampling of loading conditions will be constructed. The data from these experiments will be used to validate the numeric model. After this validation, the model will be a design tool which can assist in the rapid development of O-ACS, and consequently allow potential users of the technology the ability to test its utility in their desired application.

The process for design tool development has been outlined in the flowchart of Figure 3. The following paragraphs summarize each block. The components which form the basis of this thesis are dark blue; the chapters which detail their creation is noted in the figure.
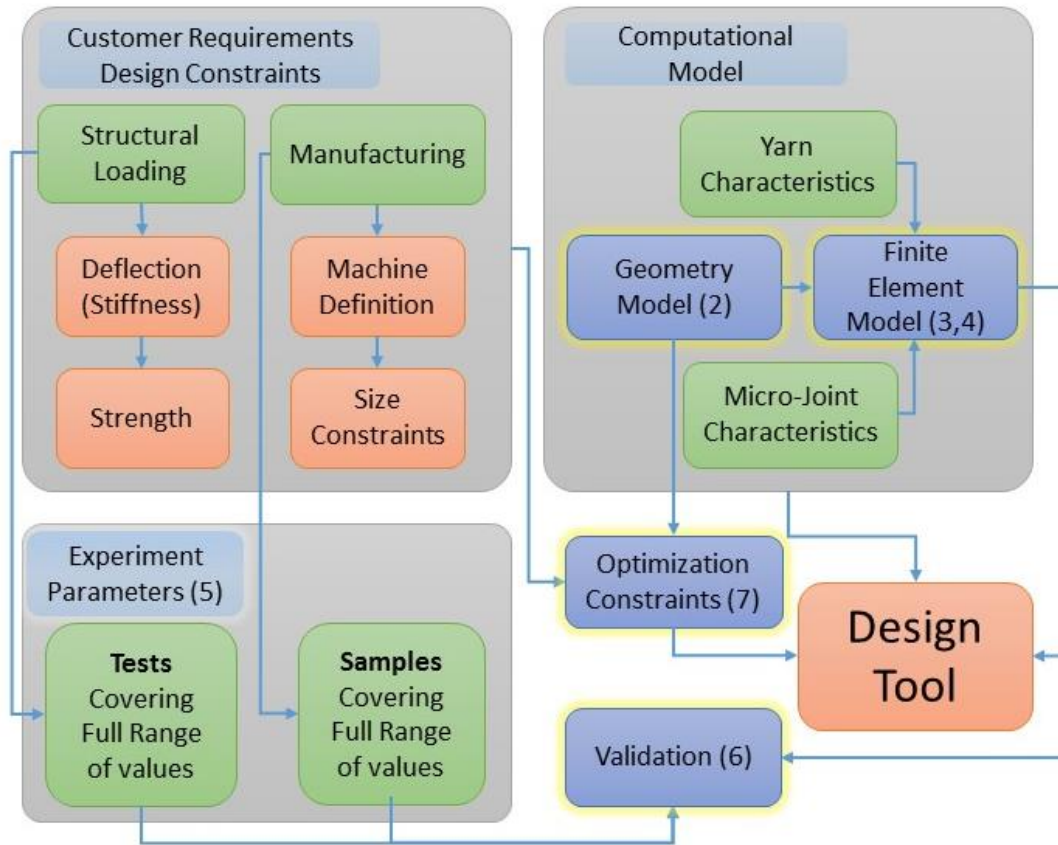
Figure 3 – Flowchart of O-ACS Design Tool Development

Customer Requirements and Design Constraints

Customer requirements will determine both the scope and limits of the design. Desired loading conditions come from the expected implementation of open-structures as struts or beams. From the desired loading conditions, the Finite Element Analysis (FEA) model constraints will be simplified and characterized. Test methods will be utilized that correspond to these loads for model validation and characterization of the open-structure. Manufacturing constraints expose the feasible bounds of O-ACS design. The manufacturing limits imposed when braiding, and farther limitations if a particular braiding machine is used, will guide the geometry modeling. All the desires of the end-user (customer) are incorporated in the optimization. The machine will limit the initial conditions of the optimization statement. The required deflection and strength characteristics will impose bounds on the optimal design. More detail on the mathematical statement of these constraints can be found in Chapters 2, 3, and 4.

Experimental Parameters and Validation

A test-matrix of structures has been designed to test open-structure configurations through a wide range of useful sizes and configurations. The selection of samples is made to fully utilize the range of manufacturing capabilities, while ensuring a designed experiment model can be accurately derived from the results. Some constraints are limited by the braiding process, others by the particular braiding machine in use, and still others by geometric relationships among yarns which make up the structure. A thorough set of tests provides enough data to interpolate smoothly between the variable for prediction of structure properties. An empirical model will be fitted to the experiments, which will yield insight into the importance and the interactions among design variables. These physical trends will be compared to the FE model predicted properties for validation of the computer model. The details of the samples tested, the testing methods employed, and the result are detailed in Chapter 5 and 6.

Computation Model and Optimization

The primary contribution of this work to the development of O-ACS as a feasible engineering material is in predictive modeling of the structure behavior. The computational model must incorporate the geometric constraints of Maypole braiding and the particular machine used. It must also utilize the material properties of the constituent yarns for stiffness and strength characteristics. The geometry and material combined are analyzed using the finite element method. The finite element model is explored in Chapter 3 and 4. The model uses beam element formulations to represent both the yarns and joint intersections, allowing accurate geometry preservation as well as fast solutions (for optimization work). To ensure the model is truly capable of accurate prediction, it is compared against the full range of samples (Chapter 6). The model is shown to accurately predict the stiffness of O-ACS tubes in axial, bending, and torsional loading scenarios.

The ultimate goal of this work lies in the optimization component. Using the FE model, the yarn properties, and structure design requirements, the optimal O-ACS solution will be found. The details of the optimization method are given in Chapter 7. Because this component of the model is the end goal of this research, it is worth keeping in mind when considering the preceding chapters (which are all leading to this goal). The thesis mission can be stated as follows:

To create design tools, useful to an engineer unfamiliar with the intricacies of O-ACS design, which compute optimal stiffness-to-weight O-ACS geometries – within constraints of design loads, a machine definition, and material properties.

Braided Lattice Geometry Model

The initial concern in creating open-structure simulation is to adequately reproduce the structure geometry mathematically. The mathematical model must be capable of generating geometries based on the machine parameters and settings, incorporate the effects of compression against a mandrel, and be organized such that the model is accessible to the Finite Element tools developed later. Because of the novelty of O-ACS, there is essentially no useful literature on the production of O-ACS geometries. Most braid geometry models are concerned with fabrics that have very fine fibers; these models are not capable of producing the large undulations found within the O-ACS tubes (Ko, Pastore, & Had, 1989). Some simulations have been created that directly calculate the exact motions of a braiding machine and the interlacing of the yarns onto a surface. Simple models are capable of solving these motions for fine yarns (Akkerman & Rodriguez, 2008), however, when capable of solving for large yarns such as constitute O-ACS structures the simulation requires slow and intensive computation of dynamic finite element models (Schneider, Pickett, & Wulfhorst, 2000). The geometry model here uses a much more heuristic approach to modeling. The geometry is based on braiding machine kinematics, but convergence to a final shape is solving using 'artificial' or logical means, rather than a method driven by dynamic modeling. Comparison between the model and physical samples shows that this method sufficiently describes the desired characteristics.

In order to make the most general model possible, consideration is given to the variables available to the braider. Some of these are limits of the maypole braiding process, and others are limited based on the machine being used. The variables needed to fully describe a braid are given in Table 1. Note that these parameters become design variables later in the optimization stage of design. Sometimes variable are described in a manner that may seem over-complicated, but was chosen such that a designer best understands the choices made. For instance, it is perhaps intuitive that 'Diameter' means the 'average diameter' of the structure; here 'Diameter' refers to the 'Mandrel Diameter' since that is the design parameter which will be chosen later in manufacturing. Also, it is important to realize that some of the parameters are not independent - for instance 'helix angle' and 'pitch' describe the same motion, and are inter-related by the mandrel diameter.

Table 1 - Braid Geometry Design Variables

Parameter	Symbol	Notes
Machine Diameter	D	used for initial calculation
Mandrel Diameter	d	
Number Horn Gears	g	
Horn Gear Diameter	Θ	function of D and g
Carrier Position	n	varies from 1 to g
Number of Horn Gear Forks	f	typically $= 4$
Yarn Location in Space	X_i, Y_i, Z_i	$i = warp, weft, axial$
Time/Step	t	used for discretization
Helix Angle	ψ	
Pitch	$pitch$	
Yarn Diameter	ϕ	constant for each yarn

Geometry Model - Maypole Braider Kinematics

The first step in deriving a mathematical geometry model is to make observations about the physical braiding machine and its product. The machine consists of a set number of horn gears which interlace; each partner gear rotating counter to its neighbors. Packages are carried around on these gears, passing from one to the next in an oscillating manner. This oscillation provides the first concept. If all the horn gears were connected in a straight line, the path taken by a single carrier would be predominantly sinusoidal, and could be described by a cosine with amplitude equal to the horn gear radius

$$y = \Theta * \sin(t)$$

<div align="right">(1)</div>

Or, perhaps more accurately by a repeated arc-length which more closely replicates the round horn gears (referred to henceforth as a synchroid) (Figure 4)

$$y = \Theta * sign\left(\sin\left(\frac{g\left(t - \frac{\pi}{16}\right)}{2}\right)\right) * \sqrt{1 - \left(mod\left(\frac{g\left(t - \frac{\pi}{16}\right)}{\pi}, 2\right) - 1\right)^2}$$

<div align="right">(2)</div>

Where Θ is the horn gear diameter, g is the number of horn gears on the machine, and t is time. While this equation may better replicate the motion of carriers on the track-plate, after the

manipulations of the geometry (described in the next sections) it is not sufficiently improved to warrant its complexity. The subsequent derivations will use the much simpler sinusoid.
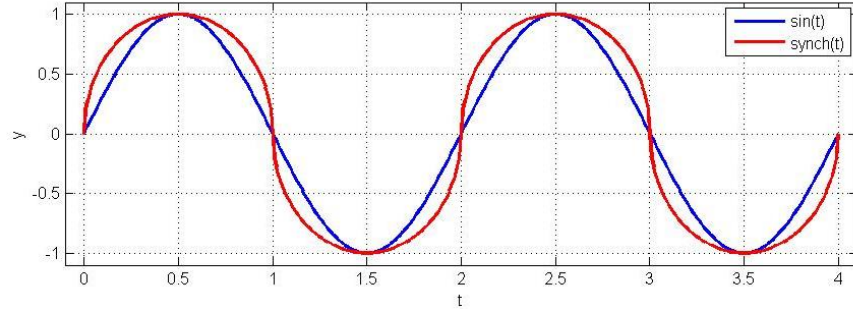
Figure 4 – comparison of track-plate equations

In conventional maypole braiding, the horn gears are arranged in a circle, and the path made by each package is continuous around a loop. This simulation is capable of making all the braid geometries which can be manufactured using a maypole braiding machine that has two carriers per horn gear, and four forks in each horn gear. Starting with the machine motion sinusoid, the distance from the center of the machine to the warp carriers is given by (Branscomb, 2007):

$$X = \left[\frac{15}{8}\cos(2\pi t) + \frac{16.5}{2}\right]\cos\left(-\frac{\pi}{4}t\right) \qquad Y = \left[\frac{15}{8}\cos(2\pi t) + \frac{16.5}{2}\right]\sin\left(-\frac{\pi}{4}t\right)$$

Which can be written far more generally using the following development:

Begin with an equation which dictates the radius of the yarn path

$$R_1 \equiv \Theta * \cos\left(\frac{g}{2}\left(t - \frac{n\pi}{fg}\right)\right) + D/2$$

(3)

Where D is the major diameter (distance from center of leftmost horn gear to center of rightmost horn gear) of the machine. Note that the position is shifted based on which n of the g carriers is of interest and the number of forks f in each horn gear. The path of the weft carriers is found similarly, but must account for a phase shift (the fact that carriers do not crash at horn gear intersections implies this relationship).

$$R_2 \equiv -\Theta * \cos\left(\frac{g}{2}\left(t - \frac{n\pi}{fg} + \frac{(2f-1)\pi}{g}\right)\right) + D/2$$

(4)

8

The path of the warp and weft carriers in Cartesian coordinates is simply the transformation of R and an angular displacement that is a function of t.

$$X_1 = R_1 * \cos(-t - \frac{n\pi}{fg})$$

<div align="right">(5)</div>

$$Y_1 = -R_1 * \sin(-t - \frac{n\pi}{fg})$$

<div align="right">(6)</div>

$$X_2 = R_2 * \cos(t + \frac{n\pi}{fg} - \frac{(2f-1)\pi}{g})$$

<div align="right">(7)</div>

$$Y_2 = R_2 * \sin(t + \frac{n\pi}{fg} - \frac{(2f-1)\pi}{g})$$

<div align="right">(8)</div>
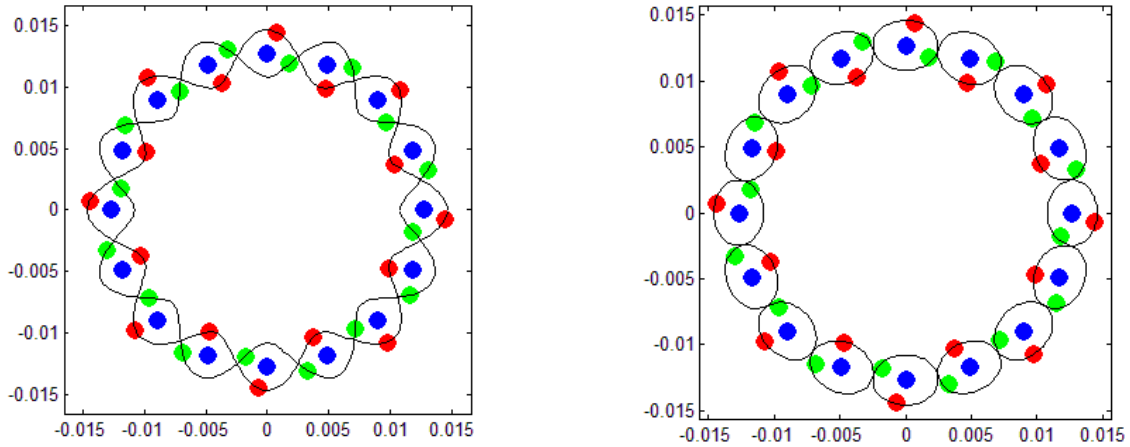
Figure 5 – effect of track-plate equations on braid geometry

The synchroid in this case is found to be only a slight improvement over the sinusoid (Figure 5). Also, with the intention to later compress the structure against the mandrel, the purpose of this geometry is simply to describe the interlacing periods, for which the sinusoid amply suffices. A synchroid has the addition mathematical disadvantage that its slope is infinite once per period.

When implemented to construct the braid geometry the phase shift terms can be removed as the final braided structure is found, from observation, to be symmetric. However, only the phase

shift model properly determines the stacking sequence of the yarns in the final braid. The geometry must 'pick' the yarns at intersections based on phase-shifted stacking (Figure 6).
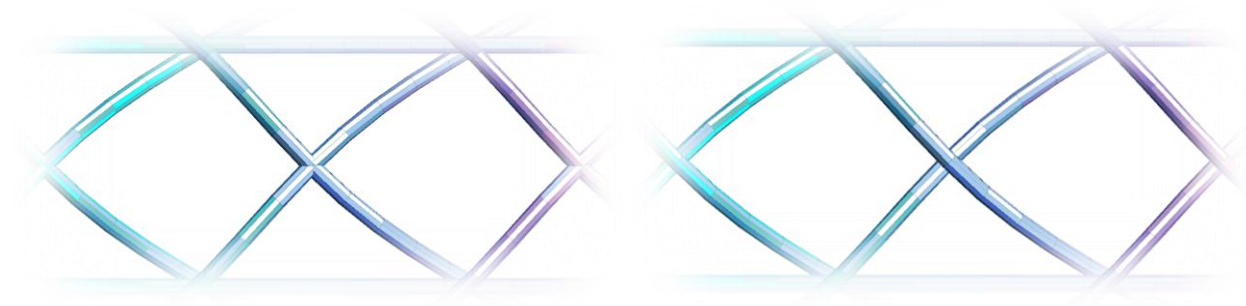
Figure 6 – model braided joint with and without 'picking' motion

A final step is required to transform braiding machine kinematics into Open Structure geometry; it must be carried into the third dimension giving the structure a height. Each yarn is carried upward in the Z direction linearly as time increases. The wrapping (helix) angle ψ is determined by the size of the z step (or vice versa) using the equation

$$Z_1 = Z_2 = \frac{2t}{g} * pitch = \frac{2\pi D t}{g} \tan(\psi)$$

(9)

This final equation has given enough to construct a first model, shown below. Note that the axial yarns are simply vertical lines centered above their respective horn gear locations. In the foregoing discussion, the size of the machine was used for sizing. Obviously when constructing the structure model, the major diameter is the diameter of the structure d not that of the machine D. Similarly, the diameter of the yarn ϕ should be substituted for the horn gear diameter Θ. Typical results of the kinematics model (as derived thus far) are shown in Figure 7.
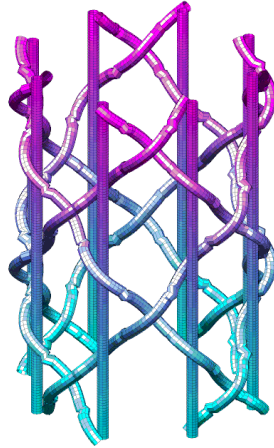
Figure 7 – structure model; kinematic geometry generation (phase I)

Joint Intersection

The open structures will be modeled as though connected by resin at joints. The details of this concept are explored in a later chapter, but the current geometry model construction will begin setting the stage for that development. In this stage, it is necessary only to define the locations at which joints will intersect. In the Open Structures, the joints contact (and subsequently bond) along lines radially outward from the structure center. Within the geometry unit of *fell_point*, the braid simulation first finds intersections of warp and weft nodes where no axial yarns are present. The program then identifies intersections of both warp and weft with axials, and uses the stacking sequence of the yarns at that point to determine which are bonded together.
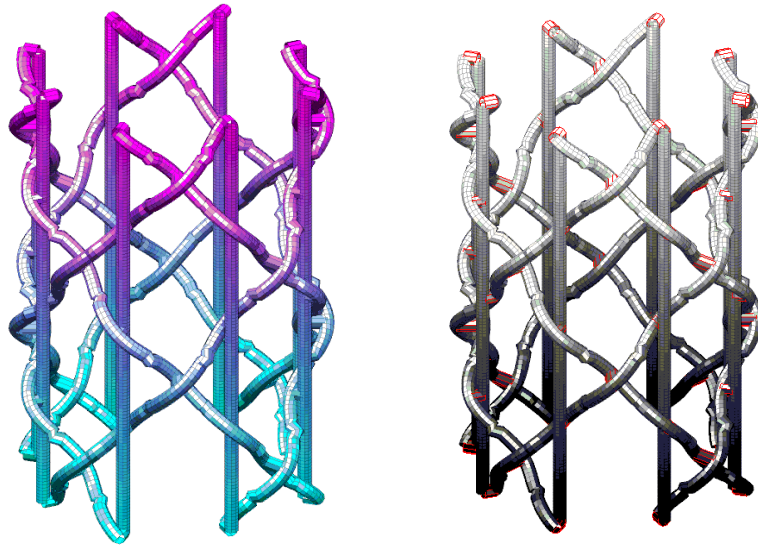
Figure 8 – structure model; joints attached (phase II)

Artificial Compression

The Open Structure is formed around a mandrel in production. The combination of tension due to the carriers and wrapping around the mandrel pulls the structure tight against the underlying mandrel shape. Because the kinematic model was based on the sinusoidal motion of the machine, it does not include this compressive effect. While the effect of yarn tension and wrapping could be modeled using finite element methods, it is prudent not to waste computing resources solving a complex problem if an adequate geometric model can be created.

The concept of artificial compression was implemented in *fell_point*. First, each overlap of yarns is sorted and identified. The joints are compressed against the mandrel as close as possible while preserving the stacking sequence at each. Each yarn is considered independently. All the nodes are pushed down a small step toward the mandrel if they have not yet reached the curvature limit. This cycle is iterated until the desired level of compression is achieved. The results of the artificial compression are demonstrated in Figure 9. Note that the earlier 'picking' results in proper braid interlacing, easily confirmed by inspection, now that the structure has been compressed.

12
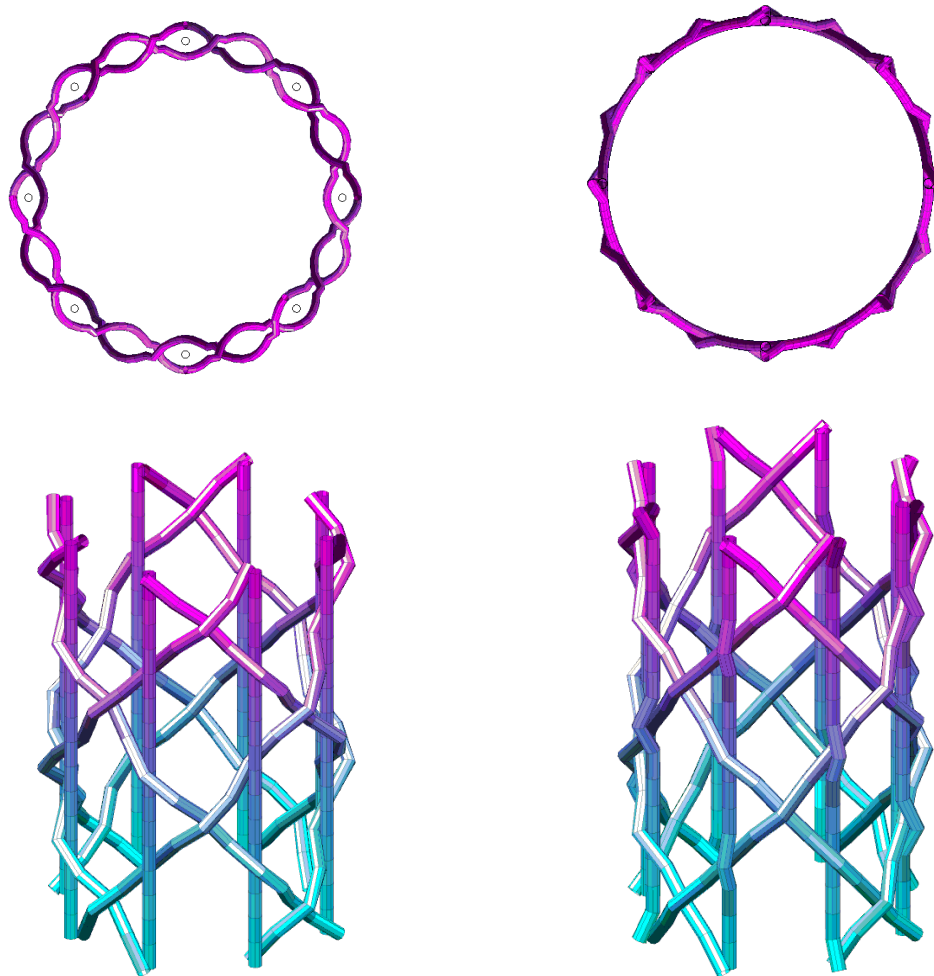
Figure 9 – structure model after artificial compression (Phase III)

Artificial Tension by Geodesics

The artificial compression model is a significant improvement over the machine kinematics model, and represents well a structure which has been pressed against a mandrel by vacuum bag or other means. However, typically the final formation of the structure is determined by tension within the yarns. Again, this could be solved using contact finite element methods, but an artificial method is computationally more attractive. The path taken by tensioned string or yarn is a geodesic, or shortest path, from one end to the other under load. This is a property of most any

13

string or cable in tension. Thus, instead of applying a tension and allowing the nodes to move towards this shortest path, logic is programmed into the software that evaluates each node and determines whether a small shift in its position would shorten the yarn. The routine is applied by testing small changes dr in radius along each yarn, and retaining only such moves which only decrease the yarn lengths. When it is found that additional changes in dr cannot improve even a single point, the step size is decreased an order of magnitude ($dr^{new} = \frac{dr}{10}$), and the tests repeated. This allows convergence to an arbitrarily small step (within machine precision) as required for accuracy. This effect was programmed into the braid simulator with fair results, as seen in Figure 10. Notice the much improved replication of axial yarn undulation, and the ability of the helical yarns to transition from straight to curved as they intersect with the mandrel. As this condition is most like the test samples made for validation of the finite element model, it will be used henceforth.
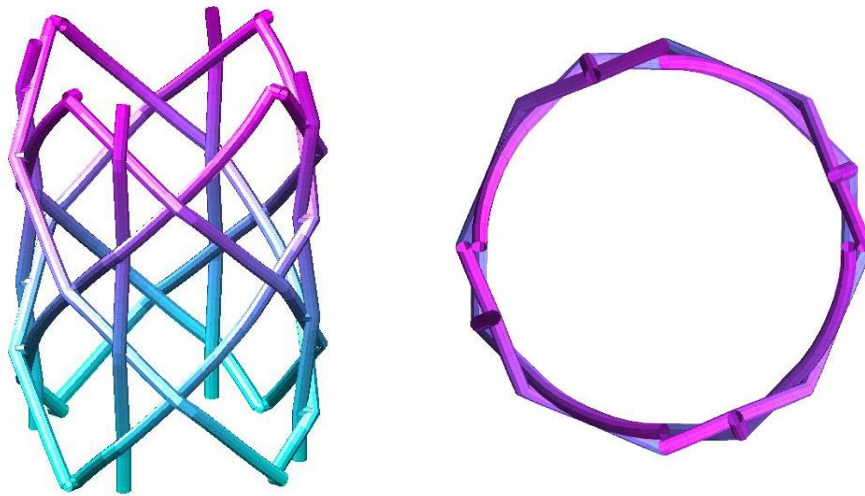
Figure 10 – Structure model after artificial tension (Phase IV, final)

Joint Intrusion

When braiding, the open-structure joints are still malleable and pliant. Under the tension of the braiding process, the joint intersections are smashed together. To simulate this effect, the compression allows yarn 'intrusion' specified as a percent of yarn diameter. An example of this effect is shown in Figure 11. The mean diameter of the free yarn is 2.3 mm, and the vertical height of the joint is only 3 mm - corresponding to a 70% intrusion. This makes for a better

structure visually, and creates more accurate paths of yarn centerlines. However, all yarns still remain round, so this approximation does not fully represent the conditions at yarn intersections.
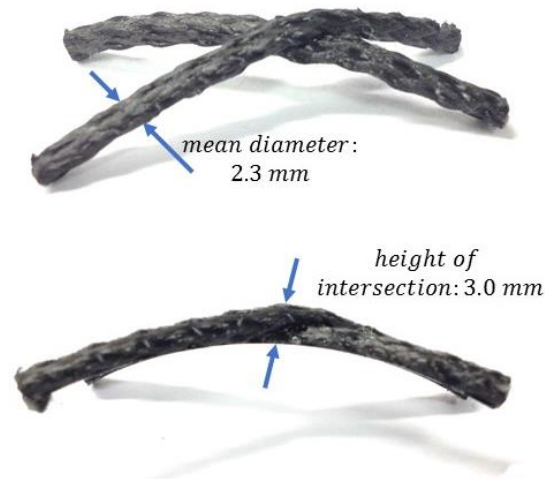
Figure 11 – An O-ACS joint showing the intersection intrusion

Discretization

When the finite element model is constructed later, the discretization of the forgoing equations will determine the number of elements in the model, and probably force a compromise between solution speed and accuracy. A control parameter is used to define the amount of discretization in the model, which is limited by the fact that the model must have discrete nodes at yarn intersections. The discretization s is defined as the number of straight 'beam' segments between the closest possible intersections of yarn. 'Closest possible intersection' is used (rather than the *actual* distance to intersection) to ensure that the discretization is compatible with the number of horn gears g on any given braiding machine. The minimum discretization between intersections shall be limited to a single element *when all carriers are loaded with yarn*. This means that a discretization $s = 2$ is not a guarantee that every free length between nodes is one straight segment; only that it be two elements at minimum. The effect of discretization on the Finite Element results will be shown in Chapter 3.

The natural discretization of the structure itself (into yarn 'beams' spanned between intersections) will be of concern when the Finite Element Analysis (FEA) program is discussed. At the end of a structure, the free-hanging yarns are very flexible since they do not have the

15

support of the joint intersections. Thus, the deflection at the very end of the structure may be large compared to that of the main body of the structure. Examples of well-conditioned and ill-conditioned structure ends are shown in Figure 12.
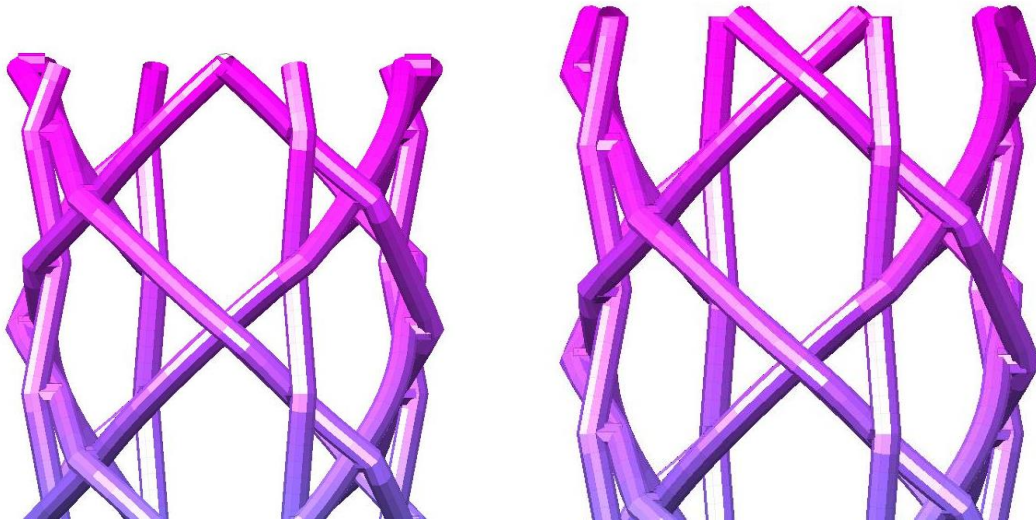
Figure 12 - Left: joint intersection at structure end, Right: yarns hang beyond the intersection

This can give rise to discretization issues which the FEA code will not understand, and care must be taken to treat the issue as it arises. For instance, a structure of a given length would be expected to have a smooth Stiffness vs. Helix angle relationship. Because of the large deflection of end-beams, the results are not smooth, as seen in Figure 13. Note that the relative effect of the ends will always decrease with an increase in structure length. These errors are discussed in more detail in Chapter 4.
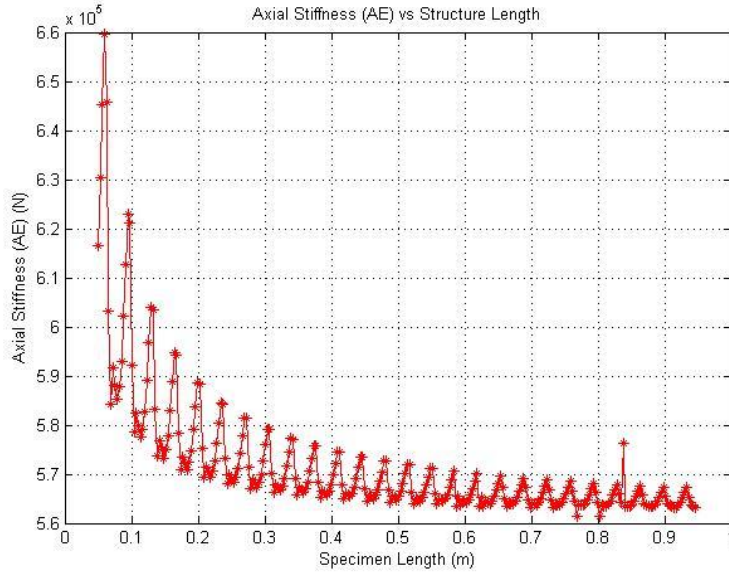
Figure 13 - Natural discretization creates periodic change in total deflection

Computation of Structure Mass

The mass of the O-ACS tube can be calculated from the discretized model. Each yarn has a density and constant diameter. The mass of each yarn is simply the product of its cross sectional area, length, and density. Length in the discretized model is the sum of all element lengths. All yarns in the structure summed together give the total mass:

$$Mass = \sum_{yarn\,1}^{\#\,yarns} \frac{\rho\pi\phi^2}{4} \sum_{element\,1}^{\#\,elements} ||node_2 - node_1||$$

(10)

This method for mass estimation was compared to fifteen experimental samples, each of unique geometry. It was found to match the mass-per-length with a Root-Mean-Squared (RMS) error of 2.5%, and a standard deviation of 2.75%.

Conclusion

An analytical interpretation of O-ACS braid geometry has been created. Several kinematics models were compared for accuracy and utility – a simple sinusoid was chosen. The equations governing the model are used to create a basic shape. Special care was taken to ensure the interlacing of the yarns is properly handled; this requires some logic in the geometry definition

17

but gives acceptable results. The structure is compressed against the mandrel diameter iteratively to better represent the cured O-ACS form. Considerations on the effect of discretization in the model were enumerated. The final model is used to generate a fairly complex physical sample in Figure 14. The model is seen to adequately replicate braid geometry.
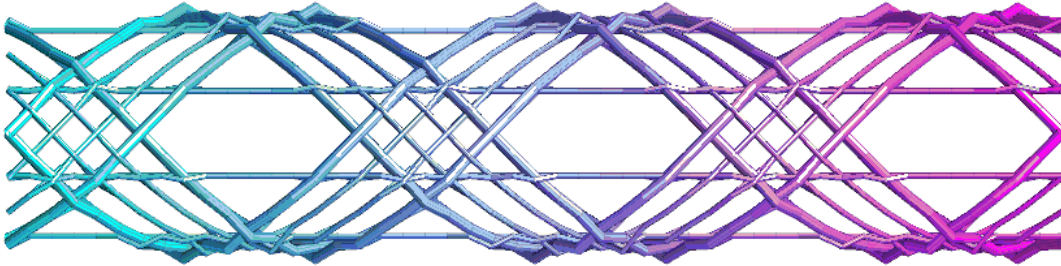
Figure 14 – Example of braid simulator capability

Finite Element Model Development

Model Goals and Objectives

The objective of the finite element model in this work is to provide a computationally lightweight model that adequately represents the geometry of the open-structure, the carbon yarns which constitute the bulk of the material, and the intersection of carbon yarns at micro-joints which interconnect the carbon yarns. The analysis will also incorporate a method for easy application of the beam loading conditions and constraints described in Chapter 1. It must finally solve for the required structure and field quantities needed in the optimization. These include structure deflection, yarn-element loads and strains, and joint-element loads and strains. These quantities are sufficient for the calculation of stresses and the computation of many common failure modes if desired (though the focus of the current work is stiffness).

The FEA solver will be constructed as generally as possible with the above-stated goals in mind. MATLAB is used as the computational and programming platform. The major components of a typical FEA process are outlined in the flowchart of Figure 15. This process is typical of structural Finite Element methods (Cook, Malkus, Plesha, & Witt, 2002) and thus only components that are unique or important in the analysis of open structures are described in detail. The primary assumptions upon which the present model is based are presented here and explained farther below:

1. Individual O-ACS yarns can be modeled as beam elements
2. The geometry model (of Chapter 2) sufficiently describes the important O-ACS form
3. A single finite-element can describe the bonded micro-joint at each yarn overlap
4. The structure behaves linearly in the deflection range of interest
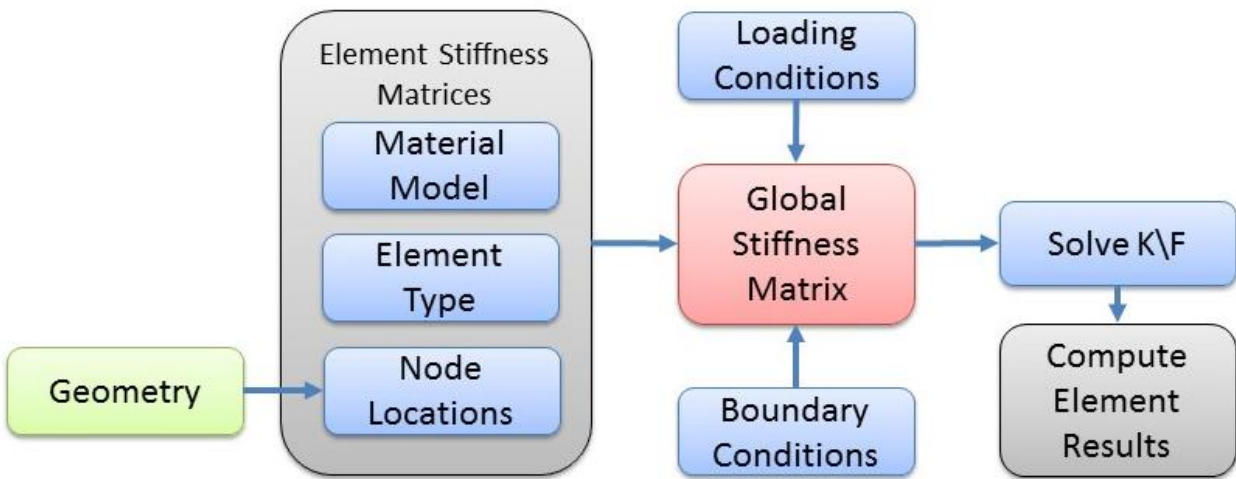
Figure 15 – Finite Element Modelling process flowchart

Modeling Yarns

During the braiding process, the pre-impregnated yarns are limp and malleable. The structure is formed from these soft yarns and then cured into the final rigid lattice. The structure is made rigid by the internal curing of the yarns, and the cured intersecting joints of overlapping yarns. Each single cured yarn in the structure is supported by the joint intersections at regular intervals. This distance between supports (i.e. yarn intersections) is long compared to the diameter of the yarn: thus it is assumed that the free-standing length of each yarn has beam-like properties.

There are a few beam element formulations which could be used. The two deciding factors in the element choice are the number of nodes and the ability to account for shear. First, because of the geometry-generation model it is very easy to increase or decrease the element spacing along each yarn. It is not convenient, however, to require the yarns have spacing compatible with three-node elements. Second, free-standing lengths between yarn intersections are not so long that shear deformation can be ignored. Finally, the yarns typically maintain a round cross section and so the ability to account for shear flow is not necessary (Cook, Malkus, Plesha, & Witt, 2002). Thus the Timoshenko shear-corrected beam is the appropriate element choice when straight beam elements are employed (Przemieniecki, 1968). However, in the development of the model, it was seen that using straight beam elements to represent the helical yarns required excessive

20

discretization to achieve desired accuracy. Thus, curved beam ('arch') elements were used for the helical yarns (Weaver & Gere, 1990). The curved beam formulation requires additional computations and transformations, thus suffers in calculation speed. A comparison of the beam element choices is shown in Table 2.

Table 2 - Comparison of the Beam Element capabilities

	Bending	**Shear**	**Curved**	**Speed (relative)**
Euler-Bernoulli Beam	yes	no	no	1
Timoshenko Beam	yes	yes	yes	1
Virtual Work Arch	yes	yes	yes	3

Another major benefit of the beam model is the easy incorporation of experimental yarn stiffness and strength properties. The diameter of the yarn is often difficult to define as the section can become oblong. The yarn jacket typically consists of materials much softer than the carbon core: thus measuring a yarn's stiffness and dividing by the cross-section to retrieve a 'modulus' is not very consistent. The most accurate model, if the yarn being used is available for measurement, is simply to measure and assign axial, bending, and torsional stiffness to the beam. The intrinsic properties Elastic Modulus (E), Flexural Modulus (E_{flex}) and Shear Modulus (G) are of course necessary for creation of the model, it is just suggested that they be derived from yarns of similar size to the ones which are being analyzed (Kothari, 2014). This also facilitates the consideration of experimental failure limits instead of the extrapolation from intrinsic properties and dimensions. The experimental yarn properties assigned in this way are given in Chapter 4.

Development of Timoshenko Beam Element Stiffness and Rotation Matrix

The derivation of the Timoshenko Shear-corrected Beam Element is now presented. The development follows Przemieniecki's derivation and notation (Przemieniecki, 1968). A diagram of the beam element is presented in Figure 16. The beam has two nodes along its x-axis. Each node has six degrees of freedom – three displacements and three rotations – and loads on each degree of freedom – three forces and three moments. It is useful to split the derivation into

separate axial, torsional, and bending computations. The primary assumptions made in this derivation are as follows:

- Yarns are transversely isotropic (y and z directions are equivalent)
- The circular yarns do not need a shear area correction term
- Thermal effects are neglected
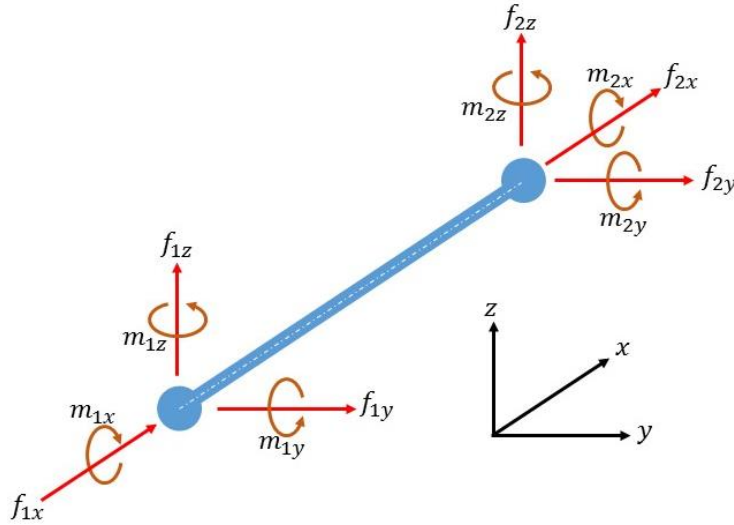
Figure 16- Straight beam element; diagram

Axial Forces - Axial Stiffness (X-direction) is found by integration of the governing differential equation

$$F_{1x} = -\left(\frac{du}{dx}\right)EA$$

And, considering equilibrium

$$f_{1x} = -f_{2x}$$

To yield

$$k_{1,1} = \frac{f_{1x}}{d_{1x}} = \frac{EA}{L}$$

(11)

$$k_{7,1} = \frac{f_{2x}}{d_{1x}} = \frac{-EA}{L}$$

(12)

A similar argument yields the reciprocal relationship for node 2, and the equations can be combined in the matrix form

22

$$\{d_{1x} \; d_{2x}\}$$

$$\begin{Bmatrix} f_{1x} \\ f_{2x} \end{Bmatrix} k_x = \frac{AE}{L} \begin{bmatrix} 1 & -1 \\ -1 & 1 \end{bmatrix}$$

Twisting Moments - Torsional Stiffness (Z-direction) is found by integration of the governing differential equation

$$m_{1x} = -GJ \frac{dr}{dx}$$

And from equilibrium it is known that

$$m_{1z} = -m_{2z}$$

To yield

$$k_{4,4} = \frac{m_{1x}}{r_{1x}} = \frac{GJ}{L}$$

(13)

$$k_{10,4} \frac{m_{2x}}{r_{1x}} = \frac{-GJ}{L}$$

(14)

A similar argument for the second node yields the full set of torsion relations, in matrix form;

$$\{r_{1x} \; r_{2x}\}$$

$$\begin{Bmatrix} m_{1x} \\ m_{2x} \end{Bmatrix} k_x = \frac{GJ}{L} \begin{bmatrix} 1 & -1 \\ -1 & 1 \end{bmatrix}$$

Shearing Forces – Lateral deflection (d_{1y}) due to shearing forces has two components, one from bending strain (v_b) and a second from shear strain (v_s).

$$v = v_b + v_s$$

The two governing differential equations are given by

$$\frac{dv_s}{dx} = -f_{1y}$$

$$EI \frac{d^2 v_b}{dx^2} = f_{1y}x - m_{1z}$$

Integration of these equations and application of boundary conditions yields

$$EId_{1y} = \frac{f_{1y}x^3}{6} - \frac{m_{1z}x^2}{2} - \frac{f_{1y}\Phi x L^2}{12} + \frac{(1+\Phi)L^3 f_{1y}}{12}$$

Where

$$\Phi = \frac{12EI}{GAL^2}$$

And from equilibrium

$$f_{2y} = -f_{1y}$$

$$m_{2z} = -m_{1z} + f_{1y}L$$

Applying boundary conditions, the four reactions can be found

$$k_{2,2} = \frac{f_{1y}}{d_{1y}} = \frac{12EI}{(1+\Phi)L^3}$$

(15)

$$k_{6,2} = \frac{m_{1z}}{d_{1y}} = \frac{6EI}{(1+\Phi)L^2}$$

(16)

$$k_{8,2} = \frac{f_{2y}}{d_{1y}} = \frac{-12EI}{(1+\Phi)L^3}$$

(17)

$$k_{12,2} = \frac{m_{2z}}{d_{1y}} = \frac{6EI}{(1+\Phi)L^2}$$

(18)

Considering the same calculations from the second node:

$$k_{8,8} = \frac{12EI}{(1+\Phi)L^3}$$

(19)

$$k_{12,8} = \frac{-6EI}{(1+\Phi)L^2}$$

(20)

Bending Moments – Using the same governing bending equation, but with boundaries that only allow deformation in rotation, the deflection for a pure moment is given as

$$EIv = \frac{f_{1y}}{6}(x^3 - L^2x) + \frac{m_{1z}}{2}(Lx - x^2)$$

$$f_{1y} = \frac{6m_{1z}}{(4 + \Phi)L}$$

$$r_{1z} = \frac{m_{1z}(L + \Phi)L}{EI(4 + \Phi)}$$

From these relationships, the reactions are found

$$k_{6,6} = \frac{m_{1z}}{r_{1z}} = \frac{EI(4 + \Phi)}{(1 + \Phi)L}$$

(21)

$$k_{3,6} = \frac{f_{2y}}{r_{1z}} = \frac{6EI}{(1 + \Phi)L^2}$$

(22)

$$k_{12,6} = \frac{m_{2z}}{r_{1z}} = \frac{(2 - \Phi)EI}{(1 + \Phi)L}$$

(23)

And from symmetry

$$k_{12,12} = k_{6,6} = \frac{EI(4 + \Phi)}{(1 + \Phi)L}$$

(24)

The same derivation can be used for shear deformation in the Z direction and bending deformation about the Y direction. The full set of equations (11) through (24) are combined to form the beam element stiffness matrix shown on the following page (25).

$$
\begin{array}{c}
\{d_{1x} \quad d_{1y} \quad d_{1z} \quad r_{1x} \quad r_{1y} \quad r_{1z} \quad d_{2x} \quad d_{2y} \quad d_{2z} \quad r_{2x} \quad r_{2y} \quad r_{2z}\}
\end{array}
$$

$$
\begin{Bmatrix} f_{1x} \\ f_{1y} \\ f_{1z} \\ m_{1x} \\ m_{1y} \\ m_{1z} \\ f_{2x} \\ f_{2y} \\ f_{2z} \\ m_{2x} \\ m_{2y} \\ m_{2z} \end{Bmatrix}
\begin{bmatrix}
\dfrac{AE}{L} & 0 & 0 & 0 & 0 & 0 & -\dfrac{AE}{L} & 0 & 0 & 0 & 0 & 0 \\[2ex]
* & \dfrac{12EI_z}{L^3(1+\Phi)} & 0 & 0 & 0 & \dfrac{6EI_z}{L^2(1+\Phi)} & 0 & -\dfrac{12EI_z}{L^3(1+\Phi)} & 0 & 0 & 0 & \dfrac{6EI_z}{L^2(1+\Phi)} \\[2ex]
* & * & \dfrac{12EI_y}{L^3(1+\Phi)} & 0 & -\dfrac{6EI_y}{L^2(1+\Phi)} & 0 & 0 & 0 & -\dfrac{12EI_y}{L^3} & 0 & -\dfrac{6EI_y}{L^2(1+\Phi)} & 0 \\[2ex]
* & * & * & \dfrac{GJ}{L} & 0 & 0 & 0 & 0 & 0 & -\dfrac{GJ}{L} & 0 & 0 \\[2ex]
* & * & * & * & \dfrac{(4+\Phi)EI_y}{L(1+\Phi)} & 0 & 0 & 0 & \dfrac{6EI_y}{L^2(1+\Phi)} & 0 & \dfrac{(2-\Phi)EI_y}{L(1+\Phi)} & 0 \\[2ex]
* & * & * & * & * & \dfrac{(4+\Phi)EI_z}{L(1+\Phi)} & 0 & -\dfrac{6EI_z}{L^2(1+\Phi)} & 0 & 0 & 0 & \dfrac{(2-\Phi)EI_z}{L(1+\Phi)} \\[2ex]
* & * & * & * & * & * & \dfrac{AE}{L} & 0 & 0 & 0 & 0 & 0 \\[2ex]
* & * & * & * & * & * & * & \dfrac{12EI_z}{L^3(1+\Phi)} & 0 & 0 & 0 & -\dfrac{6EI_z}{L^2(1+\Phi)} \\[2ex]
* & * & * & \text{symmetric} & * & * & * & * & \dfrac{12EI_y}{L^3(1+\Phi)} & 0 & \dfrac{6EI_y}{L^2(1+\Phi)} & 0 \\[2ex]
* & * & * & * & * & * & * & * & * & \dfrac{GJ}{L} & 0 & 0 \\[2ex]
* & * & * & * & * & * & * & * & * & * & \dfrac{(4+\Phi)EI_y}{L(1+\Phi)} & 0 \\[2ex]
* & * & * & * & * & * & * & * & * & * & * & \dfrac{(4+\Phi)EI_z}{L(1+\Phi)}
\end{bmatrix}
$$

$$
\Phi = \frac{12EI}{GAL^2}
$$

(25)

Three Dimensional Rotation

Because the beams will be arbitrarily oriented in 3d-space, a rotation matrix is defined. Following the notation of (Logan, 2007), the transformation matrix is

$$T = \begin{bmatrix} \lambda_{3x3} & 0 & 0 & 0 \\ 0 & \lambda_{3x3} & 0 & 0 \\ 0 & 0 & \lambda_{3x3} & 0 \\ 0 & 0 & 0 & \lambda_{3x3} \end{bmatrix}$$

$$(26)$$

Where

$$\lambda_{3x3} = \begin{bmatrix} C_{x\hat{x}} & C_{y\hat{x}} & C_{z\hat{x}} \\ C_{x\hat{y}} & C_{y\hat{y}} & C_{z\hat{y}} \\ C_{x\hat{z}} & C_{y\hat{z}} & C_{z\hat{z}} \end{bmatrix} = \begin{bmatrix} x \cdot \hat{x} & x \cdot \hat{x} & x \cdot \hat{x} \\ x \cdot \hat{x} & x \cdot \hat{x} & x \cdot \hat{x} \\ x \cdot \hat{x} & x \cdot \hat{x} & x \cdot \hat{x} \end{bmatrix}$$

$$(27)$$

is the direction cosine matrix for the beam X-axis.

Simplifying the direction cosines for radially symmetric beams (round cross section):

$$\hat{x} = \cos\theta_{x\hat{x}}\, \hat{\imath} + \cos\theta_{y\hat{x}}\, \hat{\jmath} + \cos\theta_{z\hat{x}}\, \hat{k}$$

$$\cos\theta_{x\hat{x}} = \frac{x_2-x_1}{L} = l \qquad \cos\theta_{y\hat{x}} = \frac{y_2-y_1}{L} = m \qquad \cos\theta_{z\hat{x}} = \frac{z_2-z_1}{L} = n$$

Maintaining $\hat{y}$ perpendicular to $\hat{x}$ and z axes yields

$$z \times \hat{x} = \hat{y} = \frac{1}{D}\begin{vmatrix} \hat{\imath} & \hat{\jmath} & \hat{k} \\ 0 & 0 & 1 \\ l & m & n \end{vmatrix}$$

$$\hat{y} = -\frac{m}{D}\hat{\imath} + \frac{l}{D}\hat{\jmath}$$

$$D = (l^2 + m^2)^{\frac{1}{2}}$$

And, for $\hat{z}$

$$\hat{z} = \hat{x} \times \hat{y} = \frac{1}{D}\begin{vmatrix} \hat{\imath} & \hat{\jmath} & \hat{k} \\ l & m & n \\ -m & l & 0 \end{vmatrix}$$

$$z = -\frac{ln}{D}\hat{\imath} - \frac{mn}{D}\hat{\jmath} + D\hat{k}$$

Combined;

$$\lambda_{3x3} = \begin{bmatrix} l & m & n \\ -\dfrac{m}{D} & \dfrac{l}{D} & 0 \\ -\dfrac{ln}{D} & -\dfrac{mn}{D} & D \end{bmatrix}$$

<div align="right">(28)</div>

Unless $\hat{x} = z_{global}$ or $\hat{x} = -z_{global}$, for which, respectively;

$$\lambda_{3x3} = \begin{bmatrix} 0 & 0 & 1 \\ 0 & 1 & 0 \\ -1 & 0 & 0 \end{bmatrix} \quad \text{or} \quad \lambda_{3x3} = \begin{bmatrix} 0 & 0 & -1 \\ 0 & 1 & 0 \\ 1 & 0 & 0 \end{bmatrix}$$

Finally, the transformed stiffness matrix is found:

$$\hat{k} = T^T k T$$

<div align="right">(29)</div>

This completes the derivation of the beam element stiffness matrix.

Development of Curved Beam Element Stiffness and Rotation Matrix
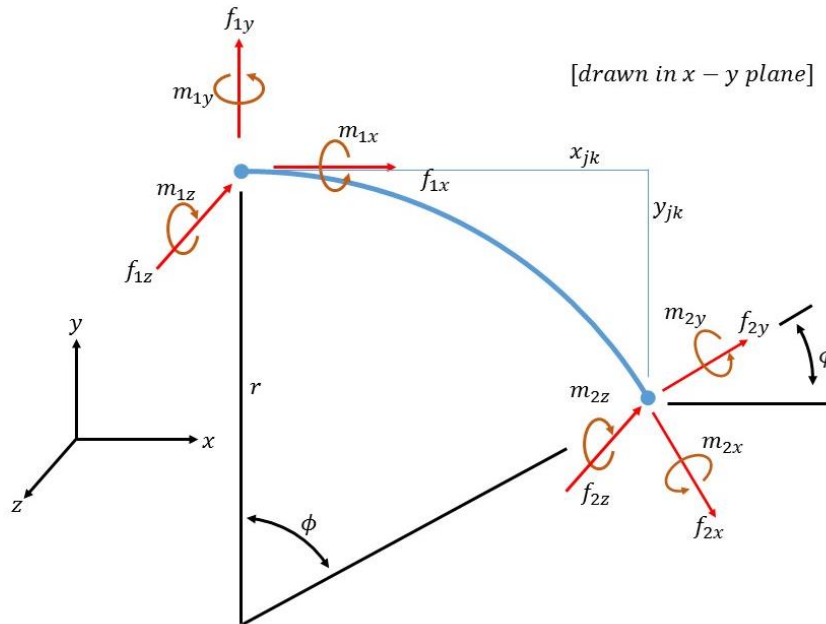
Figure 17 – Curved beam element; diagram

The stiffness matrix for the curved beam (Figure 17) will now be developed. It has the same degrees of freedom as the straight beam. Following Weaver (Weaver & Gere, 1990), the compliance matrix $f_{M_{kk}}$ for the 'frame' loads in the curved beam is given by:

$$\begin{Bmatrix} d_x \\ d_y \\ r_z \end{Bmatrix} = \frac{r}{2EI_z} \begin{bmatrix} r^2(3\phi - 4\sin\phi + \sin\phi\cos\phi) + \Phi_x & -r^2(2 - 2\cos\phi - \sin^2\phi) & -2r(\phi - \sin\phi) \\ * & r^2(\phi - \sin\phi\cos\phi) + \Phi_y & 2r(1 - \cos\phi) \\ sym. & * & 2\phi \end{bmatrix} \begin{Bmatrix} f_x \\ f_y \\ m_z \end{Bmatrix}$$

$$\Phi_x = \frac{(1 - \cos\phi)r}{GA} \qquad \Phi_y = \frac{r\sin\phi}{GA}$$

Where a shear correction term has been directly added on each of the relevant degrees of freedom. The frame-load (forces acting in the element plane) stiffness matrix is the inverse of the compliance matrix.

$$k_{M_{kk}} = \left(f_{M_{kk}} \right)^{-1}$$

End-loads must be transformed into element coordinates. Because the local coordinate system is in the x-y plane, this requires a simple rotation about the z-axis

$$k_{MS_{kk}} = R_k^T k_{M_{kk}} R_k$$

$$R_k = \begin{bmatrix} \cos\phi & \sin\phi & 0 \\ -\sin\phi & \cos\phi & 0 \\ 0 & 0 & 1 \end{bmatrix}$$

The complete stiffness matrix (to include both nodes) can be found using transformation matrices

$$k_{frame} = \begin{bmatrix} T_{jk} k_{MS_{kk}} T_{jk}^T & -T_{jk} k_{MS_{kk}} \\ -k_{MS_{kk}} T_{jk}^T & k_{MS_{kk}} \end{bmatrix}$$

$$T_{jk} = \begin{bmatrix} 1 & 0 & 0 \\ 0 & 1 & 0 \\ -y_{jk} & x_{jk} & 1 \end{bmatrix}$$

The 'grid' loading (forces acting perpendicular to the element plane) compliance matrix has two components: the flexural component $\left(f_{M_{kk}} \right)_{flex}$ is

$$\begin{Bmatrix} r_x \\ r_y \\ f_z \end{Bmatrix} = \frac{r}{2EI_Y} \begin{bmatrix} \phi - sin\phi cos\phi & -sin^2\phi & r(\phi - sin\phi cos\phi) \\ * & \phi + sin\phi cos\phi & -rsin^2\phi \\ sym. & * & r^2(\phi - sin\phi cos\phi) \end{bmatrix} \begin{Bmatrix} m_x \\ m_y \\ f_z \end{Bmatrix}$$

<div align="right">(33)</div>

The torsional components is $\left(f_{M_{kk}} \right)_{torsion}$

$$\begin{Bmatrix} r_x \\ r_y \\ f_z \end{Bmatrix} = \frac{r}{2GJ} \begin{bmatrix} \phi + sin\phi cos\phi & sin^2\phi & r(\phi - 2sin\phi + sin\phi cos\phi) \\ * & \phi - sin\phi cos\phi & -r(2 - 2cos\phi - sin^2\phi) \\ sym. & * & r^2(3\phi - 4sin\phi + sin\phi cos\phi) + \Phi_z \end{bmatrix} \begin{Bmatrix} m_x \\ m_y \\ f_z \end{Bmatrix}$$

$$\Phi_z = \frac{rsin\phi}{GA}$$

<div align="right">(34)</div>

Which can be summed and inverted to find the grid-load stiffness matrix

$$k_{M_{kk}} = \left(\left(f_{M_{kk}} \right)_{flex} + \left(f_{M_{kk}} \right)_{torsion} \right)^{-1}$$

The full stiffness matrix k_{grid} is found using the same transforms as for the frame loading, but replacing (32) with the following:

$$T_{jk} = \begin{bmatrix} 1 & 0 & y_{jk} \\ 0 & 1 & -x_{jk} \\ 0 & 0 & 1 \end{bmatrix}$$

The full 12x12 stiffness matrix is constructed,

$$k = \begin{bmatrix} k_{frame} & \emptyset \\ \emptyset & k_{grid} \end{bmatrix}$$

Noting that the node numbering must be resorted to match that of the straight beams (25). This completes the local stiffness matrix construction.

Because the curved member is circular, the orientation of the curved beam must match the expected curve around the cylindrical mandrel. Only beams which lie against the mandrel surface are curved, and the beam is oriented as shown in __. Because of the curvature, the element axes must be aligned in the global system completely (i.e. the exact direction-cosine matrix of (27) must be used). The model construction which finds the orientation of the helix also specifies completely the local beam coordinates system. Note that the beam does not lie

exactly on the mandrel surface: that would require an elliptical element. However, the curved beam as presented here provides significant benefit over the straight element, as shown in the coil-spring test case in the next section.
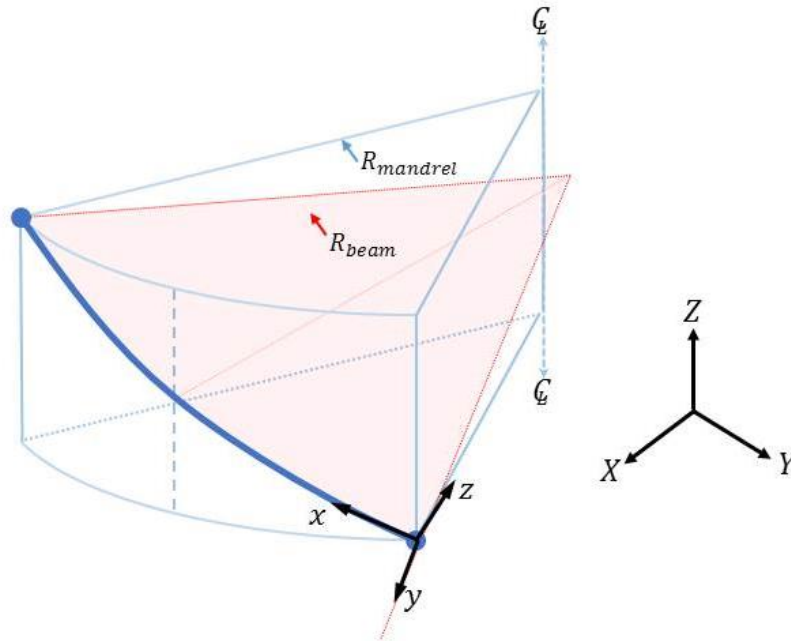
Figure 18 - Curved beam element orientation on the mandrel surface

Modeling Joint Intersections

The geometry model determined the yarn intersection locations and set the spacing between the yarns to the sum of the two intersecting yarn's radii. The intersection physically consists of the yarn radius composite, with a thin film of resin between them. The length of this intersection is small compared with other dimensions in the structure, and thus could lead to an ill-conditioned solution if incorporated with the rest of the model. Finally, physical measurement of the joint intersection as a 'unit' is easy compared with calculating the stiffness that arises from the constituent materials. In physical testing it has been found that the strength of joints (and so perhaps the area of intersection) does not vary significantly with yarn diameter. With these concerns, yarn intersections from one yarn centerline to the next are modeled with a '3-d Spring' element (Figure 19). This element is very similar to the beam element – it can deflect axially, bend, and twist – however it is given (extrinsic) spring rates on each degree of freedom rather than calculating them from material (intrinsic) properties. It is assumed that all joints in the

31

structure have comparable stiffness, regardless of yarn diameter (and hence regardless of element length). Using these concepts, the joints are modeled using an element specified by three parameters: axial stiffness k_a (N), bending stiffness k_b (Nm^2), and torsional stiffness k_t (Nm^2). The element stiffness matrix is given by (35).

$$
\begin{bmatrix}
k_a & 0 & 0 & 0 & 0 & 0 & -k_a & 0 & 0 & 0 & 0 & 0 \\
* & 12k_b & 0 & 0 & 0 & 6k_b & 0 & -12k_b & 0 & 0 & 0 & 6k_b \\
* & * & 12k_b & 0 & -6k_b & 0 & 0 & 0 & -12k_b & 0 & -6k_b & 0 \\
* & * & * & k_t & 0 & 0 & 0 & 0 & 0 & -k_t & 0 & 0 \\
* & * & * & * & 4k_b & 0 & 0 & 0 & 6k_b & 0 & 2k_b & 0 \\
* & * & * & * & * & 4k_b & 0 & -6k_b & 0 & 0 & 0 & 2k_b \\
* & * & * & * & * & * & k_a & 0 & 0 & 0 & 0 & 0 \\
* & * & * & * & * & * & * & 12k_b & 0 & 0 & 0 & -6k_b \\
* & * & sym. & * & * & * & * & * & 12k_b & 0 & 6k_b & 0 \\
* & * & * & * & * & * & * & * & * & k_t & 0 & 0 \\
* & * & * & * & * & * & * & * & * & * & 4k_b & 0 \\
* & * & * & * & * & * & * & * & * & * & * & 4k_b
\end{bmatrix}
$$

$$(35)$$

Though the stiffness of the joint intersection used is comparable to the yarn stiffness, strength considerations should not use the yarn strength. The resin is significantly weaker than the yarns in certain loads, and any failure mechanisms should use physical experiments or micromechanical modeling to determine the limits of joint strength. In the same way that a physical measurement could be made of joint 'spring rates' in the preceding discussion, a similar measurement of (extrinsic) joint strength could also be made.
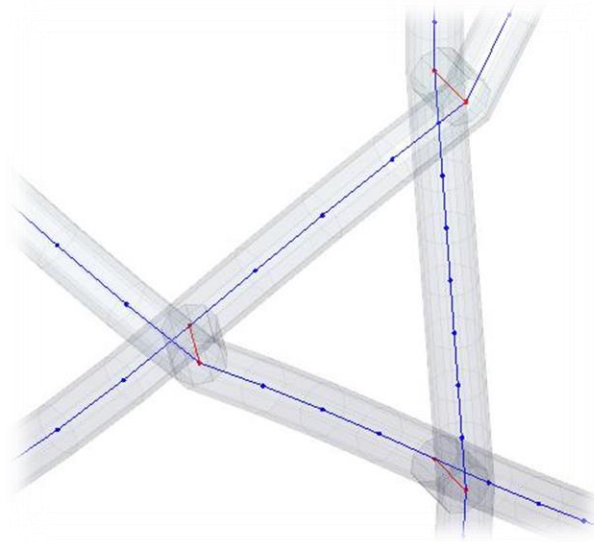
Figure 19 - Example of joint-intersection beam elements

Application of Loads and Boundary Constraints

The loads and constraints will be applied only to the ends of the structure. To facilitate this connection, all the endmost nodes of the structure are joined together radially; creating a single 'master node' to which loads and constraints can be directly applied. The radial 'plate' is formed of essentially rigid (4 orders of magnitude more rigid than the yarns) bar elements. The program automatically determines the number of yarns and appropriate node locations for the connection (Figure 20).

Figure 20 - Demonstration of the rigid bodies to which constraints and loads are applied

The loads and boundaries are applied in the six degrees of freedom available to the master node on each end of the structure. Without loss of generality and to help ensure no redundancy, displacement constraints can be applied to both ends of the structure, while forces and moments can only be applied to the upper end. The naming convention used for each of the constraints is as follows (Table 3):

Table 3 – Degree of freedom labels and notation

	Linear X	Linear Y	Linear Z	Angular X	Angular Y	Angular Z
Lower Displacement	ldx	ldy	ldz	lrx	lry	lrz
Upper Displacement	udx	udy	udz	urx	ury	urz
Upper Load	Fx	Fy	Fz	Mx	My	Mz

Each of the load scenarios which will be tested in the physical experiments (Chapter 4) can be implemented as shown in Table 4. This completes the description of both the internal model (mesh) and boundary conditions. The next stage is the construction of the matrix problem, the solution, and the post-processing of the model.

Table 4 – Displacement and Load Boundary Conditions for each load scenario

	Lower Displacement	Upper Displacement	Upper Load
Tension Tension	ldx=ldy=ldz=0 lrx=lry=lrz=0	* all DoF free*	Fz > 0
Compression Compression	ldx=ldy=ldz=0 lrx=lry=lrz=0	* all DoF free*	Fz < 0
Torsion Torsion	ldx=ldy=ldz=0 lrx=lry=lrz=0	urx=ury=0	Mz > 0
Pure Bending Pure Bending	ldx=ldy=ldz=0 lrx=lry=lrz=0	* all DoF free*	Mx > 0
3-Point Bending (complex example)	ldx=ldy=0 lrz = 0	udz = 0 urx=ury=0	Fx>0

Solution and Post-Processing

The simple form of the Finite Element solution is shown in equation (36) .

$$F = Kx \ \leftrightarrow \ K \backslash F = x$$

(36)

The specification of all the node locations and their interconnections was given in Chapter 2 and the foregoing discussion. These geometry descriptions are then combined with the element stiffness model into the global stiffness matrix K, for a description of the process see, for

example, (Cook, Malkus, Plesha, & Witt, 2002). The constraints on the boundaries remove degrees of freedom from the master nodes, and the loads to be used constitute the F component of Equation (36). It is now possible to solve for the deflection of the structure x using matrix algebra.

When solving the finite element problem, it is common, as occurs here, that the size of K be very large, and the solution of Equation (36) very computationally expensive. A typical O-ACS finite element solution has over 8000 degrees of freedom. To remedy this, sparse matrix abilities within MATLAB were used in the construction of K and in the solution (Gilbert, Moler, & Schreiber, 1991). The size is not so large that a direct solution of the matrix cannot be readily found, and so iterative methods for FE solutions were not considered useful in this work.

Visualization of Results

As *fell_point* is to be used as a design tool, it is useful to include a method for visualizing FEA results. This allows verification that the loads and constraints were properly applied, as well as quick confirmation that the deflection is of the magnitude expected. The geometry model provided a basis for the visualization; Each yarn path is swept with a tubular cylinder of the appropriate diameter to generate the initial (un-deformed) shape. After the FE solution is found, this same path sweep is used along each yarn using the locations of the (now displaced) nodes. Some examples of deformed shapes are shown in Figure 21. The blue and purple structure is the tube after deformation and the gray 'shadow' is the original shape.
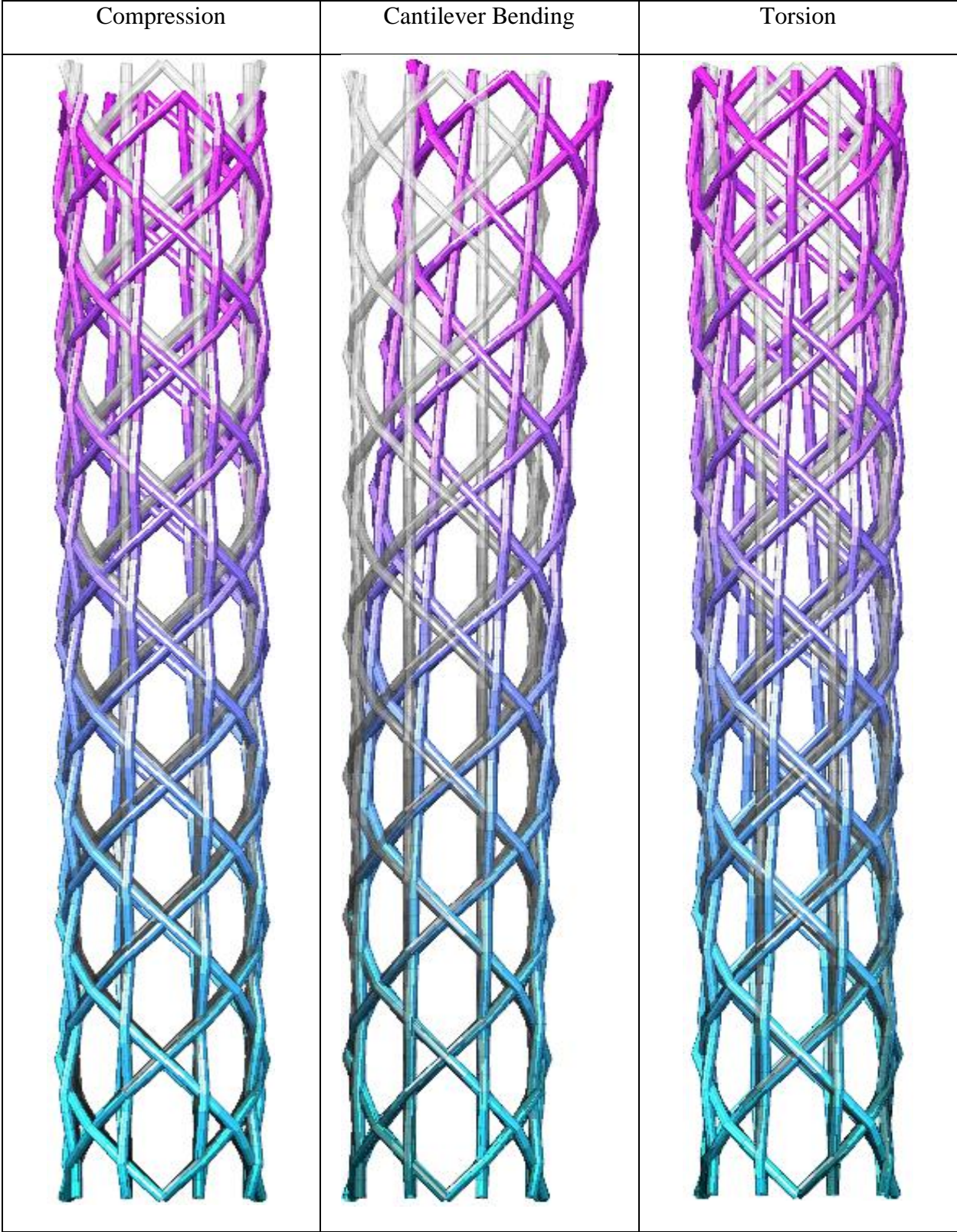
Compression	Cantilever Bending	Torsion

Figure 21 – Visualizing the model after deformation has occured

Sources of Error

The primary concept used in the finite element model development was the beam element. Because the yarns are slender and connect at interspaced points, it was considered to be advantageous to use beams rather than (e.g.) 3D solid elements or shells. This allows an easy connection between the geometry and the finite element model as well. Some limitations of the model have been enumerated already in the geometry chapter which similarly effect the finite element model. These include the fact that yarns are round, yarns are not limited in their radius of curvature, and intersections are approximated by intrusion. All these assumptions give individual yarns more stiffness (in general) than they might have if such effects were modeled. The beam concept relies heavily on the fact that yarn properties are taken from the testing of actual yarns, and not extrapolated from intrinsic properties of their constituents.

Another source of model weakness is treatment of the yarn intersection joints. The complex interaction of two tangent yarns and a resin film have been combined into a single spring rate. This is a good method if joint properties are to be measured in physical testing, however it does not allow the development of structural stiffness from more basic properties such as the resin and yarn individual moduli.

One of the aspects of beam elements which detracts from accuracy is they do not inherently predict buckling failure. The O-ACS concept concentrates mass into bundles that are more stable than a thin sheet. However, if the structure becomes 'open' enough, those bundles will certainly themselves be prone to instability. This effect should be considered if structural strength is to be determined. The current model is designed for stiffness concerns, and thus does not include these effects.

As mentioned in the chapter on geometry, the yarns at the end of the structure are not supported as well as the rest of the O-ACS yarns. The effect of this natural discretization is discussed in detail in the next chapter.

A key goal of the finite element model is to provide a platform for the subsequent geometry optimization. Hence, compromises made in these regards are deemed valid for the purposes of this work. A balance has been made between speed and comprehension of the model vs. inherent accuracy; the former concepts have been emphasized.

Conclusion

This concludes the development of the Finite Element solver in *fell_point*. The underlying assumptions of the model have been stated, and a modeling method built on those. The primary art used in the model is the beam finite element and its advanced forms. Straight and curved beam elements form models of the individual yarns. At the intersections of yarns, a beam-spring formulation is used to represent the connection. A method for application of loads distributed to the end of an O-ACS tube model was created, and shown to be capable of representing the load-cases under which a beam is loaded, as required by the thesis simulation objectives.

The following chapter will evaluate the accuracy of the Finite Element solver using test cases. After showing that the model is capable of matching theoretical results in those test cases, the model is used to evaluate the effects of O-ACS design variables on structural stiffness. Possible sources of error in the model will also be discussed therein.

Finite Element Model Application

Goals and Objectives

The finite element model and programming structure have been developed; it should now be applied. First, a series of trial problems are solved using the model. These trials will test the element stiffness', the element rotations and connectivity, the ability to apply loads, and the retrieval of deformation solutions. The theoretical deformations are presented and compared to the model, proving that it is capable of producing theoretical solutions to moderately complex scenarios. Once the model is proven valid, open-structure tubes are modeled. Several variables in the design of O-ACS tubes are known to produce large effects on the performance of the structures. A comprehensive review of all the parameters, and their effect on structural stiffness, is presented. Possible sources of model error are compared.

Comparison with Theory (Straight Beam and Software Tests)

Straight, Cantilever Beam Test

Having explored the hypothesis and assumptions used in constructing the finite element model of the open-structure, it is desirable at this stage to ensure the model behaves appropriately under common loading scenarios. Beam elements should be tested in trivial cases to show the element construction, element connectivity, load application, and post-processing are all computed properly. Two tests are performed. The first test simply shows that a line of beam elements loaded as a cantilever has the correct deflection magnitude. The solution is known from elementary beam theory. This is, of course, only a test of the programming and not of the element accuracy since the same equations used to check the model were used to create it. The second case involves element rotations and a combined loading, and is the test case used by Logan as a demonstration exercise (Logan, 2007).

The first example is simply a line of beam elements fixed at the left end and loaded in cantilever at the right end. Obviously this test is only valid for the straight beam elements. The expected deflection in the vertical direction is given by the beam bending equations as

$$w = -\frac{Pl^3}{3EI} - \frac{Pl}{GA}$$

<div align="right">(37)</div>

where the first term on the left-hand side is bending, and the second is shearing. The angular deflection is a function of the bending alone

$$\theta = \frac{Pl^2}{2EI}$$

<div align="right">(38)</div>

It is expected that the traditional beam element deflection w is only accurate on long span-lengths, and that the shear-corrected beam perfectly matches the equations in all cases. It is also anticipated that both beams accurately predict the angular deflection. The parameters for the two inch diameter beam are listed in Table 5. The model visualization output is shown in Figure 22, and the deflection results under an end load of 100 kips are shown, for various span lengths, in Table 6. The number of elements does not, of course, change the results for the tip deflection due to the nature of beam elements and beam-bending equation origins. Again, the chart is a test of the software assembly; the fact that the deflection results are exactly correct is trivial.

Table 5 – FEA Sraight Beam Test 1: Material properties

	Value
Elastic Modulus (ksi)	30000
Shear Modulus (ksi)	10000
Cross-sectional Area (in^2)	π
Area Moment of Inertia (in^4)	$\frac{\pi}{4}$
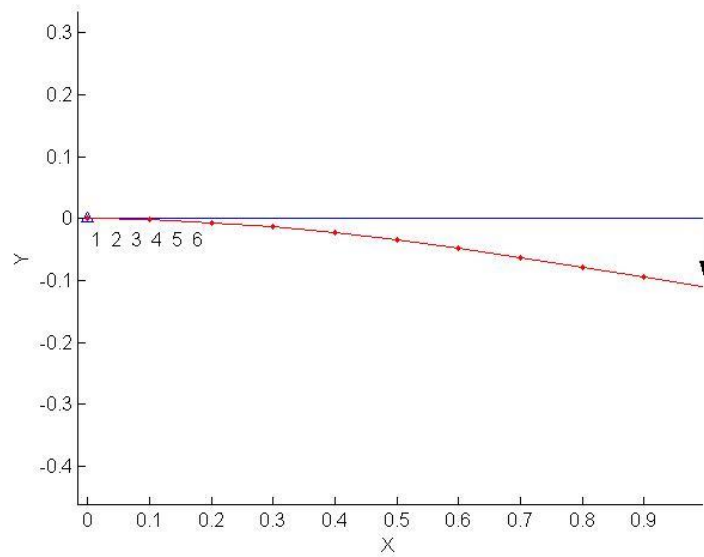
Figure 22 – FEA Test 1; a simple cantilever

Table 6 – FEA Straight Beam Test 1: Results

Beam Length (in)	1	5	10	50
Theoretical Deflection (in/1000)	-4.598	-192.8	-1447	-177000
Theoretical Rotation (rad/1000)	-2.122	-53.05	-212.2	-5305
Traditional Beam Deflection (in/1000)	-1.414	-176.8	-1414	-176800
TB Deflection % Error	225	9.00	2.25	0.09
Traditional Beam Rotation (rad)	-2.122	-53.05	-212.2	-5305
TB Rotation % Error	0	0	0	0
Shear-Corrected Beam Deflection (in)	-4.598	-192.8	-1447	-177000
SC Deflection % Error	0	0	0	0
Shear-Corrected Beam Rotation (rad)	-2.122	-53.05	-212.2	-5305
SC Rotation % Error	0	0	0	0

Test for Beam 3D Rotation and Multiple Loads

The second simple example comes from an exercise by Logan (Logan, 2007). This tests the beam element rotation matrices and the ability to handle multiple loads. The test consists of a space-frame with three mutually orthogonal beams. The intersection of the beams is loaded with

41

a force in the Y direction of -50 (kips), and a torque about the X-axis of -1000 (kips*in) as seen in the visualization (Figure 23).

Figure 23 – FEA Test 2; a space frame
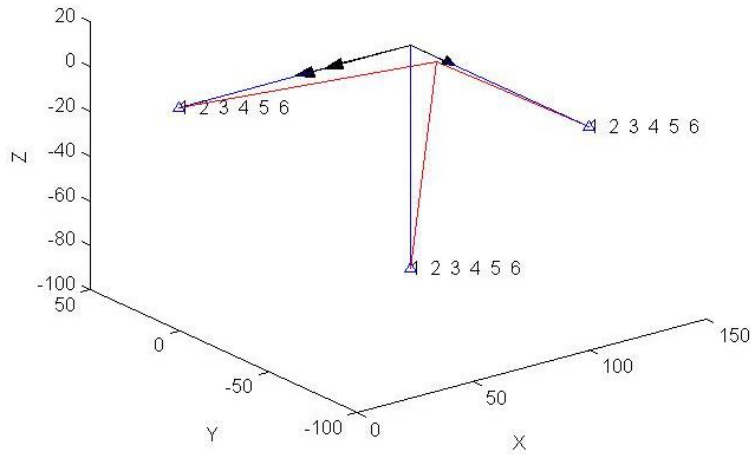
The deflection given by Logan is compared with the results of the *fell_point* and seen to match exactly; demonstrating that element connectivity, rotation in three dimensions, and load applications all work properly (Table 7).

Table 7 – FEA Straight Beam Test 2: results

	Free node Y Deflection (in)	**Free node X Rotation (rad)**
Result from Logan	-0.014	-0.004
Result in *fell_point*	-0.014	-0.004
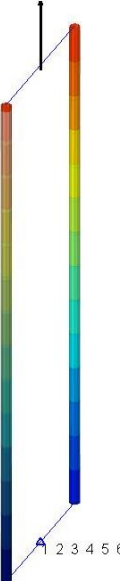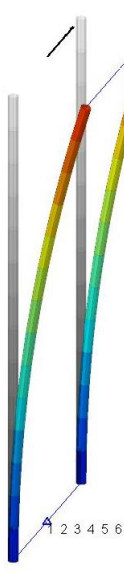
Test of the *fell_point* Load Application and Constraints

    The final simple test will check the ability for the rigid body end caps to properly transfer loads into the O-ACS yarns during simulation. The load case will be a 'structure' consisting of only two yarns. The load will deflect these two simultaneously, and the results should simply reflect the expected results of the test of a beam. The beam properties are listed in Table 8. The equations used to calculate the theoretical deflection are listed in the table of results (Table 9). Error is due to deformation of the end caps; the amount of error induced by this small deflection decreases with structure length.

42

Table 8 – FEA Straight Beam Test 3: Material properties

	Value
Elastic Modulus (Pa)	100e9
Shear Modulus (Pa)	4.0e9
Yarn Diameter (mm)	2.5
Structure Height (mm)	127
Number of Elements	14

Table 9 – FEA Straight Beam Test 3: Results

	Compression	**Cantilever**	**Applied Moment**
Governing Equation	$\delta = \dfrac{Pl}{AE}$	$w = \dfrac{Pl^3}{3EI} + \dfrac{Pl}{GA}$	$w = \dfrac{Ml^2}{2EI}$
Load	10000	10	-1
Theoretical Solution	2.5064 (mm)	133.8 (mm)	78.9 (mm)
FE Solution	2.5084 (mm)	132.35 (mm)	78.4 (mm)
% Error	0.0798	-1.096	-0.646

Comparison with Theory (Curved Beam Test)

Simple beam elements were tested in trivial cases previously to ensure proper behavior. It is now appropriate to ensure the model behaves appropriately under a more complicated loading scenario. The first test of the full model is of a single coil in compression - a coil-spring configuration. Under axial load, the spring compresses. The size of each element is identical, and with similarly identical material properties each element is found to have the same load. The theoretical axial spring rate of the coil is given by the equation (39)

$$K_t = \frac{d^4 G}{8 D^3 N}$$
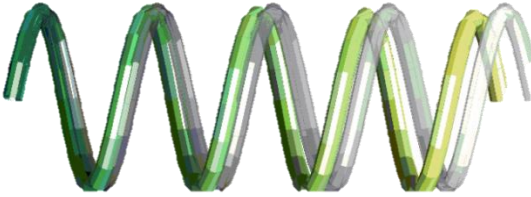
<div align="right">(39)</div>

This test particularly shows the ability of the curved beam elements to handle course mesh discretization. The values used in the analysis are presented in Table 10. A comparison between the model and theoretical values are given in Table 11. The curved beam achieves an accuracy of within 1% using only 12 elements, whereas the straight beam requires 125 elements to achieve similar accuracy; the curved beam is practically 10 times as efficient in this load case.

Table 10 – FEA Curved Beam Test: Material properties

	Specification
Minor Diameter (in)	0.245
Major Diameter (in)	1.7
Shear Modulus (psi)	10.5e6
Elastic Modulus (psi)	45e6
Number of Coils	5.5

Table 11 – FEA Curved Beam Test: Results

Number of Nodes	N=15	N=25	N=50	N=100	N = 1000
Elements per 360 deg.	2.5	4.4	8.9	18	182
Theoretical	175	175	175	175	175
Straight Beam	591.85	272.02	194.28	178.80	173.99
SB % Error	238.19	55.43	11.02	2.17	-0.57
Curved Beam	173.80	174.92	175.12	175.14	175.20
CB % Error	-0.69	-0.05	0.06	0.08	0.11

Effect of Natural Discretization

O-ACS tubes have a natural discretization into trusses which gives them their high specific stiffness, but which simultaneously makes the yarns at the structures end vulnerable to excessive deformation. This can be pictured as a girder which is missing some struts from the end of the beam: without a cross-member to transfer the tension and compression across the structure, the end of the beam is very weak (Figure 24).
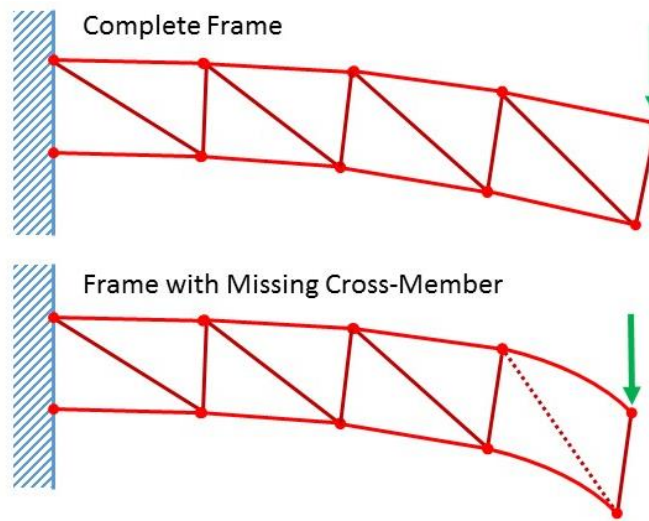
Figure 24 – The effect of a missing cross-member on girder stiffness

In the O-ACS tube, the yarns at the end are at varying distances from an intersection; and provide little stiffness beyond the closest joint. This effect will greatly change the calculated deflection (and thus, stiffness) of the structures. On a short length, the end-most yarns constitute a large portion of the structure, and so play a large role in the total deflection. As the beam grows longer, the deflection of the end-most yarns will become negligible compared to the deflection of the rest of the structure (Figure 25). The error occurs periodically as the end is closer or farther from the joint intersections. Two examples of free-end lengths are given in Figure 26 where the difference is clear. Because of this effect, the stiffness of a given geometry should only be tested on long spans. Where the effect can have large impact on results - such as during optimization – care should be taken that consistent end conditions are compared. The problem will occur when structure height is changed while keeping helix angle constant, or when changing helix angle on a constant structure length.
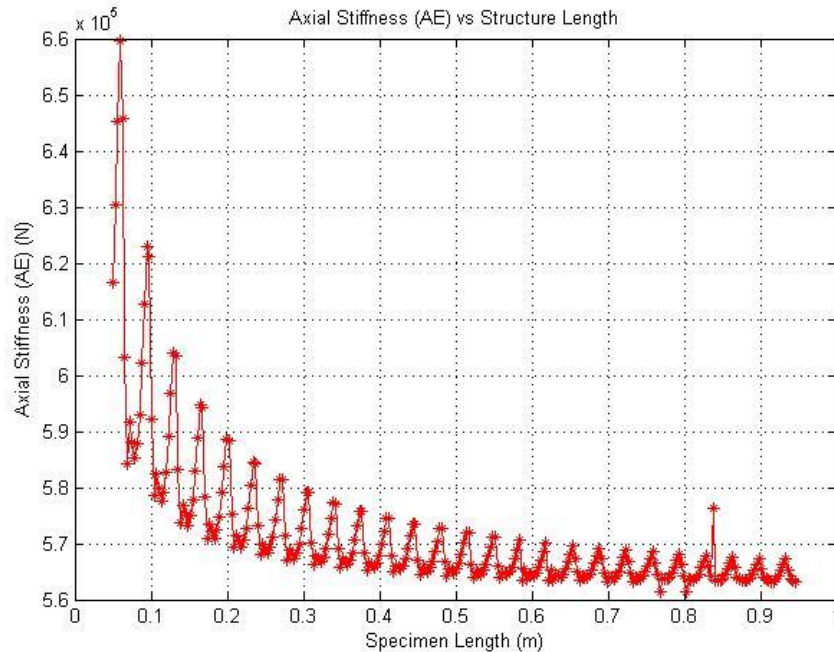

Figure 25 - Effect of natural discretization on predicted stiffness
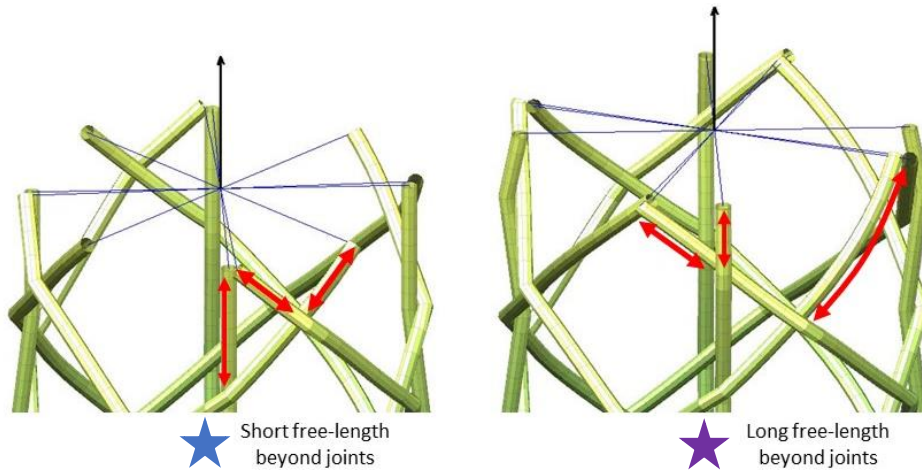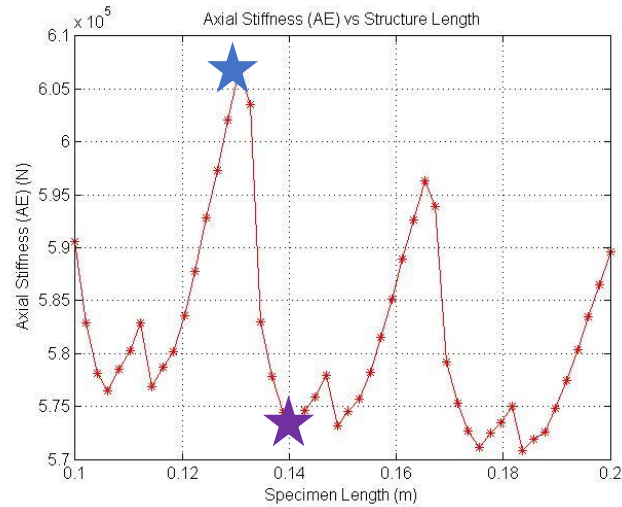
Figure 26 - Left: Short free-lengths at 0.13 m.   Right: Long free lengths at 0.14m.

Results for O-ACS Tubes

Examples of the FEA simulation of O-ACS tubes are given here. First, the examples will demonstrate the control parameters of the finite element formulation to determine the effect of discretization. Secondly, simulations are given showing the relationships among the design variables (helix angle, number of axials, etc.) which will drive the optimization (Chapter 5). Finally, a range of samples has been specified for validation of the Finite Element model with physical tests. The results of the simulation for these samples are presented here, and the results analyzed in Chapter 4.

The base trial structure is the 'typical' Open-structure (Figure 27). This particular sample serves as the mid-point for both the physical testing and for the parametric plots shown below.

47

All controllable values for this structure are given in Table 12. The parameters will be held constant in subsequent plots unless otherwise specified. Yarn properties that require special measurement are adopted from Branscomb (Branscomb, Minimal Weight Composites Utilizing Advanced Manufacturing Techniques, 2012) and Kothari (Kothari, 2014). In some cases the yarn strength may be affected by the braiding process and other variables not considered in the model: thus care must be taken that the effective yarn properties be measured from meaningful samples.
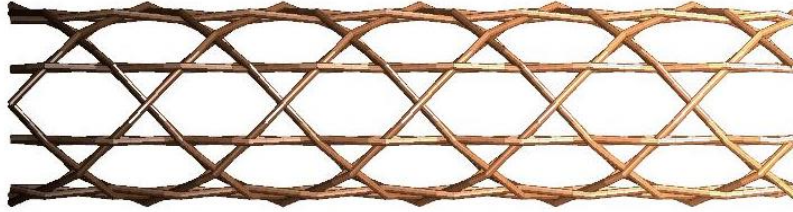

Figure 27 – The O-ACS tube model to be used as a datum

Table 12 – Starting geometry specification for Computer Experiments

Braid Geometry Specification		Material Model	
Mandrel Diameter (m)	0.0444	Yarn Elastic Modulus (GPa)	100
Helix Angle (deg.)	45	Yarn Shear Modulus (GPa)	1.5
Pitch (m)	0.1396	Effective Bending Modulus (GPa)	80
Discretization *s* (1/1)	2	Yarn Effective Diameter (mm)	2.0
warp/weft/axial carrier loading	4/4/8-TT	Joint Axial Stiffness (kN)	123
Height (m)	1	Joint Bending Stiffness (Nm^2)	0.06
Number of Wraps (1/1)	1.4322	Joint Torsional Stiffness (Nm^2)	0.12
Machine Definition *g* (1/1)	32	Yarn Density (g/cc)	1.40

The analysis of each design variable – the driving Braid and Yarn parameters in Table 12 - will be performed for compression, pure bending, and torsion. There are seven design variables not including the carrier loading conditions. The carrier loading will only be varied in meaningful combinations (increase number of axials, decrease number of wrapping yarns, etc.). Some of these characteristics are easily changed by structure design, such as helix angle or mandrel diameter. Others are material properties which are somewhat fixed so long as carbon yarns are being used. However, it is important for design and understanding that the effect of each component of the material be understood to see the strengths and weaknesses of the choice of carbon yarn and resin joints as currently employed in O-ACS design. The plots on the following pages show these simulations: the caption for each figure describes the test.
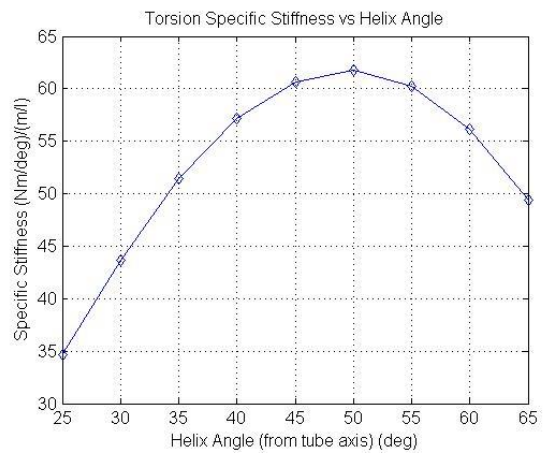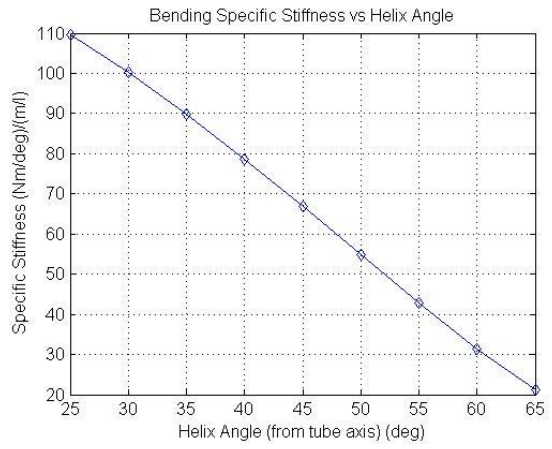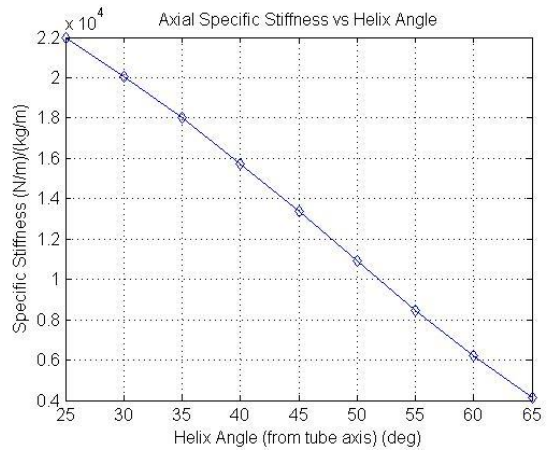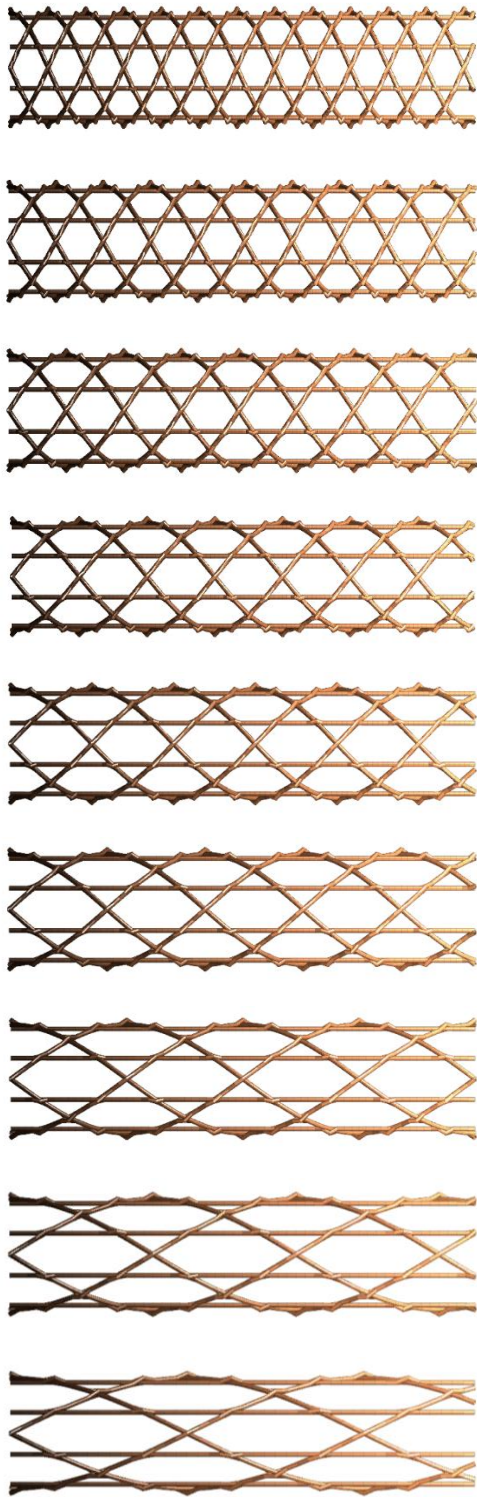
Figure 28-Effect of Varying Helix Angle on O-ACS specific stiffness
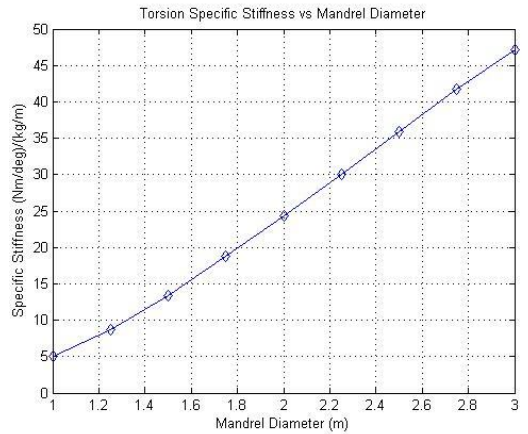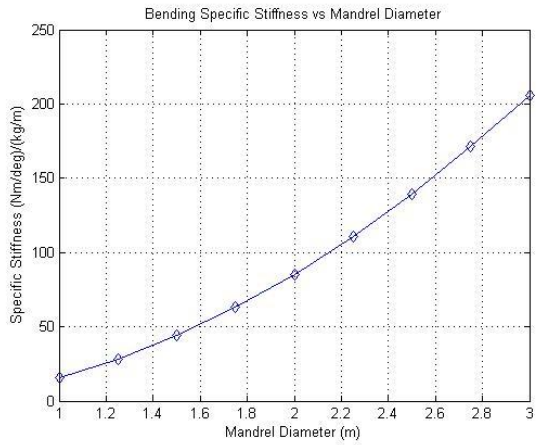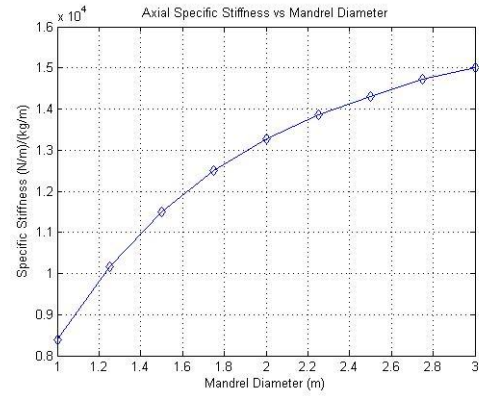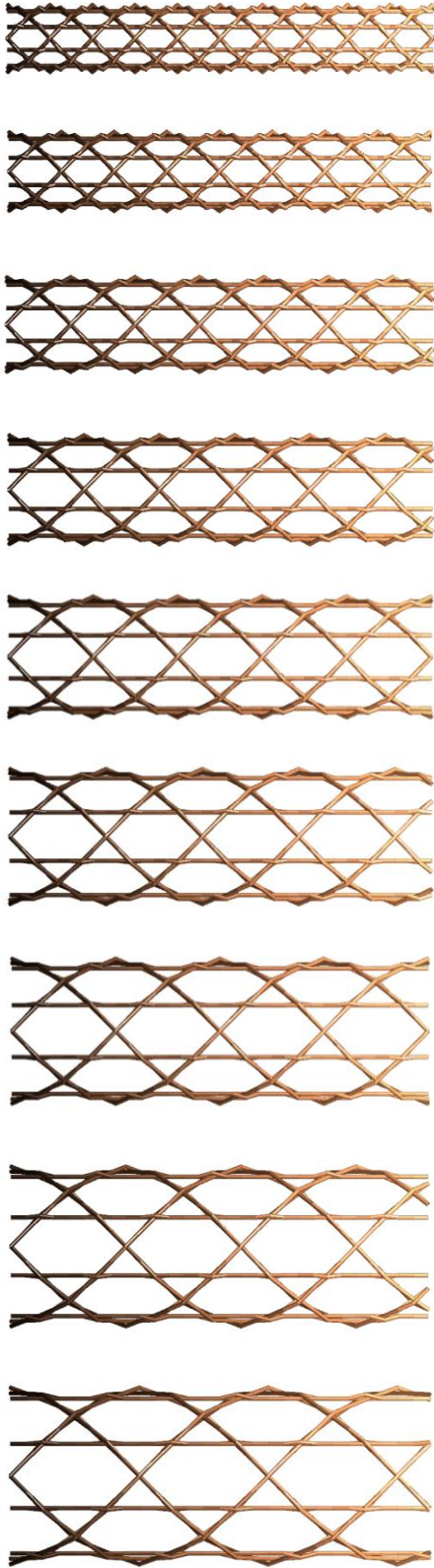
Figure 29 - Effect of Varying Mandrel Diameter on O-ACS specific stiffness
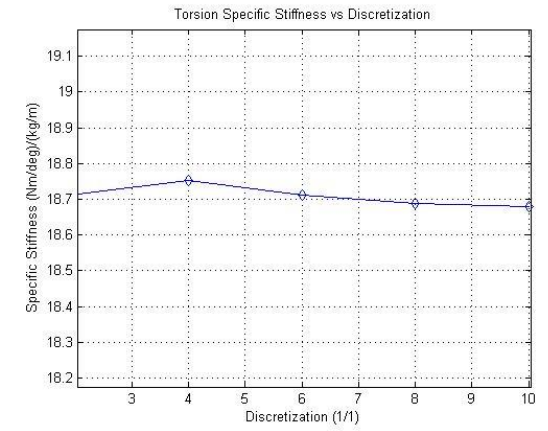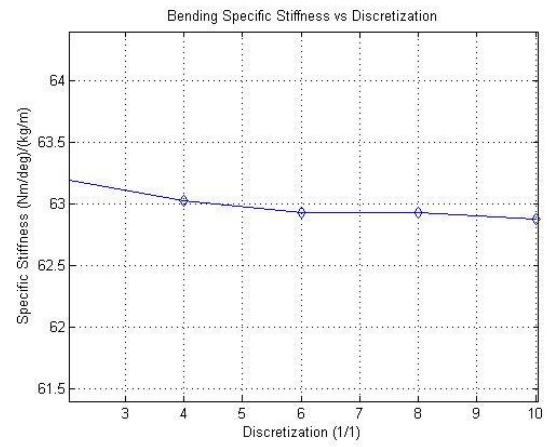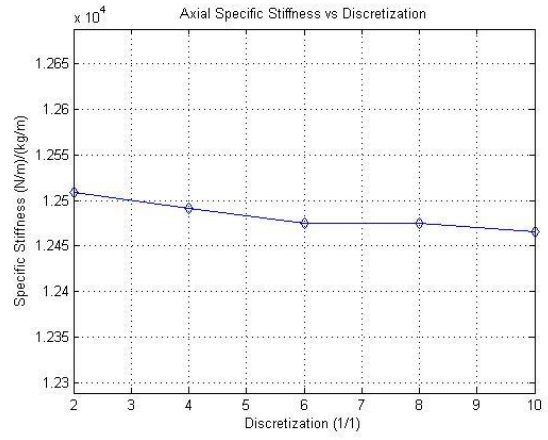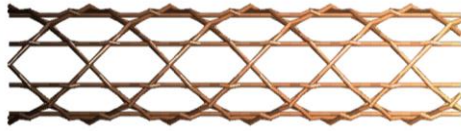
Figure 30- Variation of Discretization Step – Effect on O-ACS stiffness
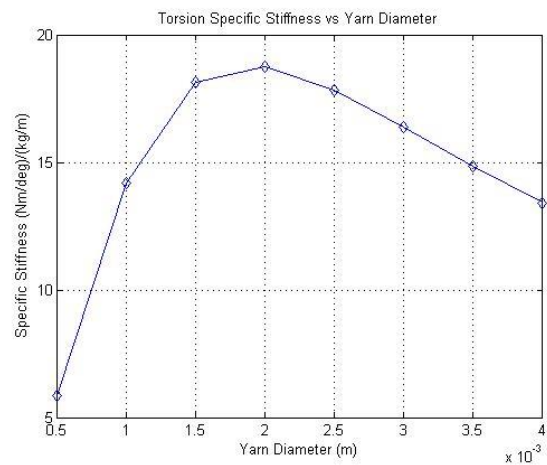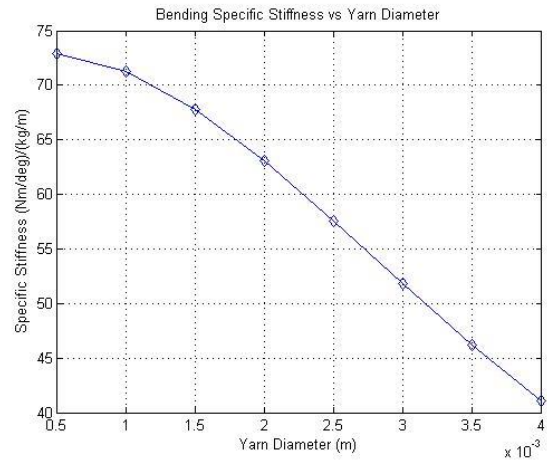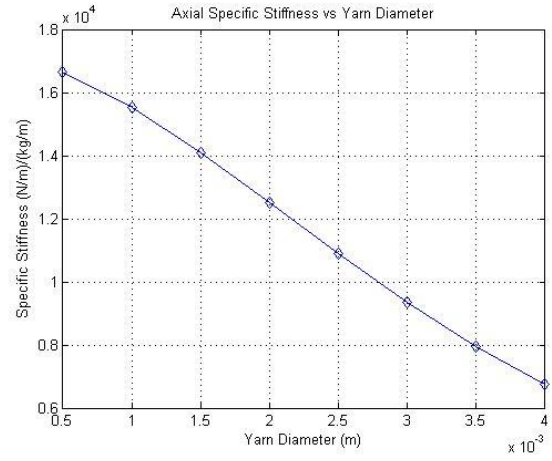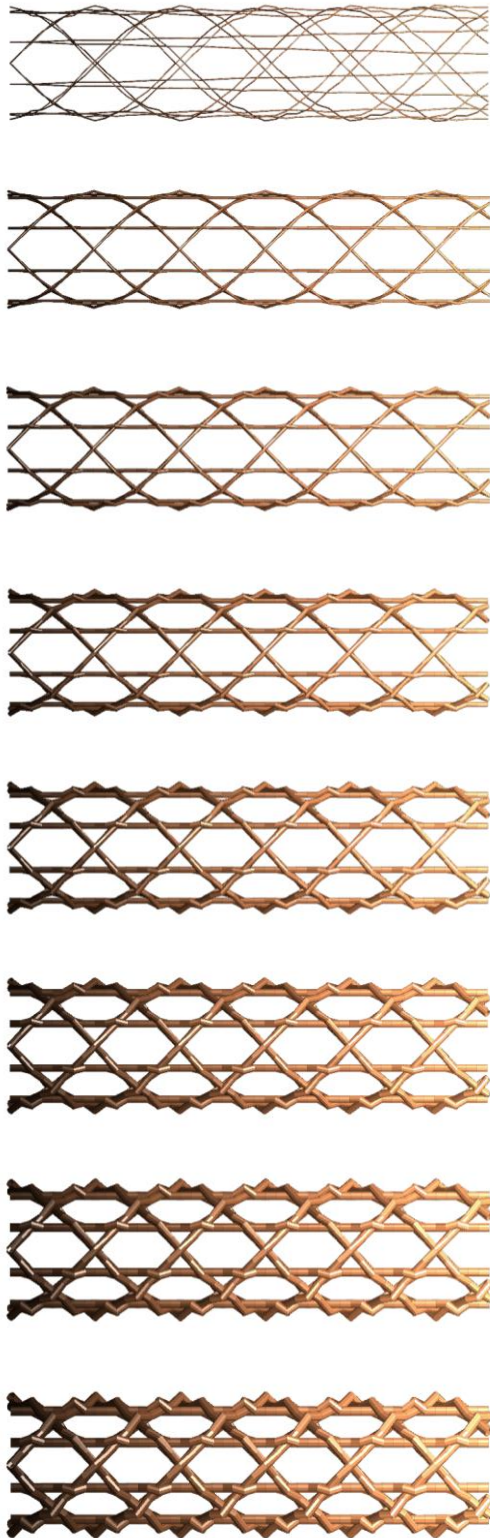
Figure 31 – Effect of variation of Yarn Diameter on O-ACS specific stiffness
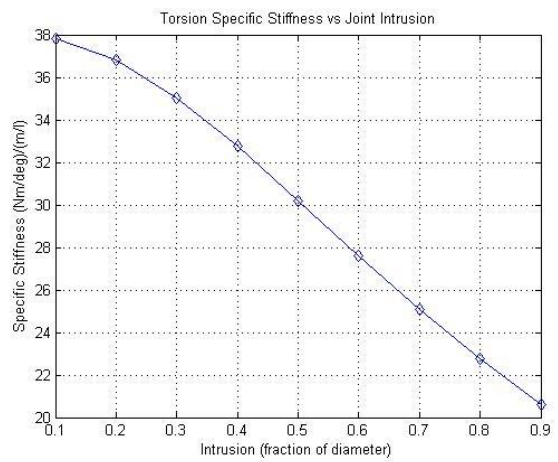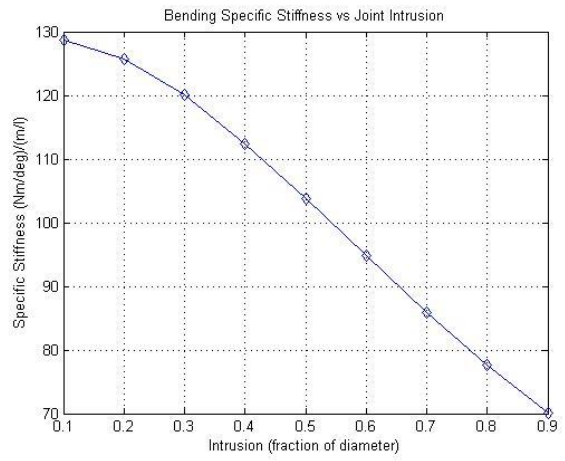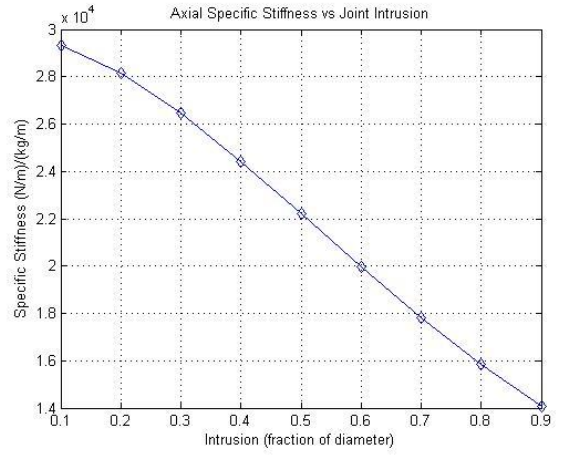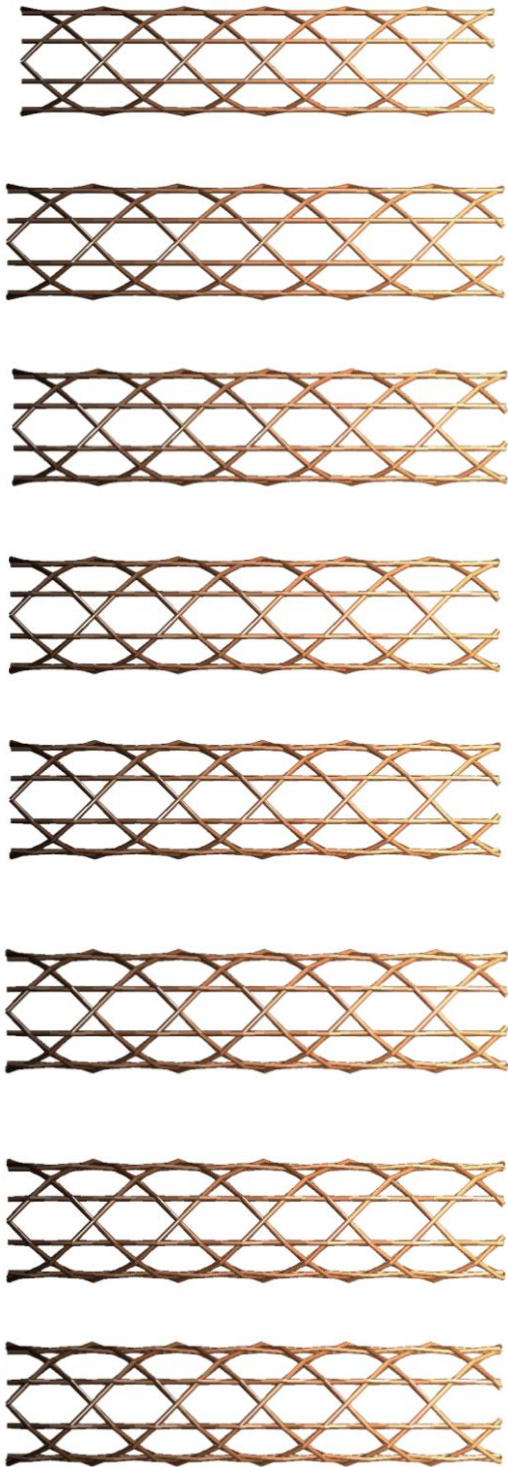
Figure 32 - Effect of variation of joint intrusion

Variation of Elastic Modulus
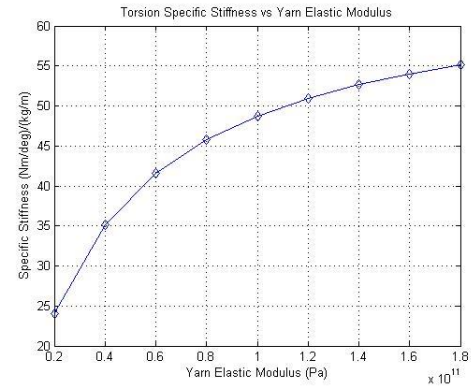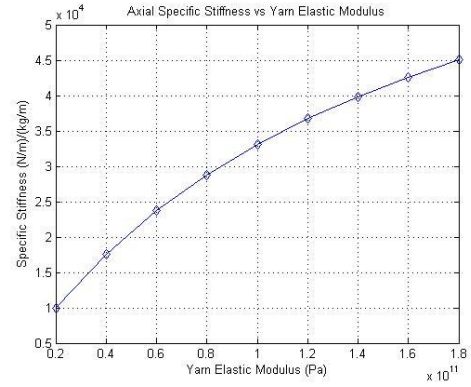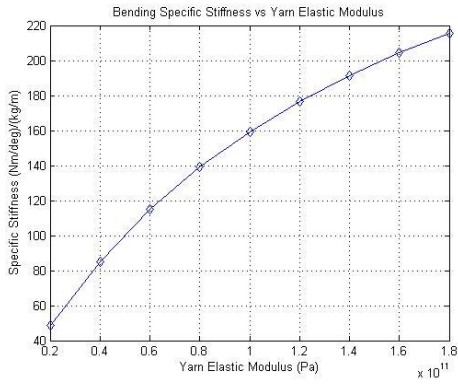
Figure 33 - Variation of Yarn Elastic Modulus

Variation of Yarn Shear Modulus
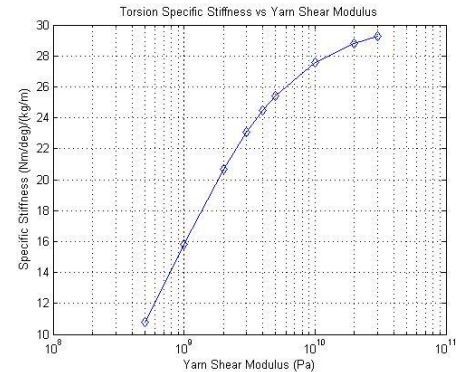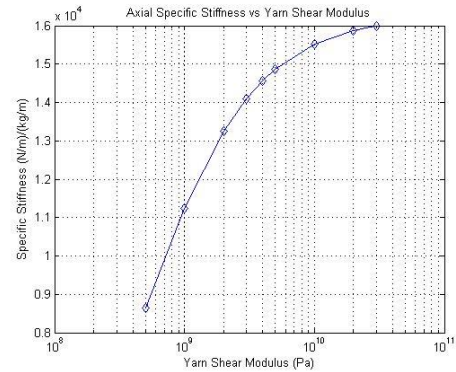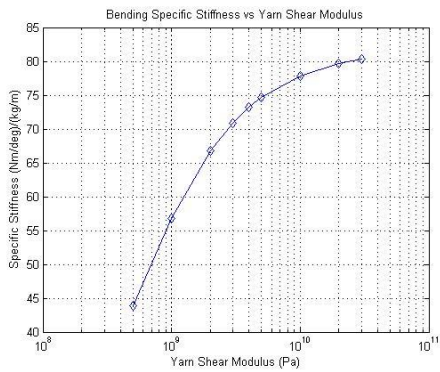
Figure 34 - Variation of Yarn Shear Modulus

54

The plots above give a complete overview of the effect of sweeping design variables through their respective, physically realistic, ranges. It is difficult to see how this information is best used in design. For this purpose, radar plots are very effective. Here are presented plots showing the effect of small variations of some parameters near the values for the 'average' tube as listed in Table 12. These charts should be compared later to those in the chapter on validation. The first three plots show the effect of design variables - helix angle, mandrel diameter, and number of axial yarns – on stiffness'. The next three show response of stiffness – axial, bending, and torsional – to variation of design parameters.

Helix Angle: Effect on Specific Stiffness

Mandrel Diameter: Effect on Specific Stiffness
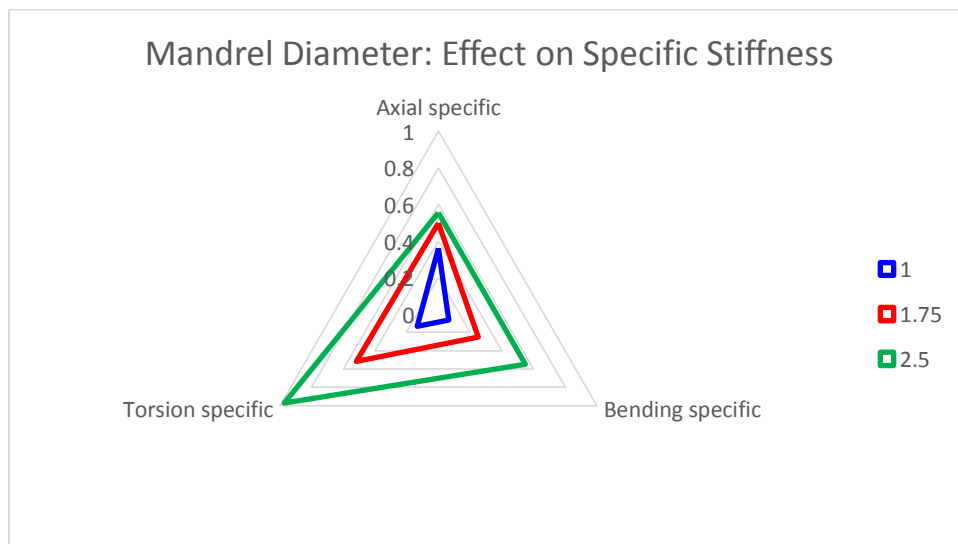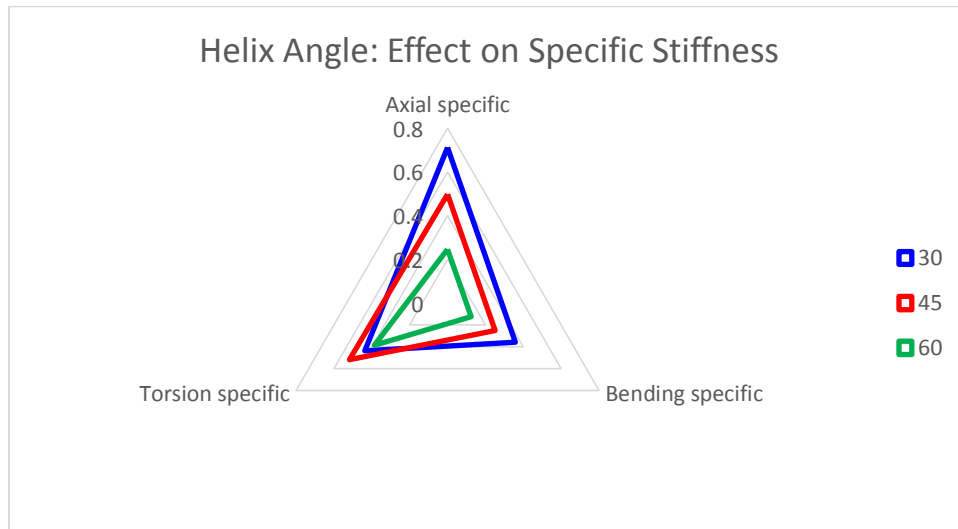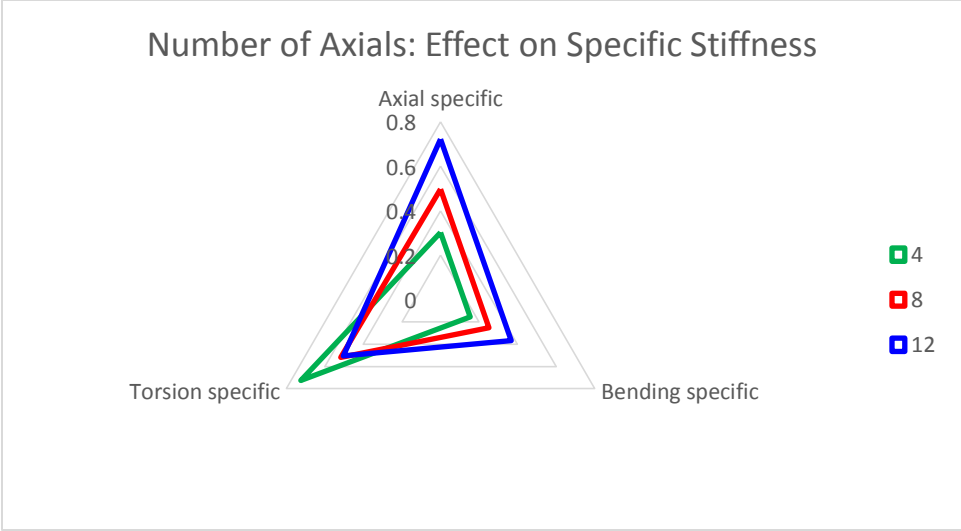
Figure 35 – Radar plots of design variables and their effect on specific stiffness
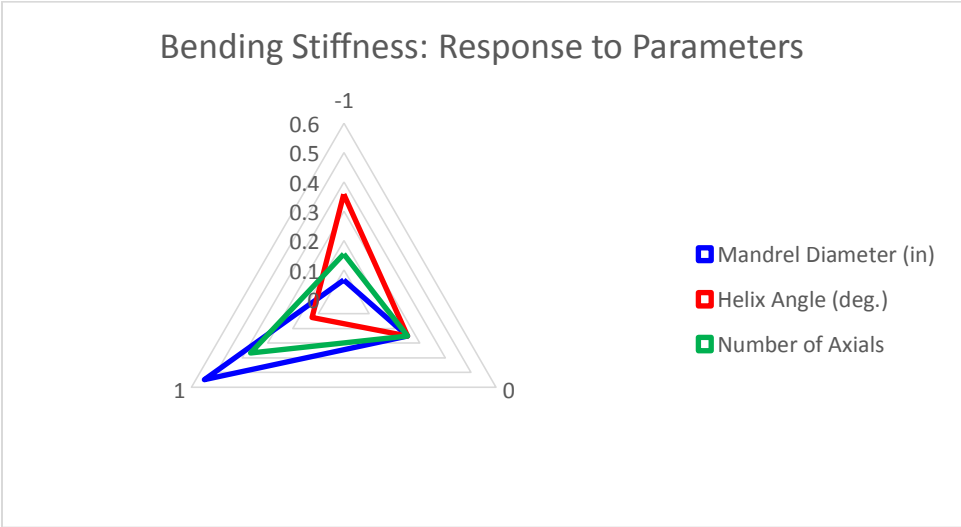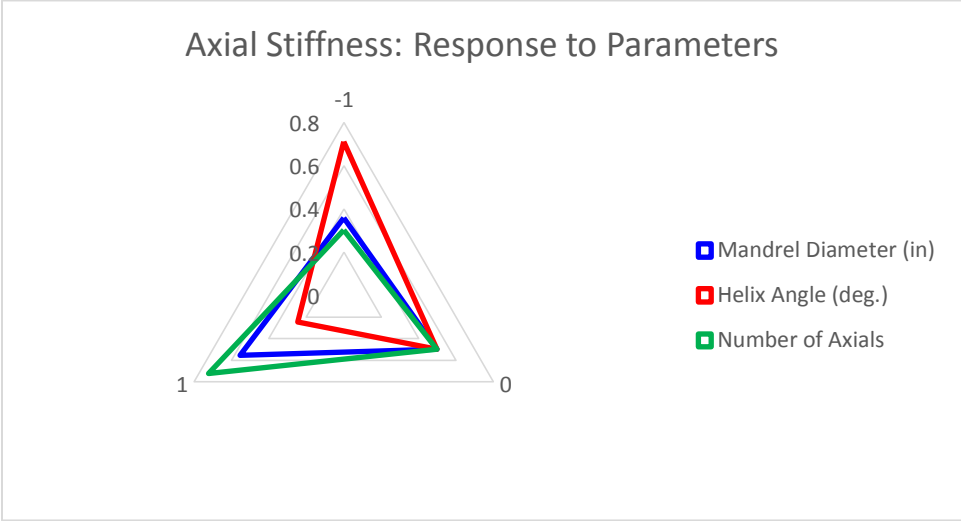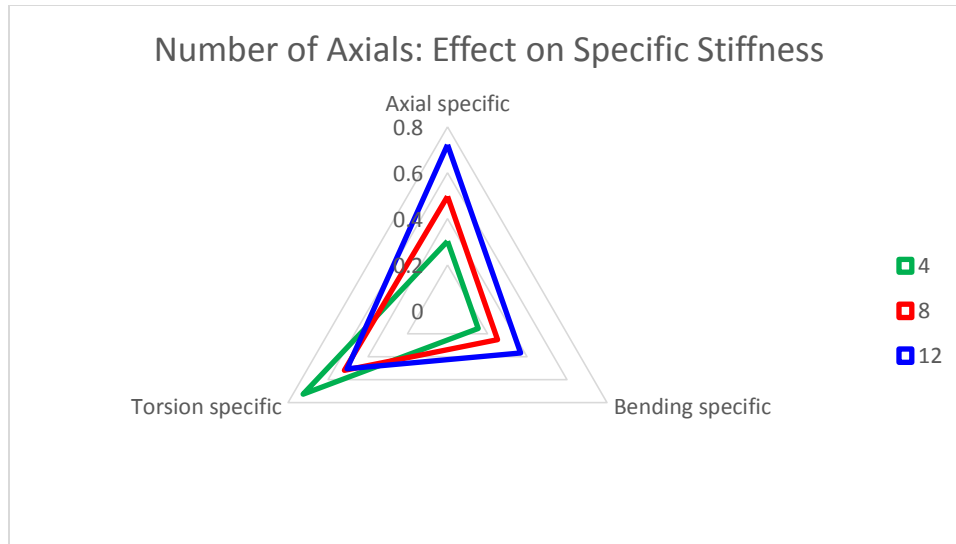
Figure 36 – Radar plots of specific stiffness and their reaction to parameter variation

Conclusion

A Finite Element processor has been developed. The model takes the discretized braid geometry model and interprets the yarns and intersection as beam elements. Common beam elements were found inadequate to represent the helical nature of the braider yarns, and a curved beam element was used. The finite element primitives such as load application and element orientation were confirmed to be accurate using simple test cases. The goal of the model is to allow extrapolation beyond physical testing for structure design. In this pursuit, several parameters of the braids were varied to find their effect on the structure. The three important stiffness 'directions' are Axial, Bending, and Torsional stiffness. In Bending and Torsion, the mandrel diameter is found to have the most beneficial effect on structure specific stiffness. This is intuitive since the weight does not increase, but the 'moment of inertia' of the cross section increases significantly. Because the amount of material does not increase, the effect of additional diameter is nearly linear, and not quartic (to the fourth power) as might be expected based on moment of inertia concepts. In compression, the axial stiffness of the yarns is most important. A key discovery is that specific stiffness in all loads increases significantly with smaller ratios of yarn diameter to mandrel diameter (until the limit of yarn stability). This helps prove the hypothesis that open-structures have an advantage as the minimal weight composite solution. Joint stiffness does not significantly affect the results within the range tested. This would not be true if they joints were made to carry more load, such as by removing all axial yarns. Finally, the

57

use of a composite yarn has many benefits: currently O-ACS could not be manufactured if the pre-impregnated yarn concept was not used. However, as with all composites, the yarns suffer greatly from a low shear modulus. An increase in yarn shear modulus of only a few GPa would increase O-ACS stiffness more than ten percent, with no cost in mass.

Experiment Design

The design of open-structures will soon encompass a huge field when they become commercially viable. Eventually, all design variables might be iterated and compared to better determine the characteristics of ideal braided lattice composites. For now, it is important to quickly cover a wide range of possible structures to find relationships among the key variables. Once a yarn material and size has been selected (currently limited by manufacturing capabilities), the next major design variables are mandrel size, yarn helix angle, and the ratio of axial to braid reinforcement. The specimen collection in the test sample is chosen such that empirical models can be fit to the measured data. Next, the loads to be applied to the structure are determined, and proper test methods for those developed. The description of the test methods is brief as the design of test methods is not the focus of this work.

Designing the Sample

To date, a systematic study of the effects of O-ACS structural parameters and their effect on structure performance has not been completed. The current application targets for the O-ACS are for structures where size and weight limits impose constraints. A range from one to three inches is the focus. While there are thousands of combinations of structures that can be made on the maypole machine, this study focuses on isolating the effect of geometry, and maintains symmetric forms throughout. Some of the main 'degrees of freedom' in the design of open-structure tubes are shown in Figure 37. The first structure shown is a basic true tri-axial: eight axial yarns, four warp, four weft, and a 45 degree helix angle. The structure can be modified in several ways. First, helical yarns could be added to the basic structure; perhaps for torsional stiffness. Alternately, axial yarns could be added to increase compressive strength. Yet another alternative is to keep the yarn-count the same as the basic structure, but to change the helix angle; perhaps affecting both torsional and bending stiffness. Any combination of these is also valid.
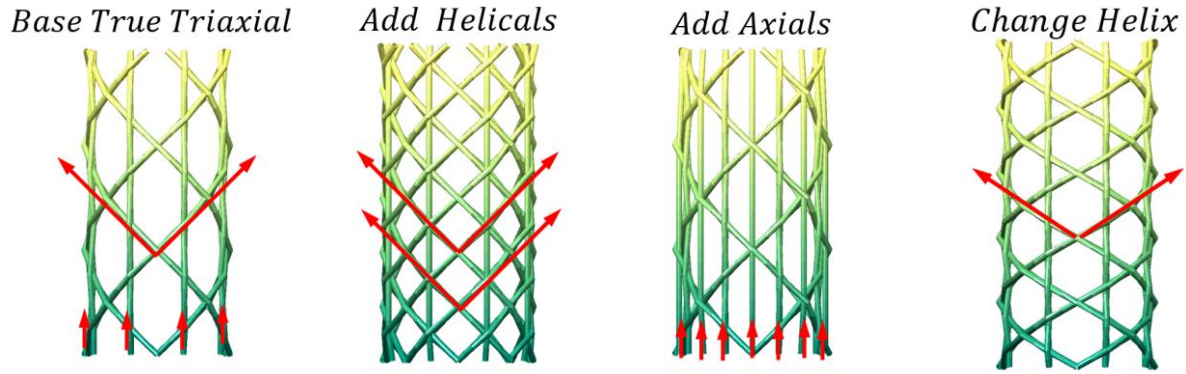
Figure 37 – Major design variable sof the O-ACS structure

Each of these parameters is a dimension that the structure can be designed on. Practically, some of these directions are limited. A clear example is the helix angle variation (Figure 38). Angles which are too shallow do not provide good compression in the helical yarns at the braid point, and so are impractical. Similarly, a very high helix angle will not provide proper axial tension. Some constraints are also placed on the ratio of yarn-to-mandrel diameters. If this ratio is large, the structure begins to close and form a traditional tube. If too open, the structure lacks any geometric reinforcement benefits of the O-ACS concept.
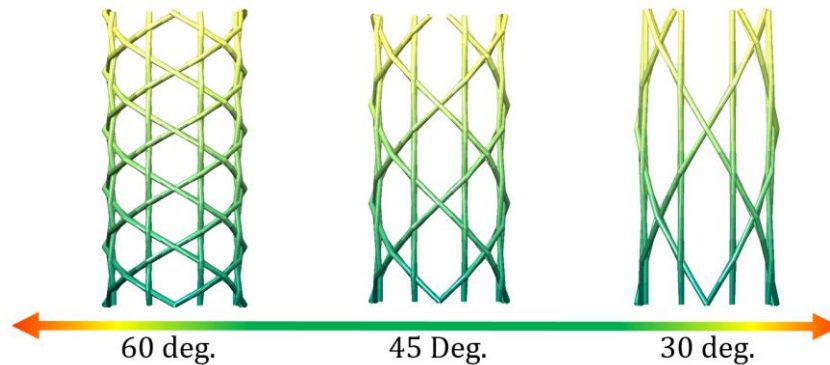
Figure 38 – Example of Design Variable with limited range

The range of structure parameters tested for this work is presented in Table 13. These degrees-of-freedom were chosen as they have the largest influence on structure performance once a particular yarn has been chosen. The range of dimensions specified are within the manufacturing capabilities of a composite braider, and represent a full range of expected structure performance.

60

Table 13 – Range of test sample design variables

	Low	Mid	High
Non-dimensional	(-1)	(0)	(1)
Mandrel Diameter (in)	1.00	1.75	2.50
Helix Angle (deg.)	30	45	60
Number of Axials (#)	4	8	12

If every possible combination of the above were tested, 27 unique samples would be required. Design-of-experiment techniques can greatly reduce the number of test samples by assuming certain polynomial relationships between variables (Lundstedt, et al., 1998). If the relationships among variables were assumed to be linear, only 8 experiments would be needed. For more generality here, a quadratic (2nd order) relationship is assumed. The equation for the relationship among the three variables is assumed to be adequately approximated by (40).

$$y = \beta_0 + \sum_{i=1}^{3} \beta_i x_i + \sum_{i=1}^{3} \sum_{j=i}^{3} \beta_{ij} x_i x_j + \varepsilon$$

(40)

Expanding terms, this relationship can be written

$$y = \beta_0 + \beta_1 x_1 + \beta_2 x_2 + \beta_3 x_3 + \beta_{11} x_1^2 + \beta_{12} x_1 x_2 + \beta_{13} x_1 x_3 + \beta_{22} x_2^2 + \beta_{23} x_2 x_3 + \beta_{33} x_3^2 + \varepsilon$$

(41)

The x_i terms are the independent variables, each β_i is a constant parameter, ε is a random experimental error present in each experiment, and y is the dependent relationship between variables. Because it is an experiment and some error is expected, the equation will be solved in a least squares sense. As there are 10 unknown parameters, the model requires a minimum of ten experiments to be constrained. However, the error is unknown, and additional experiments will reduce the modeling error. Using a modified central composite design, 15 experiments are required. A true central composite design cannot be used since some parameters (the number of axials for instance) are very difficult to vary in a continuous manner. The experiments still

include a 'neutral' experiment (using values labeled 'Mid' in Table 13), and an experiment along each parameter direction. For the present work, the experiments required are listed in Table 14.

Table 14 – Designed experiment specimen list

Experiment #	Mandrel Diameter (in)		Helix Angle (deg.)		Number of Axials	
1	-1	1.00	-1	30	-1	4
2	1	2.5	-1	30	-1	4
3	-1	1.00	1	60	-1	4
4	1	2.5	1	60	-1	4
5	-1	1.00	-1	30	1	12
6	1	2.5	-1	30	1	12
7	-1	1.00	1	60	1	12
8	1	2.5	1	60	1	12
9	0	1.75	0	45	0	8
10	-1	1.00	0	45	0	8
11	1	2.5	0	45	0	8
12	0	1.75	-1	30	0	8
13	0	1.75	1	60	0	8
14	0	1.75	0	45	-1	4
15	0	1.75	0	45	1	12

There are several benefits to the designed experiment approach beyond the reduction in testing needed. A major benefit of the polynomial model is that it will allow some extrapolation to be done in the initial consideration of new design concepts. Once the parameters in (41) are established, new values for the variables can be entered; within a similar range of values the model will predict expected responses for the new values. Also, if an additional variable was to

be considered, it would require only 10 additional experiments to have a 2nd order model in four variables instead of three (a test of all possible combinations would require an additional 54).

Having chosen the size and shape of the samples, the method of constraint should be chosen. The method used was adopted from Branscomb (Branscomb, Minimal Weight Composites Utilizing Advanced Manufacturing Techniques, 2012), and consists of 'potted' end-caps, which encase the structure in resin within a threaded metal cap. The resin provides a solid connection between the metal cap and the structure yarns. The threaded cap is easily connected in a variety of fixtures suitable for testing the various modes. The test fixture design is explored in the next section.

The last consideration in specifying the experimental samples is the length of tube to be tested. The primary consideration is that the length includes at least one full repeating pattern of structure; this ensures local stiffness deviations within the structure do not affect the overall equivalent stiffness. To have a full repeated pattern in a 2.5 inch mandrel, 60 degree helix sample requires a 14.6 inch sample length. The next consideration is the testing equipment: the current testing equipment in use limits the length of uniaxial samples to approximately 24 inches (including the length of the potted end-caps). In most bending tests, a longer sample gives more information about the bending stiffness, and shorter samples yield more information about the shear stiffness. This effect has been eliminated by use of the pure bending test – in which no linear force is carried by the structure and therefore there is no shear effect. From the considerations above, the sample length is chosen to be 18 inches; this is the longest sample length which fits the test rig while allowing for three inches of potting in the end-caps.

Determination of Test Procedures

The open-structure samples will be tested in several modes of beam loading. As stated in the first chapter, the goal of these experiments is to validate the *stiffness predictive* abilities of the FEA model. For this reason, the experiments are designed to measure loads and deflection in a linear range of the structure response. While some observations will be made regarding strength as an extension to the core work, it is not currently a primary consideration. It is desired to determine the effect of each variable (mandrel diameter, etc.) on the deflection response. In other words, for each loading condition we seek a relationship between the variables (x_1, x_2, x_3) and

the response (y) that can be approximated by a 2nd order model (41). The loads to be considered are uni-axial tension and compression, pure moment bending, and torsion. Each case is shown in Figure 39. A brief explanation for the selection of each test, and the procedure used to conduct each one, is given in the following paragraphs.
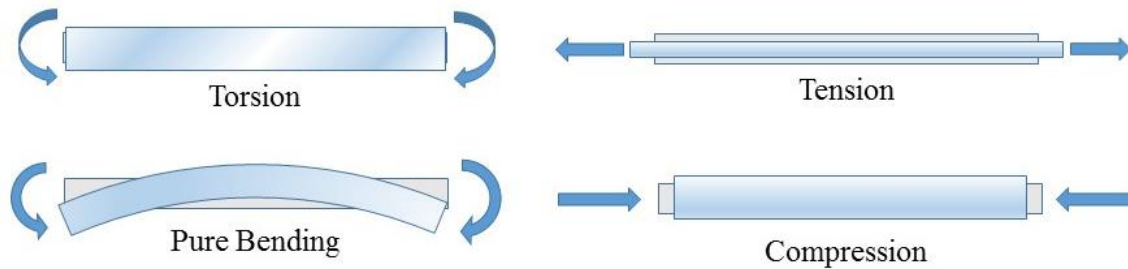
Figure 39 –Loading conditions to be tested

Torsion is a torque or twist about the main axis of the tube. This load case is seen in applications such as drive shafts, drill shafts, and wind-turbine blades (aerodynamic loads). The expected result is that the helix angle and the mandrel diameter will have the largest effect on torsional stiffness. This test is performed using a dedicated torsion testing machine which holds one end fixed and applies a rotation on the other end, measuring the torque and angle of twist. The test fixture for torsion testing is shown in Figure 40.

Figure 40 – The torsion testing setup

The angular deflection and Torque applied are measured. The torsional stiffness 'JG' is retrieved from the raw torque vs angular deflection data using

$$JG = \left(\frac{Nm}{deg}\right) L \quad (\text{Nm\textasciicircum 2})$$

<div align="right">*(42)*</div>

Tension/compression is a pull/push along the tube main axis. This is the most likely loading that the O-ACS will encounter. Applications include truss members and many other uses in a similar condition. While this is perhaps conceptually the easiest test to perform, it is expected that the strength of the structures in tension will exceed the testing machine capacity. NASA has expressed interest in the fabrication of O-ACS trusses as a major component in the Space Launch System (SLS). In that application (and many like it) the primary load will be compression. Connections for the open-structures will certainly ensure that the O-ACS itself be loaded only in tension and compression as a 'two-force member'. Compression is also the most obvious condition in which open-structure tubes should exceed equivalent weight thin-walled tubes; where a thin-walled tube will become unstable and buckle, the individual yarns in the open-structure will not fail. Because the intent of this thesis is to study the stiffness (not strength) of the O-ACS, only one of the tension/compression tests is needed. Compression testing is performed so that more rigid available fixtures can be utilized: steel bearings and caps are used to ensure only compressive (i.e. no bending) loads are applied (Figure 41).

Figure 41 – The compression testing setup

The linear deflection and force applied are measured. The axial stiffness 'AE' is retrieved from the raw force vs. deflection data using

$$AE = \left(\frac{N}{m}\right)L \quad \text{(N)}$$

<div align="right">(43)</div>

Bending is a relatively untested loading condition for common tubes. Examples of bending loads include camera booms, cranes, and robotic arms. Most of the cases are actually cantilever bending. Cantilever bending has loads due both to shear and bending moments – the relative effects of which are significant when the beam length and beam diameter are within an order of magnitude. To isolate only the bending load, a 'pure bending' test will be used. This test involves the application of a bending moment to each end of the structure, but no net force is applied. This presents several convenient results. Shear is not induced and can be safely ignored in calculation of the effective stiffness. The shape taken is nominally a circular arc, allowing easy measurement of the deflection. Finally, it prevents applying force locally to yarns within the structure – an important consideration when the entire beam stiffness is sought. The test fixture developed for this test is shown in Figure 42.
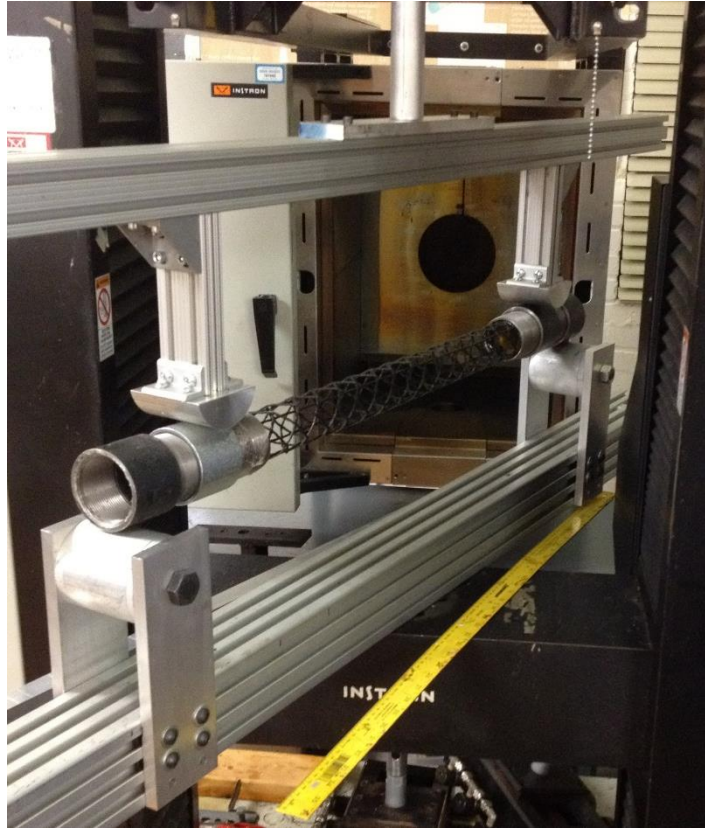
Figure 42 – The pure bending testing setup

The linear deflection and load applied are measured. The end supports each have a known spacing 'a' between supports. The bending stiffness 'EI' is retrieved from the raw force vs. deflection data using

$$EI = \left(\frac{N}{m}\right) * \frac{La^2}{4}$$

<div align="right">(44)</div>

Test Fixture Design

Because the computational tests will involve end-loading with rigid end-plates, this condition is replicated in the test samples. To facilitate connecting the structures to various test equipment, steel threaded couplers (pipe nipples) are placed at each end. The structure is potted in epoxy within this coupler ring. It is important that these end caps be collinear, and that the potted structure be also aligned within them. The procedure for potting the structure is shown in Figure 43. Because epoxy should not be allowed to jam in the coupler threads, a sheet of plastic vacuum-bagging material is used to keep the epoxy from leaking. Step 1 shows the necessary

materials: Pipe nipple, pipe coupler, plastic sheet, and rubber band. Step 2 is to thread the coupler and nipple together with plastic sheet between: this will contain the resin. It was found to be very helpful to glue the sheet in place first with (e.g.) superglue to prevent resin leakage. In Step 3, the rubber band is used to support the free ends of the plastic, which can be trimmed as desired at this point. The two end caps ready, Step 4 shows the fixture; the ends of the structure are wrapped with a cloth material to evenly space it from the walls of the nipple and keep it aligned therewith. Finally, Step 5 shows the fixture completed; the couplers are bound to the rod with (e.g.) hose clamps, the fixture is placed in a vertical orientation, and the ends can be subsequently potted. It is desirable that the rod have a channel in it to help align the couplers. The sixth step is the finished sample, ready for testing.
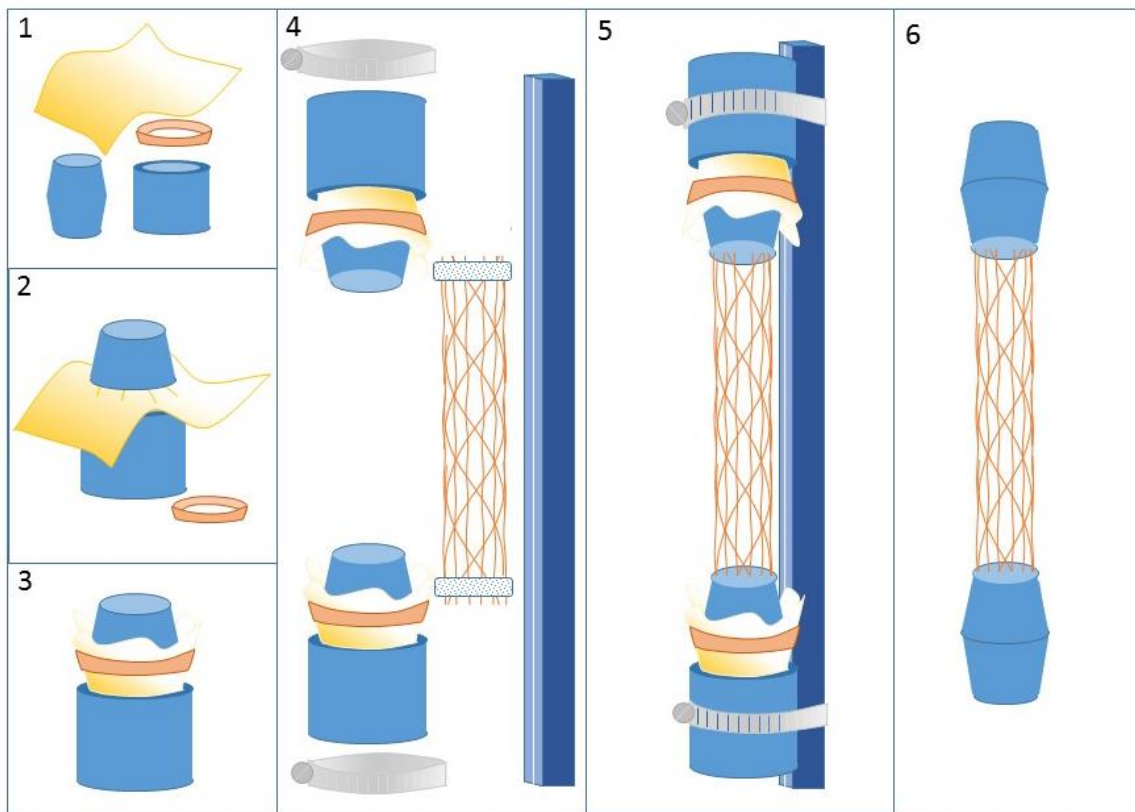
Figure 43 – Demonstration of end-cap potting

68
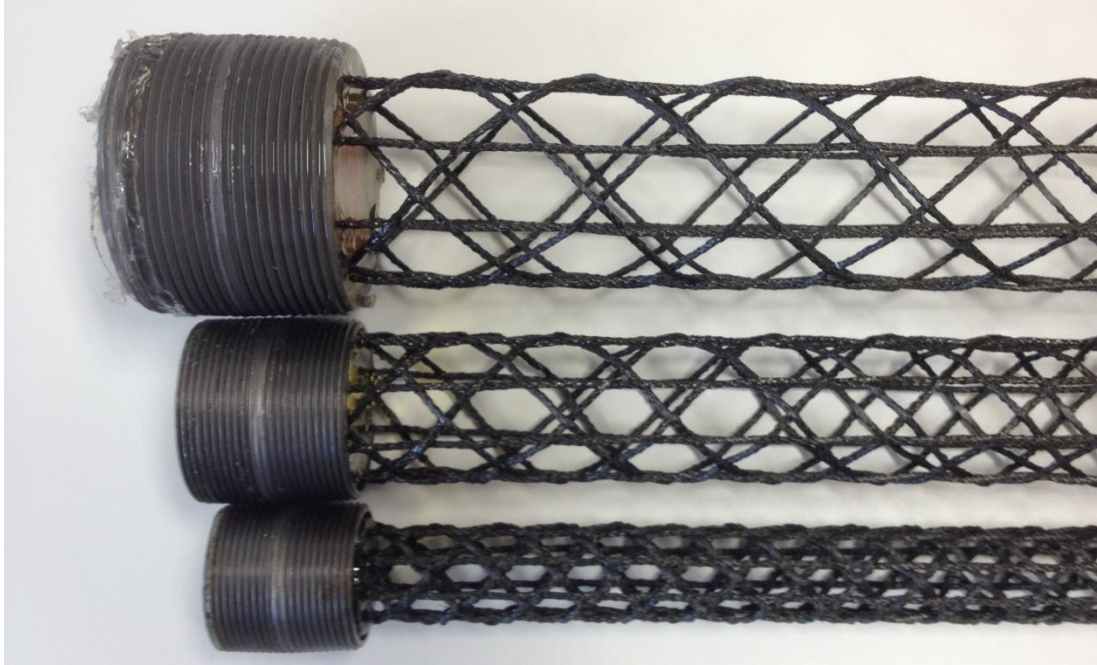
Figure 44 - Example of potted end-caps on various diameters

Conclusion

An experiment was designed to test several major O-ACS design variables in an efficient manner. The testing procedures for the different load scenarios were briefly described. A method for constraining the ends of the open structure tubes was adopted and formalized (Branscomb, Minimal Weight Composites Utilizing Advanced Manufacturing Techniques, 2012). The actual test results are presented in the next chapter. Possible sources of error resulting from these test procedures are described there. The experiment is designed such that a very wide range of samples is tested. This may lead to inaccuracy of results since no test is repeated multiple times to find error bounds on the test. Doing so would not be helpful with the current state of O-ACS manufacture: the braiding process is not yet consistent enough for such statistics to be meaningful when the process is automated. Instead, the assumed polynomial model will give an estimate of the test error, as well as comparison with the finite element model.
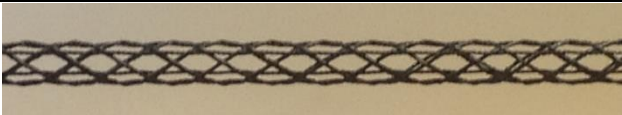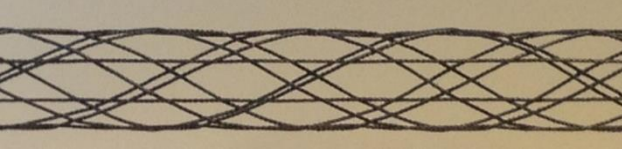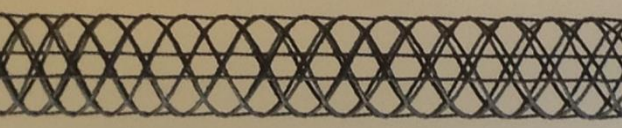
Experiment Results and Model Validation
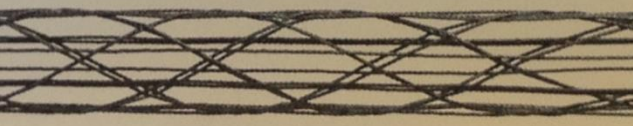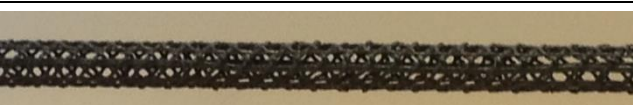
Having described previously an experiment of fifteen specimens, the test results are now presented. The experiment produces an empirical (curve fit) model which can be used for design of structures with properties near the tested values. The mode also helps see the relative strength of effects among the design variables. The same fifteen tests were repeated in the finite element model. Comparisons between the physical and finite-element results demonstrate the relative utility, strengths, and weaknesses of the two forms of design. Graphical methods are presented to help utilize the test data in future O-ACS design.

Physical Experiment Results

The results of the physical testing are recorded in Table 15. The results for a thin carbon tube are also included for comparison.

Table 15 – Physical Experiment test samples and results

Visualization		Sample Stiffness		
		Axial AE (kN)	Bending EI (Nm^2)	Torsion JG (Nm^2)
1		501.7	130.2	53.51
2		511.8	386.2	148.43
3		541.8	90.5	53.06
4		560.5	381.2	270.79

5		1055	279.0	43.15
6		1264	1178.6	126.91
7		1114	328.1	43.19
8		1314	1224.7	306.55
9		957.8	501.2	138.39
10		929.9	170.2	47.30
11		1031	725.5	266.40
12		996.7	422.8	102.20
13		987.5	427.4	145.00
14		617.9	240.4	131.41
15		1219	571.2	151.38

Physical Experiment Polynomial Model Fit

The results of the experiments were used to construct a polynomial model in the form of equation (41). The simple quadratic model can be seen to do a fair job of predicting the axial stiffness within the range tested. Each of the three modes of testing is presented below. The results for each mode of testing are presented graphically. The interpretation of results follows the listed graphs and tables of fit. Note while reading that the values of the coefficients yield insight into the physical relationships. Larger magnitude coefficients demonstrate strong effects of their associated variables in (41).The prediction ability of the simple quadratic model is very good considering the efficiency of the model.

Axial Compression

Table 16 – Physical Test: Axial Empirical Model Coefficients

	β_0	β_1	β_2	β_3	β_{11}	β_{12}	β_{13}	β_{22}	β_{23}	β_{33}
Value	-218.0	110.5	10.25	101.5	-51.29	0.269	16.28	-0.106	-0.009	-0.236
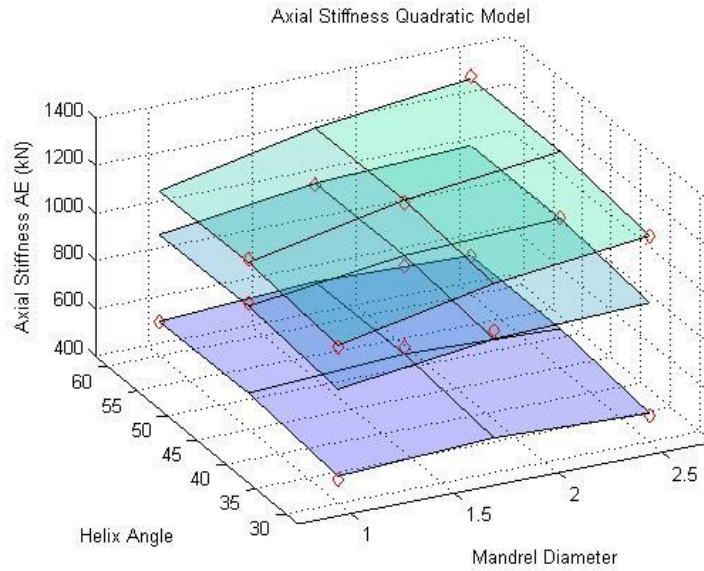
Figure 45 – Physical test: axial model
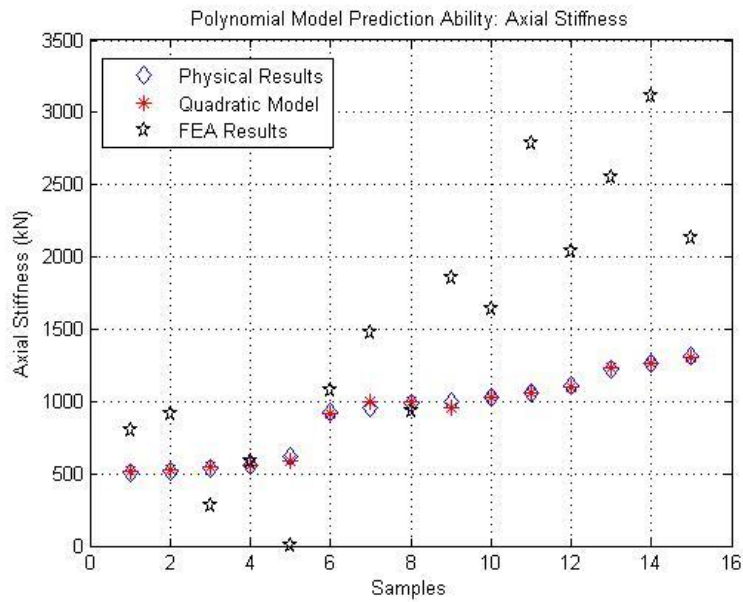
Figure 46 - Physical test: axial model

73

Pure Bending

Table 17 – Physical Test: Bending Empirical Model Coefficients

	β_0	β_1	β_2	β_3	β_{11}	β_{12}	β_{13}	β_{22}	β_{23}	β_{33}
Value	496.1	-382.3	-5.23	-46.3	92.2	0.719	51.51	0.0263	0.223	0.026
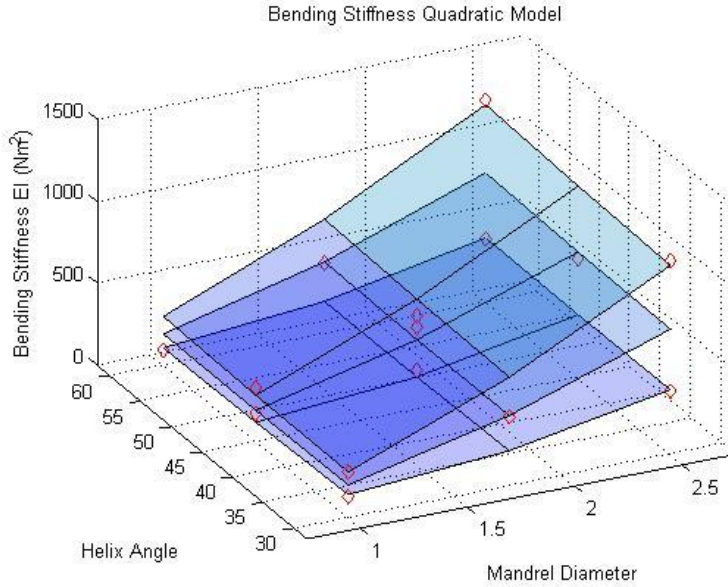
Figure 47 - Physical test: bending model
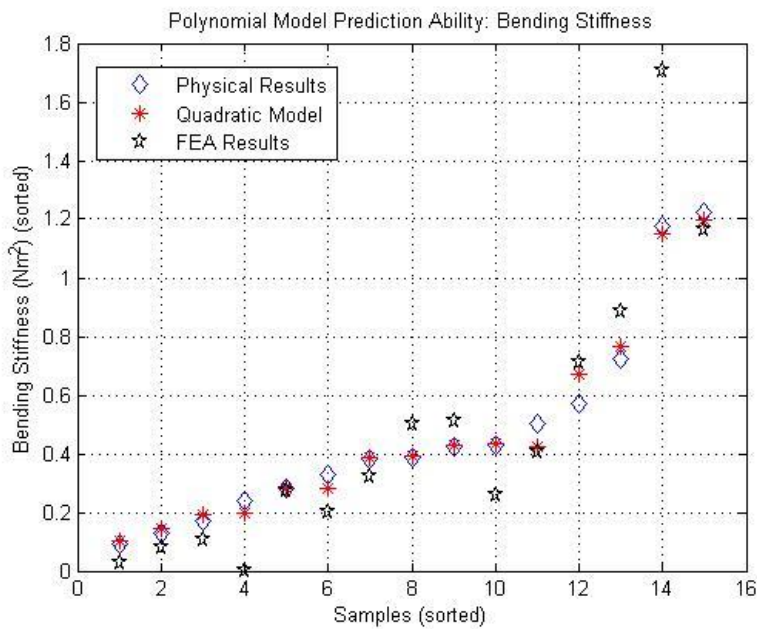
Figure 48 - Physical test: bending model fit

74

Torsion

	β_0	β_1	β_2	β_3	β_{11}	β_{12}	β_{13}	β_{22}	β_{23}	β_{33}
Value	42.64	-117.8	2.994	-5.53	17.994	3.484	2.234	-0.085	0.097	-0.014
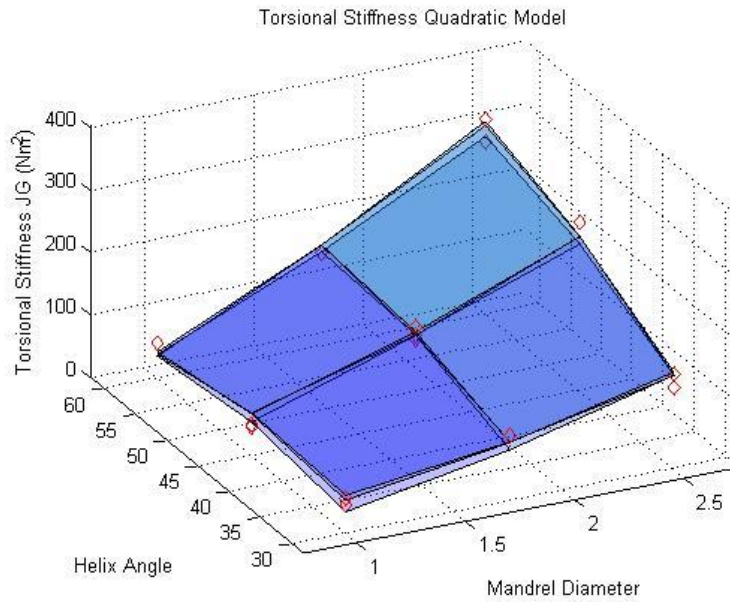
Figure 49 - Physical test: torsion model
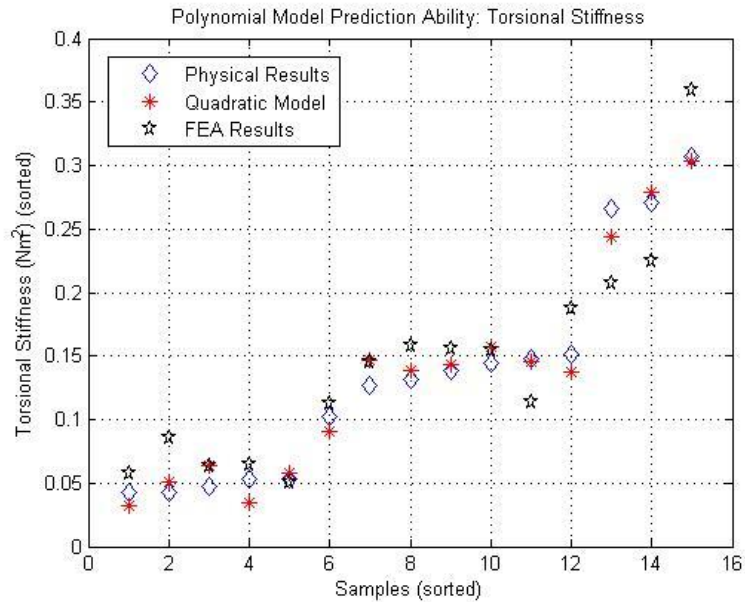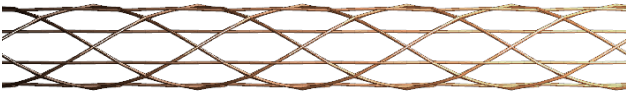
Figure 50 - Physical test: torsion model fit

75
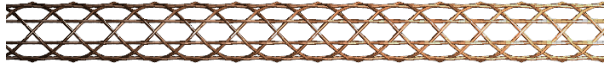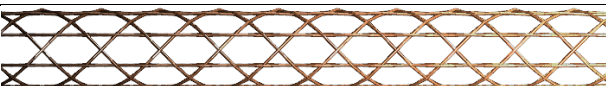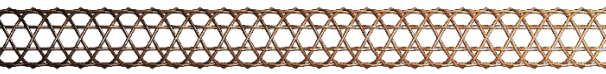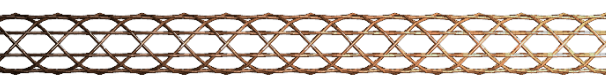
FEA Experiment Results

The Geometry and Finite Element model was used to create a simulation of each of the fifteen test specimens, and simulated them in each of the four loading conditions. The results of the simulation, and images of each structure, are listed in Table 19.

Table 19 – Finite Element experiment test samples and results

	Visualization	Sample Stiffness		
		Axial AE (kN)	Bending EI (Nm^2)	Torsion JG (Nm^2)
1		818.0	81.6	38.5
2		912.5	500.2	164.4
3		276.9	27.9	39.4
4		585.5	320.1	233.5
5		2821.1	280.7	36.9
6		3149.4	1724.4	169.5
7		2019.4	201.2	43.9
8		2128.6	1166.4	323. 4

9		1484.9	410.6	128.9
10		1106.2	110.2	34.4
11		1638.7	889.0	240.1
12		1869.0	512.2	95.8
13		948.8	264.0	124.4
14		719.6	200.6	143.9
15		2596.7	722.6	151.3

FEA Experiment Polynomial Model Fit

The results of the FEA simulations were also used to construct polynomial models in the form of equation (41). The results for each test are presented below. A discussion of their interpretation follows.

Axial Compression

	β_0	β_1	β_2	β_3	β_{11}	β_{12}	β_{13}	β_{22}	β_{23}	β_{33}
Value	-46.55	325.06	1.696	212.7	-177.4	7.381	30.99	-0.182	-3.29	0.459
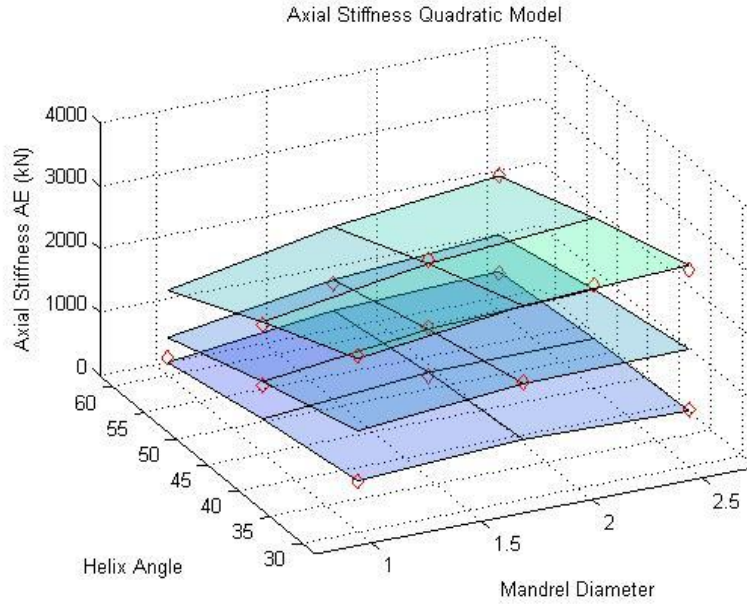
Figure 51 – FEA test: axial model
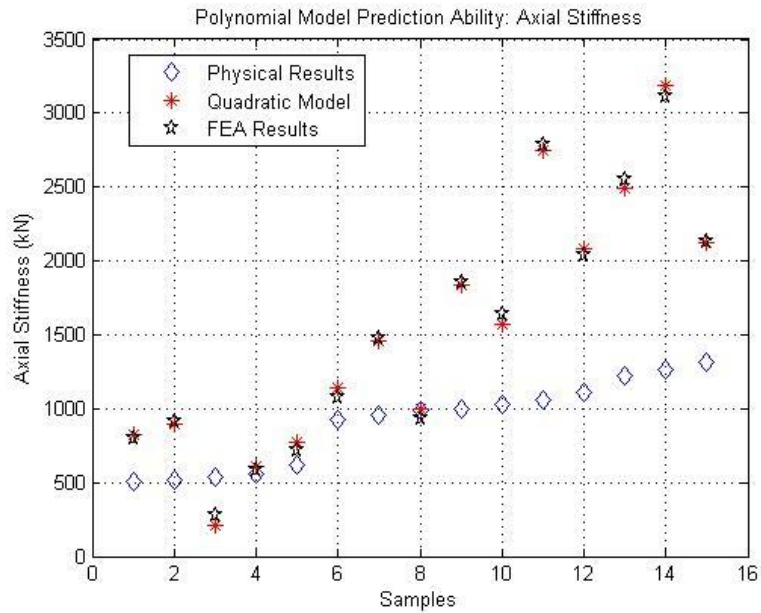
Figure 52 - FEA test: axial model fit

78

Pure Bending

	β_0	β_1	β_2	β_3	β_{11}	β_{12}	β_{13}	β_{22}	β_{23}	β_{33}
Value	-104.3	-437.6	23.67	-35.89	154.3	-4.07	78.24	-0.169	-1.264	0.116
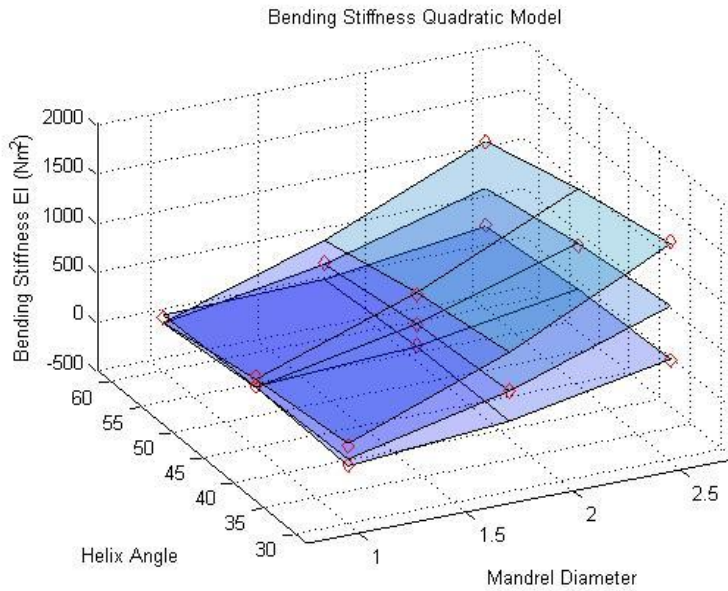
Figure 53 - FEA test: bending model
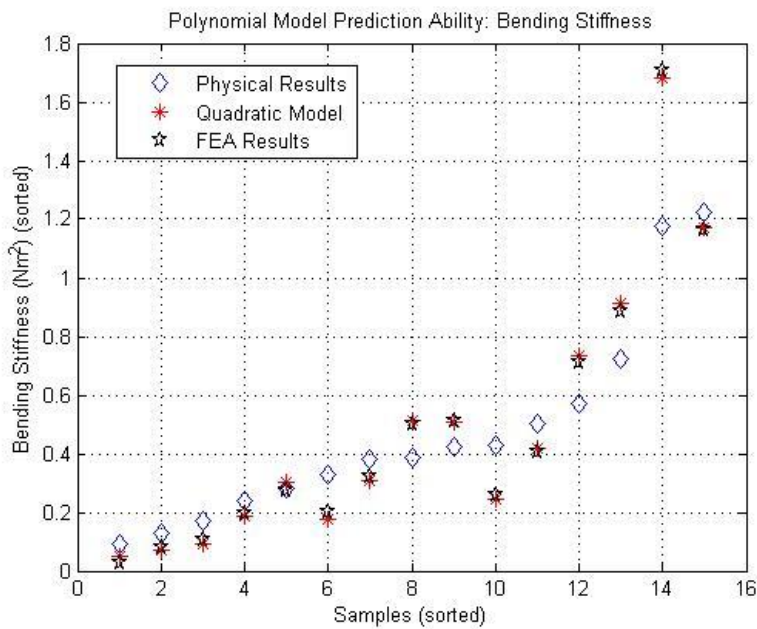
Figure 54 - FEA test: bending model fit

79

Table 22 – FEA Test: Torsion Empirical Model Coefficients

	β_0	β_1	β_2	β_3	β_{11}	β_{12}	β_{13}	β_{22}	β_{23}	β_{33}
Value	52.91	13.64	1.447	-25.67	-26.7	2.96	5.28	-0.067	0.273	0.049
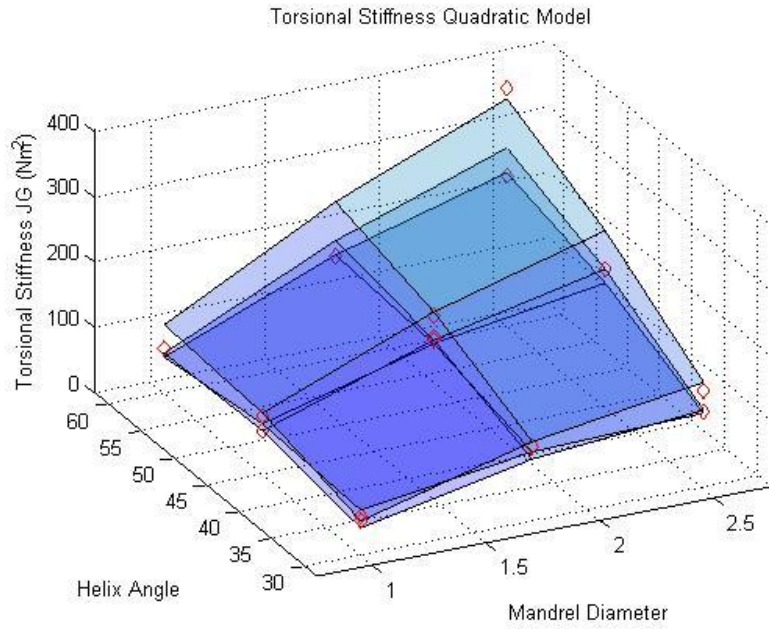
Figure 55 - FEA test: torsional model
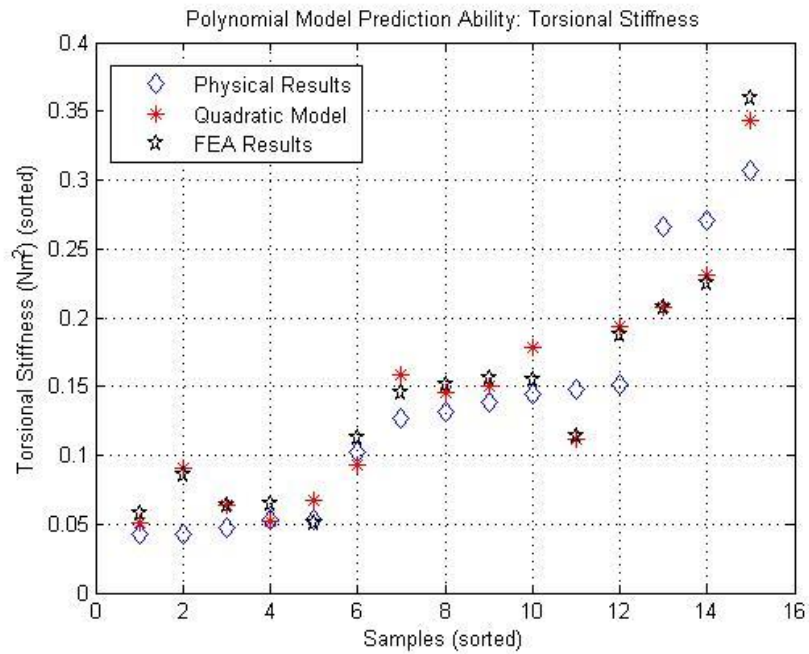
Figure 56 - FEA test: torsion model fit

80

Comparison of Physical and Simulation Results

The chief goal of this validation process is to confirm that the model adequately represents the relationship among structure design variables. The polynomial model allows a way to compare the effects seen in physical testing with those predicted by the model. For reference, Table 16 through Table 18 and Table 20 through Table 22 are consolidated into Table 23, below. To compare the model's fitting ability, the error given is the difference between the FEA and physical coefficient value, divided by the largest coefficient of the table.

Table 23 – Comparison of FEA and Physical Experiment Results

		β_0	β_1	β_2	β_3	β_{11}	β_{12}	β_{13}	β_{22}	β_{23}	β_{33}
Compression	Exp.	-218.0	110.5	10.25	101.5	-51.29	0.269	16.28	-0.106	-0.01	-0.24
	FEA	-46.55	325.06	1.696	212.7	-177.4	7.381	30.99	-0.182	-3.29	0.459
	% max	N/A	66.0	-2.63	34.2	-38.8	2.18	4.52	-0.02	-1.01	0.22
Bending	Exp.	496.1	-382.3	-5.23	-46.3	92.2	0.719	51.51	0.0263	0.223	0.026
	FEA	-104.3	-437.6	23.67	-35.89	154.3	-4.07	78.24	-0.169	-1.26	0.116
	% max	N/A	-11.1	5.83	2.1	12.5	-0.96	5.38	-0.04	-0.3	0.018
Torsion	Exp.	42.64	-117.8	2.994	-5.53	17.994	3.484	2.234	-0.085	0.097	-0.01
	FEA	52.91	13.64	1.447	-25.67	-26.7	2.96	5.28	-0.067	0.273	0.049
	% max	N/A	111.6	-1.31	-17.09	-37.9	-0.44	2.58	0.016	0.149	0.053

Each loading condition (Compression, Bending, and Torsion) is now summarized. The effect of design variables will be explained, as well as the ability of the model to accurately predict the response to design variables. The polynomial model is useful for prediction and extrapolation, but it is hard to directly visualize the independent effect of each design variable: plots are

provided below summarizing these effects as seen in physical data. Some of the qualitative remarks below are the author's opinion of these data as he interprets them.

The **compression** test shows a strong dependence on Diameter and Number of Axials. The Diameter effect is a regressive polynomial, that is; there is a point at which increasing the diameter will no longer increase the structure stiffness. This is due to the increase of free span-length between joint intersections, which are increasingly weak in bending. The shear modulus of the composite yarn is significantly lower than elastic modulus, thus making the yarn 'beams' weak in lateral loading. The Axial yarns, as expected, contribute most to the axial stiffness. The relationship is nearly linear with number of axials present. Alignment of the axials could also affect this: fewer braider yarns or lower braid angles improve alignment at the cost of increasing free span length (decreasing support from the helical yarns). The relative merit of the two effects should be considered in design. The effect of directly varying single parameters is shown in Figure 57. The x-axis is non-dimensional using the values from Table 13. The compression testing method may not be adequate for the range of stiffness seen in the open structures. The potted end compliance may affect the measured stiffness. This would explain the slightly nonlinear response to the number of axials, which one would expect a direct increase in stiffness as more axial yarns are added. The finite element model properly represents the response to design variables, but the magnitudes it gives are too high. This could be due to the poor alignment of the yarns in the test samples, and could be fixed by the use of higher tension carriers when braiding.
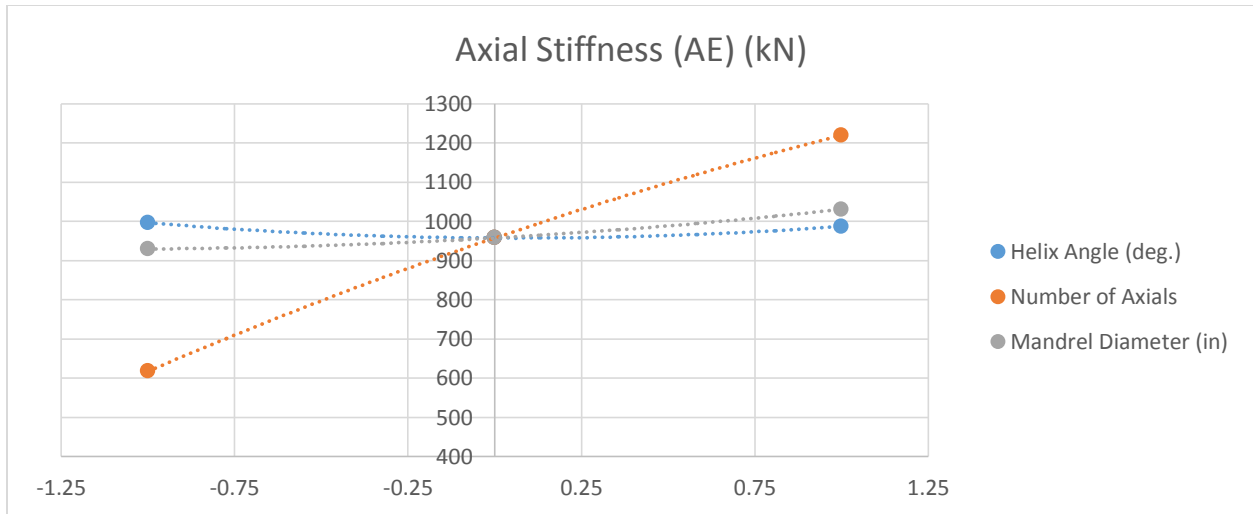
Figure 57 – Axial Stiffness in a narrow band of test variables
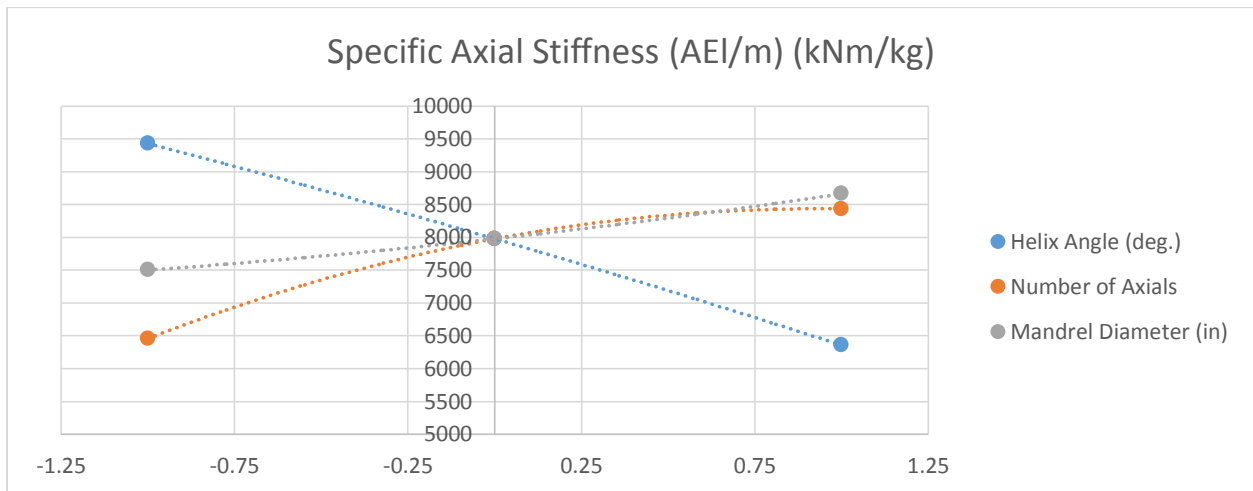
Figure 58– Axial Specific Stiffness in a narrow band of test variables

The **pure bending** test shows much interaction between variables. Number of axials adds to the stiffness significantly, though the axials on the sides of the structure do not add much support: thus the response is regressive with respect to number of axial yarns. The helix angle does not significantly affect the stiffness: while lower angles align more fibers with the bending stresses, it reduces their ability to stabilize the axial yarns (as was seen in the axial test). The diameter directly and exponentially increases the structure stiffness, though the effect of opening the span is again seen here (Figure 59). The Finite Element model again over-predicts the actual stiffness, though it does a very good job of modeling the relationships between variables. Error in the physical test may again have been introduced through the potted end-caps.
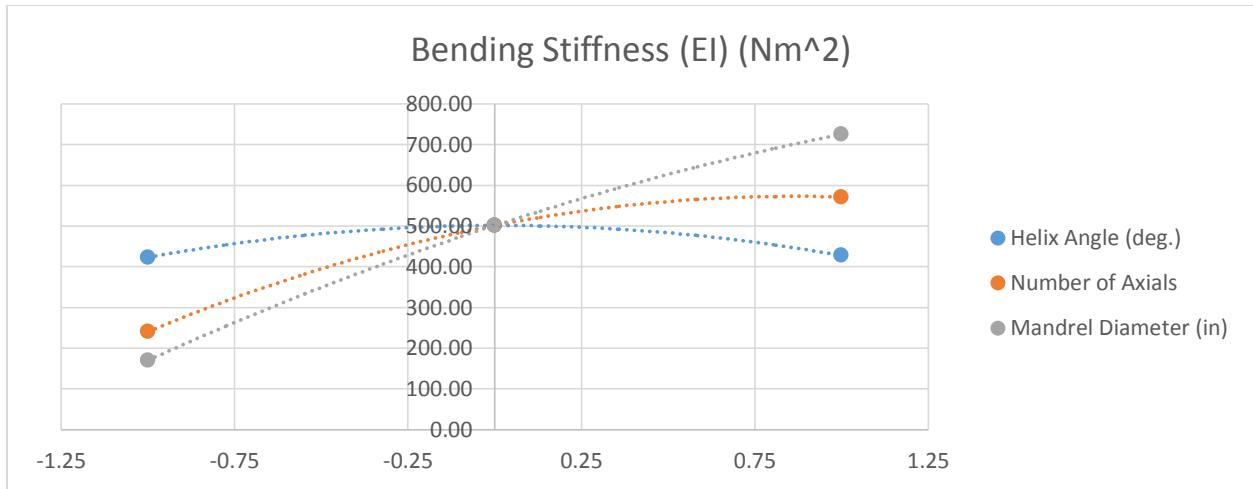
Figure 59 – Bending Stiffness in a narrow band of test variables
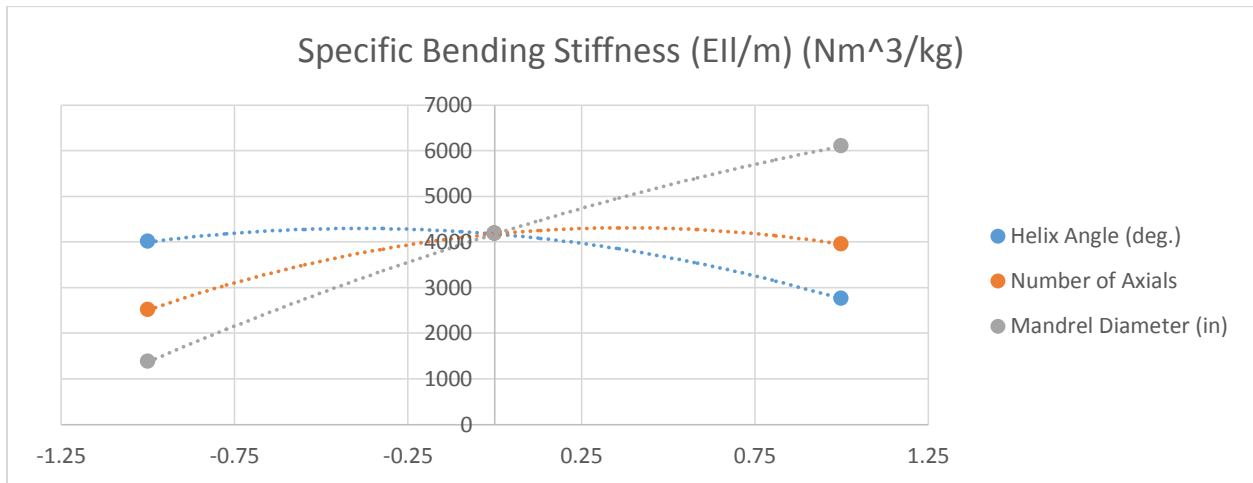
Figure 60 – Bending Specific stffness in a narrow band of test variables

The **torsion test** showed the best fit between physical testing and the finite element model. The torsional stiffness is seen to be nearly linearly dependent on mandrel diameter. Number of axials has little or no effect on the torsional stiffness. The helix angle has an effect that is more pronounced when the tube is of a large diameter. In particular it is seen that helix angles near 56 degrees provide the most support, probably due to stability against axial loading. The test was very stable and repeatable, and requires low loads (relative to the other two tests). This could be a reason for improved correlation between these tests and the FEA model.
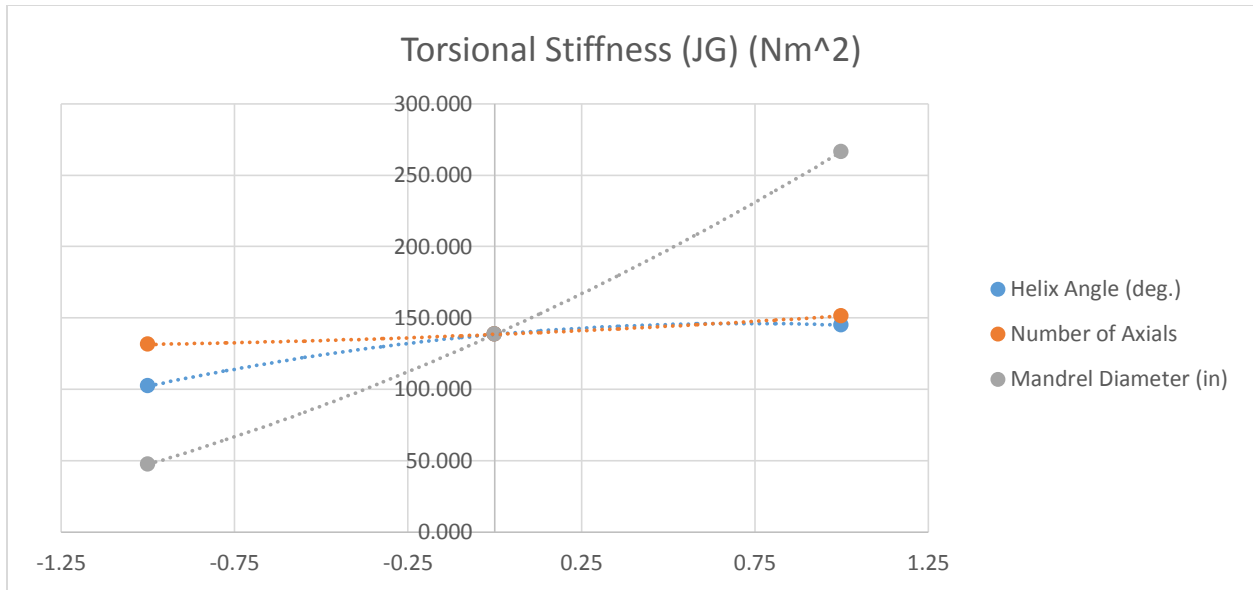
Figure 61 – Torsional Stiffness in a narrow band of test variables
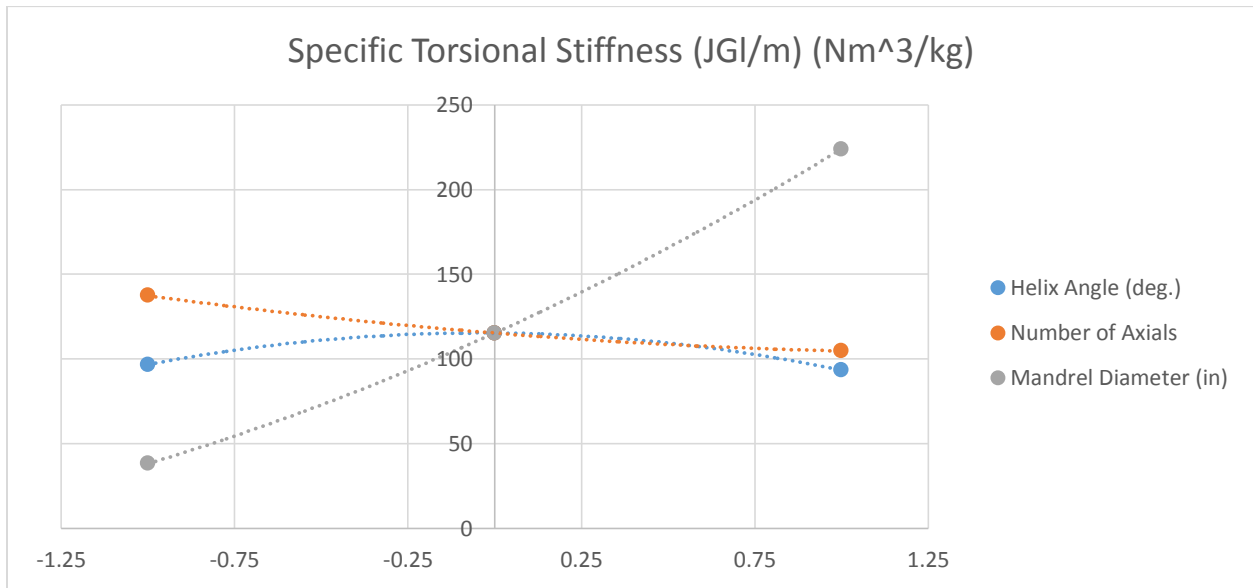
Figure 62 – Torsional Specific Stiffness in a narrow band of test variables

A final method for visualizing the designs is the radar plot, adopted from Broderick (Broderick, 1985). The radar plot allows quick understanding of the effect of each variable on the structure. The plots shown below demonstrate the specific stiffness change due to a change in design variable. The first three (Figure 63) show how a single variable affects all load cases. The next three (Figure 64) show how a load case is affected by all three variables. The plots are non-

85

dimensional, such that they can show the relative effect of each variable in a clear manner. The numeric values can be found in the plots above.
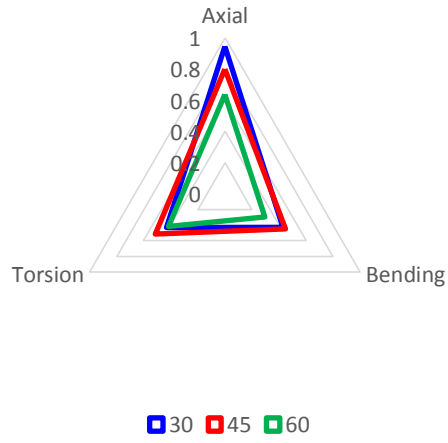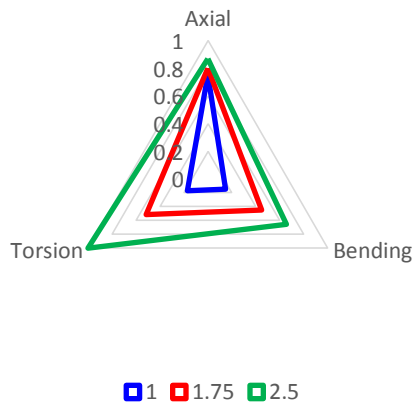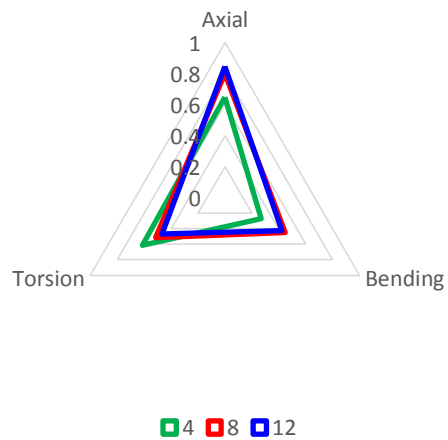
Figure 63 – Effect of design variables on specific stiffness

87

Axial Stiffness: Response to Parameters

-1
1
0.8
0.6
0
.2
0

1
0
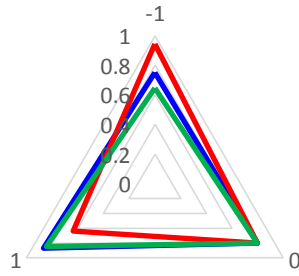
☐ Mandrel Diameter (in)   ☐ Helix Angle (deg.)   ☐ Number of Axials

Bending Stiffness: Response to Parameters

-1
0.8
0.6
0.4
0.2
0

1
0
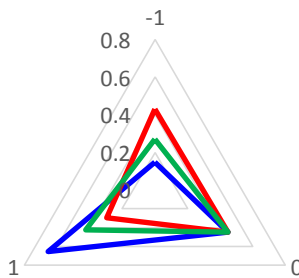
☐ Mandrel Diameter (in)   ☐ Helix Angle (deg.)   ☐ Number of Axials

Torsional Stiffness: Response to Parameters

-1
1
0.8
0.6
0.4
0.2
0

1
0
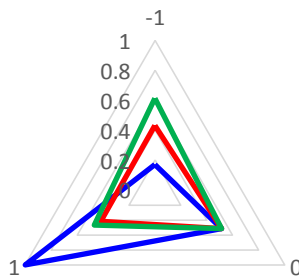
☐ Mandrel Diameter (in)   ☐ Helix Angle (deg.)   ☐ Number of Axials

Figure 64 – response of specific stiffness to design variables

88

Sources of Error

As was done for the geometry and finite element models previously, possible sources of error in the physical tests are noted here. The sources of error can be roughly divided into those induced by the prototype fabrication, and those produced by the testing procedures.

First, the manufacture of O-ACS tubes is far from mature. The machinery used is designed to braid fine fibers and tows, with far less friction and tension than the carbon yarns provide. To overcome the tension, it often requires manual intervention at the braid point to ensure yarns do not kink and bind. This intervention is irregular and causes some errors in the tubes. It produces axial misalignment from the tube axis and arching in the helical yarns, both of which weaken the tube geometry. Also, the O-ACS joints are very weak compared to the yarns. It is difficult to determine whether the joints are intact and contributing to structure stiffness: some could be broken during curing or transport without operator knowledge. Finally, the abrasion during braid formation damages the carbon yarns somewhat. The extent of this damage is not uniform and varies from structure to structure.

These sources of error in the test samples could be eliminated by the use of a different braiding machine. For example, a machine designed to braid wire would have the tension and carrier motion capable of constructing uniform structures with no human intervention. This would improve axial alignment, helical tensioning, and helix angle verification. If such a machine was used, yarns could be made with a more protective jacket to prevent abrasive harm. The yarn jacket could also, perhaps, be designed of a material which is impervious to the abrasion. Experiments have shown that fiber-glass yarn-jacket axial fibers may fulfill this purpose. The final prototype error needing solution is the joint strength. Joint strength is dominated by the resin used. A resin which has designed structural properties would assist tremendously here. The current resin is a laminating resin, which is good for maintaining fiber alignment but not suited for joint bonding. Again, experiments with a structural adhesive have shown that a different resin choice is a valid solution here, if it is cost-effective.

Secondly, the test procedures are not fully developed. The purpose of this work is to provide a platform for optimization, and effort is being made by others in the Auburn Advanced Braiding lab to develop suitable test procedures. A preliminary review of the ASTM testing standards shows a lack of methods for thin-walled tubes, and for composite tubular structures in general.

The author believes that his testing method for compression is washing out O-ACS results due to compliance in the resin potting used. This method was adopted from a time when the development of open-structures was comparative and not predictive; it is now time a more rigorous testing system be designed as models are made needing confirmation. A possible solution is to pot the structures in machined aluminum or steel blocks of precise dimension: reducing the amount of resin which contributes to overall compliance. The main justification for these claims regarding potting is the fine results of the torsion test: because the torsional stiffness of the O-ACS is low compared to the resin potting, the potting had a very minimal effect on the test results. Another source of test error is end-cap alignment. While effort was made to keep the end caps aligned, the threaded caps are not perfectly re-aligned between structure potting and subsequent testing. A final computation of the error in the model is presented in

Table 24 - Error between physical testing and finite element

	Mean Error	**Standard Deviation**	**Plotted in:**
Compression	60.2%	57%	Figure 46
Bending	-8.4%	32.6%	Figure 48
Torsion	-5.7%	16.6%	Figure 50

Conclusion

An experiment was designed which covered a wide range of O-ACS geometries. Fifteen open-structure prototypes were fabricated, and a design-of-experiment method was used to fit a polynomial model between samples. The results of the physical testing yielded insight into the relationship of design variables on the structure stiffness and specific stiffness. The most important revelation from the testing is that diameter is a very effective design decision: increasing the diameter of O-ACS tubes does not effectively increase their weight, but significantly affects their bending and torsional stiffness. This advantage should be used when finding applications of the tubes for commercial purposes. Another revelation is that the helical yarns often do very little for the structure besides stabilizing axial yarns. To this end, it is expected that they could be made much smaller than the axials to increase the specific stiffness in both axial compression and bending.

The same fifteen O-ACS configurations were tested in *fell_point*. The model fits the bending and torsional data well (Figure 53 and Figure 55), but consistently over-estimates the axial stiffness (Figure 52). The possible reasons for mismatch have been explored in the Finite Element chapter. The model sufficiently simulates the effect of major structure design variables - helix angle, mandrel diameter, number of axials, and yarn diameter – and is a valid basis for extrapolating open-structure design and designing optimal braided lattice structures.

Optimization Model

Having developed tools that automate the analysis of lattice composites, focus can now be given to tools which design them. Structural optimization – the programmatic design of shapes and topologies based on cost function minimization - is a mature field which has developed to suit many diverse engineering disciplines. Starting with the seminal paper by Michell a century ago (Michell, 1904), based on principles applied by Maxwell (Maxwell, 1864), structural optimization has found application in the design of frame structures. The concept of frame structures as more efficient topologies than smooth or continuous media can be derived quite heuristically by observations of nature, or rigorously by application of General Relativity (Vasiliev & Gurdal, 1999). The present objective is to apply established optimization techniques within the special constraints imposed by the braiding process.

Establishment of the Optimization Technique

Developments in optimization of structures have been summarized by several authors, many of whom write work specific to one application or topic (Bendsoe & Sigmund, 2003). Much of the literature on engineering optimization is not specific to structural design, though the principles of general optimization often find their way into structural applications (Vanderplaats, 1984) (Arora, 1989). The particular topics covered specifically by 'structural optimization' can roughly be broken into size, shape, topology, and truss optimization. Size optimization is the selection among similar designs, within a narrow range, to best achieve the objective. An example would be the design of a structural tube diameter and wall thickness, without considering whether the tube is in the ideal location to maximize its contribution to the objective. Shape optimization seeks to modify the *boundaries* of a structure to yield a more efficient whole. Determining the ideal arrangement of crenulation within a plate would fit in this field. Topology optimization is the penalization of *internal* structural mass, which does not contribute to design objectives. These techniques are usually the most general as they allow algorithms the most design freedom in establishing efficient structures. Because of the freedom inherent in the technique, careful constraint must be placed to ensure designs can be manufactured after design. Finally, truss optimization – closely related to size optimization – finds the ideal connection of a

frame network between nodes which are set in space. One of the accepted modern references on topological and shape optimization is the work of Bendsoe and Sigmund (Bendsoe & Sigmund, 2003). All of the methods described above are summarized neatly in that work.

The unique aspect of this research is the design of optimal geometries within the constraint of the braiding process. The possible geometries of the O-ACS must conform to the abilities of Maypole braiding. It is within this scope that an optimum is sought. A major concern in the choice of procedures is that the design-space be smooth within these limits. It was found during the Finite Element development previously that open-structure efficiencies will always be improved by the increase of mandrel diameter; thus the design diameter should be as large as the application allows. The ideal helix angle can be solved by simple Newton iteration, and again does not require the application of any special techniques. The remaining concerns primarily consider the location and loading of the yarns. In this work, the optimal structure is the 'most efficient' in a stiffness sense; that is, it is the structure within the design space which provides the highest stiffness for its weight. Where is this design to be found? The most rigid structure will, generally, be the one with the most material; meaning the maximum stiffness will always be the braid with all carriers loaded with their largest possible yarn. This structure will not be, however, the most efficient design possible, as it probably contains some portions which contribute significantly to the stiffness, and some portions which are barely loaded at all. Thus we seek to find the sub-space within the set of 'fully loaded machine' that contains only portions which contribute to the stiffness against a given load. The goal of the optimization algorithm to choose which yarns contribute best to the structure stiffness, and which yarns are oversized (or completely unnecessary) based on their individual contribution to structural rigidity. The implementation of these concepts in the mathematical statement of the optimization procedure is described below.

Optimization Statement and Constraint Discussion

It was seen in the previous section that the heart of the optimization lies in selection of yarn diameters (or removal of yarns as diameter goes to zero). The optimization procedure for O-ACS design is now formalized. Formalization requires the mathematical description of an objective function, design variables, and constraints. The objective is a mathematical description of the goal or mission of the simulation. Design variables are the engineering quantities which can be

93

modified and which affect the achievement of the objective. Constraints are limits imposed on the design variables which ensure the resulting design does not reach forbidden spaces (practical or physical limits and requirements). These design components are outlined in *Figure 65*, and described in detail below. The method for solving the optimization problem should be conducive to the form of the problem (finite element) and to the types of constraints imposed on the system. The Optimality Criteria method will be used for its speed with the number of degrees of freedom present in the simulation, and its suitability for topological optimization (Haftka, Gurdel, & Kamat, 1990) (Sigmund, 2001).
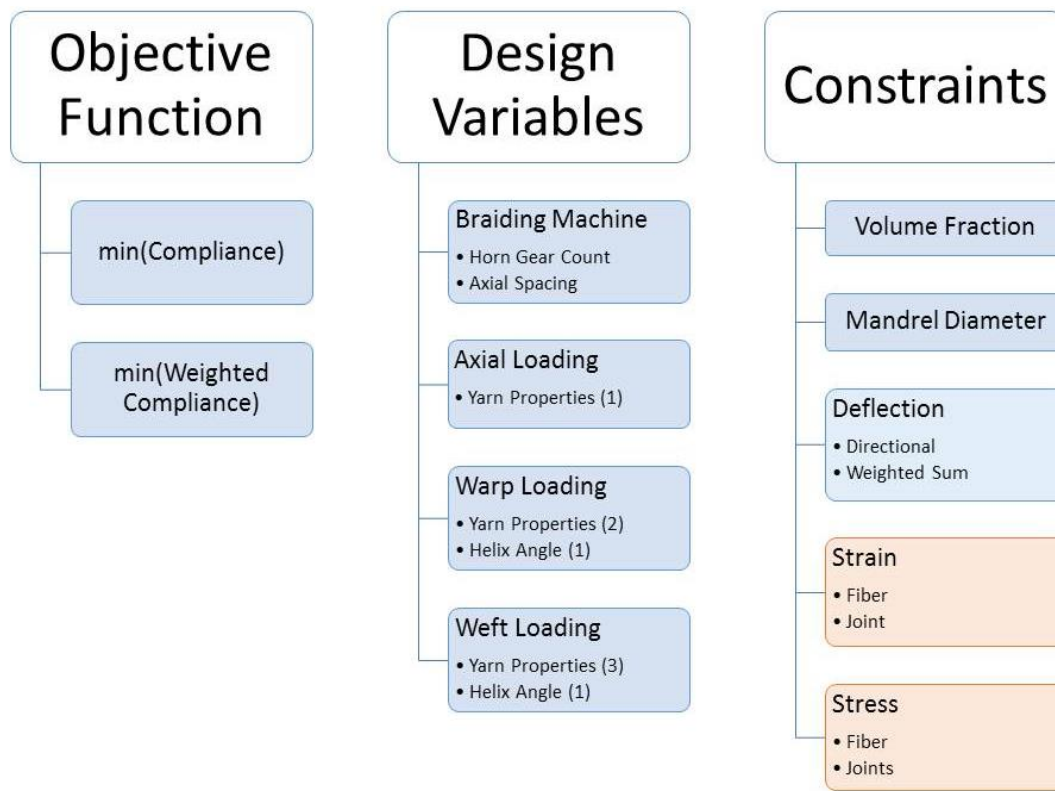
Figure 65 – Optimization Statement Outline

The design variables and constraints are most easily considered. The present problem has two forms of constraints active. First, there are constraints *inherent* to the simulation, a feature of the mathematical model used. It has already been stated that a structure can be completely specified once the machine, helix angle, and all yarn diameters (including 0 diameter) have been declared. One additional constraint is, of course, that the deflection comes from the finite element solution.

$$U = K \backslash F \qquad\qquad 0 \leq \phi \leq \phi_{max}$$

94

Second are the constraints that serve as *boundaries* on the design. These constraints are the desired design results. First, it is clear that one essential goal in this work could always be to minimize the weight of the structure, subject to displacement and stress constraints. However, a more practical formulation at present in creating efficient structures is to make the weight itself the constraint, and let the objective be to minimize the compliance (external energy). Using this approach, the structure will be 'the most rigid for its given weight', rather than 'the lightest weight for a given deflection'. This concept is now clarified and formalized.

The objective of 'specific stiffness' has been mentioned throughout this work, but not yet clarified as a proper mission for O-ACS design. The applications for O-ACS, originally designed as 'minimal weight', are closely tied to creating structures which, for their weight, are the most rigid possible. This concept in an 'external' sense is easy to see; given a structure of a certain length, subject to a known load vector, determine the structure which *for its weight* will deflect the least. The deflection and the applied force define the external work done on the structure. The structure will gain energy exactly proportional to this load and deflection. The most efficient structure can be considered the one which will provide the least deflection under that load (i.e. it will have the least external energy or 'compliance'). Yarns within the structure will be strained due to the external work, and thus in any structural element, the work is known. Because the yarns are not (necessarily) aligned with the external load, the amount of work done on the structure is affected more by some yarns than by others due to the loads they carry and their individual deformation due to that load. Thus the objective is to minimize the compliance of the structure. The mathematical statement of this objective is

$$minimize[c(x) \equiv U^T K U]$$

(45)

for the entire structure (Bendsoe & Sigmund, 2003) (Sigmund, 2001). This statement must be interpreted in a way that makes sense for the analysis at hand. In the 'power-law' approach to topological optimization (Bendsoe & Sigmund, 2003), this statement is solved by computing the element-wise contribution to compliance, and penalizing element density $0 \leq x_e \leq 1$ with a power p. Note that this is not quite the same as (45), but is an objective which will try to force the removal of elements with intermediate density:

$$c(x) \equiv U^T K U = \sum_{e=1}^{n} (x_e)^p u_e^T k_e u_e$$

<div align="right">(46)</div>

Using this equation, each element is evaluated for its contribution to the compliance, and updated on each iteration (the update technique is described in the next paragraph). However, elements in the current analysis should not be allowed freedom to change independently; yarns should have a constant diameter ϕ along their entire length l. The objective is reformulated and grouped to find the yarn-wise compliances:

$$c(x) \equiv U^T K U = \sum_{i=1}^{N} \sum_{e=1}^{n} u_{e,i}^T k_{e,i} u_{e,i}$$

$$k_{e,i} = f(\phi_i, \phi_i^2, \phi_i^4, l_e)$$

<div align="right">(47)</div>

Thus, on every iteration, each yarn's compliance will be computed, and the diameter updated. It is clear that this is nearly equivalent to (46), since a change in diameter will affect the stiffness of the element as well. In other words, the penalization was added as a somewhat heuristic way to force a solution where $x \in \{0,1\}$, and in our current problem intermediate values of yarn diameter $x \in \{0 \leq x \leq 1\}$ are acceptable.

Review of the Optimality Criteria Method

The objective is now clear, but it is yet undecided how each yarn's *relative* contribution to compliance should be determined. More specifically, we must know how a change in the yarn diameter will affect the stiffness: then the yarns which have the largest effect are retained, and those with the smallest effect are removed. The sensitivity will be found using the Optimality Criteria (OC) method (Haftka, Gurdel, & Kamat, 1990). This method uses Kuhn-Tucker optimality formulation, and is accepted as an established topological optimization technique (Rozvany, 2009). The OC method can be summarized, for a single constraint, as follows (Haftka, Gurdel, & Kamat, 1990): Given a set of design variables and their reciprocal

$$x_i = \frac{1}{y_i} \qquad i = 1, \dots, n$$

Formulate the objective and constraints in terms of the reciprocal variable

$$\text{Minimize } f(y)$$

$$\text{Subject to } g_j(y) \geq 0$$

The Kuhn-Tucker optimality criterion (assuming the constraint g is critical and the objective is nearly linear with respect to x_i) is

$$\frac{\partial f}{\partial x_i} - \lambda \frac{\partial g}{\partial x_i} = 0 \qquad i = 1, \dots, n$$

<div align="right">(48)</div>

Which can be solved for the Lagrange multiplier

$$\lambda = \frac{\dfrac{\partial f}{\partial x_i}}{\dfrac{\partial g}{\partial x_i}} \equiv \frac{effect\ on\ constraint}{cost\ of\ change}$$

The design variables should now be resized to move closer to the objective. This can be achieved by increasing the effective variables, and decreasing the ineffective ones. A common method for the update is (Bendsoe & Sigmund, 2003) (Haftka, Gurdel, & Kamat, 1990)

$$x_i^{new} = x_i^{old}(\lambda e_i)^{1/\eta}$$

<div align="right">(49)</div>

Where

$$e_i = \frac{\dfrac{\partial g}{\partial x_i}}{\dfrac{\partial f}{\partial x_i}} \equiv effectiveness\ of\ the\ design\ variable$$

And η is a numeric damping coefficient. If the constraint is active,

$$g_0 + \sum_{i=1}^{n} \frac{\partial g}{\partial y_i}\left(\frac{1}{x_i}\right) = 0$$

And the multiplier in (49) can be determined:

$$\lambda = \left[\frac{1}{g_0}\sum_{i=1}^{n} x_i \frac{\partial g}{\partial x_i} e_i^{-\frac{1}{\eta}}\right]^{\eta}$$

$$g_0 = g + \sum_{i=1}^{n} x_i \frac{\partial g_i}{\partial x_i}$$

Of course, because the equations above assumed the objective was linear in design variables, the actual change in x_i is practically limited to a small value. This completes the general description of the optimality criteria method.

Implementation of the Optimality Criteria Method

For the problem at hand, each of the components above will be interpreted in light of (47). It would be desirable for the effect of yarn diameter (design variable) on the compliance (objective) to be simply

$$\frac{\partial c_i}{\partial \phi_i} = -u_i^T k_i u_i \quad \text{[a false equality]}$$

<div align="right">(50)</div>

Unfortunately k_i is certainly not linear in ϕ_i, as required by (48). The axial stiffness of the yarn is proportional to ϕ^2, while bending and torsional stiffness are proportional to ϕ^4 , and only the small shear term proportional to ϕ. In order to better follow the OC method, it is proposed that the design variable be transformed: instead of using the diameter, use the square of diameter

$$\rho = \phi^2 \equiv new\ design\ variable$$

If it is assumed that the axial stiffness of the yarn is significant compared to its bending and torsional stiffness, then the compliance is nearly linear in ρ, and the sensitivity therefore is nearly constant. The effect of yarn diameter squared (design variable) on the compliance (objective) is then (more accurately)

$$\frac{\partial c_i}{\partial \rho_i} = -u_i^T k_i u_i$$

<div align="right">(51)</div>

The change in volume (cost) of a change in yarn diameter (design variable) is

$$\frac{\partial V}{\partial \rho_i} = \frac{\pi l}{4}$$

<div align="right">(52)</div>

If the objective was truly linear in ρ, we could solve for the new design variables in a single step

$$\rho_i^{new} = \rho_i B_i^{\eta}$$

$$B_i = -\frac{\dfrac{\partial c}{\partial \rho_i}}{\lambda \dfrac{\partial V}{\partial \rho_i}}$$

(53)

However, to maintain careful treatment of the remaining nonlinearity in (51), the total change in diameter is limited to a step change in diameter (usually <5% of the initial diameter). Let m be this move limit, and $\eta = 1/2$ the numeric damping coefficient. The update scheme is summarized:

$$\rho_i^{new} = \begin{cases} \max(\rho_{min}, \rho_i - m) & if\ \rho_i B_i^{\eta} \leq \max(\rho_{min}, \rho_i - m) \\ \rho_i B_i^{\eta} & if\ \max(\rho_{min}, \rho_i - m) < \rho_i B_i^{\eta} < \min(1, \rho_i + m) \\ \min(1, \rho_i + m) & if\ \rho_i B_i^{\eta} \geq \min(1, \rho_i + m) \end{cases}$$

(54)

Retrieving Structural Quantities from the FE Solution

The optimization method requires computation of the internal energy (compliance) of each element in the structure. Computation of the structure compliance obviously requires the extraction of load and/or strain data from each element after the finite element solution has been computed. By storing the element stiffness matrices during construction of the global stiffness matrix, the element loads can be retrieved from the deformation solution

$$structure\ deformation: F = KX \rightarrow X = K\backslash F$$

By the computations of each element's deflection

$$element\ load: f_{el} = k_{el} T_{el} X_{el}$$

(55)

$$element\ strain: u_{el} = k_{el} \backslash f_{el}$$

(56)

$$element\ compliance: c_{el} = u_{el}k_{el}u_{el}^T$$

<div align="right">(57)</div>

If only certain dimensions of the compliance are to be considered (for instance, if only axial load is of concern) then the weighted compliance can be computed

$$c_{el} = (u_{el}w^T)^T k_{el}(u_{el}w^T)$$

<div align="right">(58)</div>

Where w is a one-by-six weighting vector, with at least one non-zero element. Using only the axial component ($w = [1\ 0\ 0\ 0\ 0\ 0]$) would result in the sensitivity function (51) being very close to linear, which helps the convergence to a global minimum and increases the solution speed.

Addition of Practical Braiding Constraints

It was specified earlier that the design variables are individual yarns, instead of single elements, because practically yarns must have constant diameter along their length. Another constraint, not accessible to the model, is in the braiding process itself; because braider yarns are in tension during the braiding process, a uniform structure will not be created unless the clockwise and counter-clockwise tensions are nearly equivalent. An easy remedy for this is to always match a warp and weft carrier, such that they carry the tension in opposite directions and balance the tension. To consider this effect, the optimization solver in *fell_point* can be commanded to group pairs of yarns such that their diameters remain the same. By considering the average sensitivity (51) of the two yarns, they are forced to update equally (53).

A similar concern arises when certain boundary conditions are used in analysis. For instance, a cantilever load-case can be used for simulation in place of three-point bending, and the boundaries are identical. However, the simulation will not be able to account for the symmetry in three-point bending which is lost in the cantilever. Thus, in addition to balancing the tensions (matching warp to weft and vice versa) the program allows an option to match yarn rotated by 180 degrees (match warp to opposite side warp, and weft to opposite side weft). An example of the difference between a balanced and matched result compared to an unlimited result are shown in Figure 66 for a short, cantilever beam under asymmetric loading. While the structure on the

left may be the actual optimal solution, clearly the one on the right is more practical in manufacturing and application.
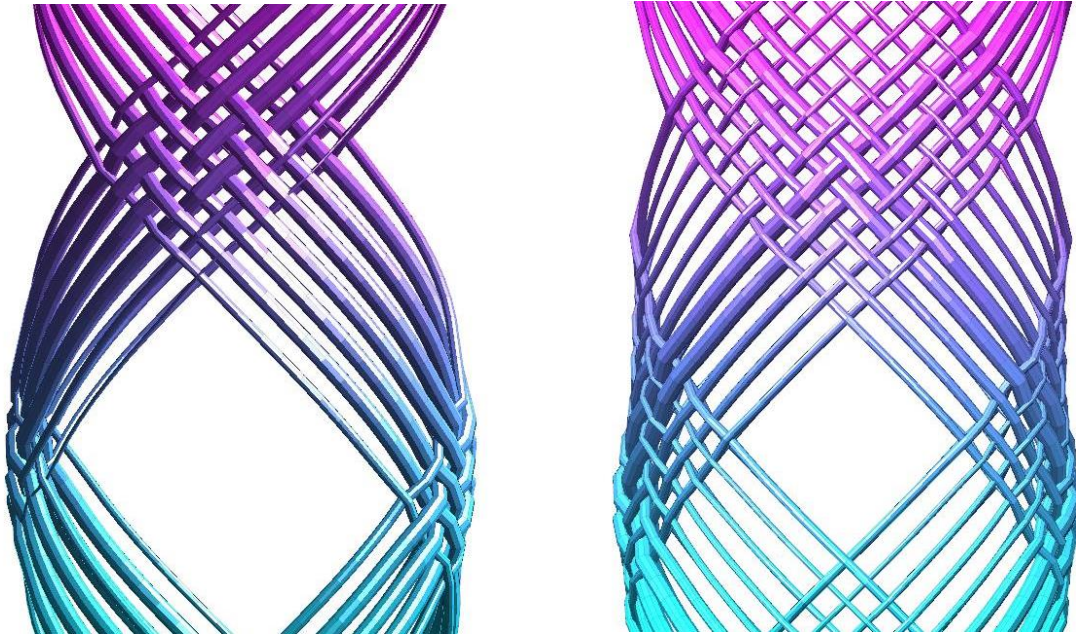
Figure 66 - Left: No braidability constraints, Right: balanced and matched

Optimal Strut Design - Uniaxial Compression

A primary application of O-ACS may be in the creation of struts for space-craft or supports in a larger space-frame. It would be expected that the ideal strut would consist of mostly axial reinforcement. In fact, without consideration of stability limits (buckling) the ideal strut is simply a ring of equally sized axial yarns; this is expected since simple axial yarns can achieve perfect structural efficiency (Michell, 1904). The axial compression load-case serves as a good test of the optimization algorithm. The solution can also be limited to a volume fraction which requires the retention of *some* braider yarns and will demonstrate those which, if present, proved the most support to the structure. The baseline configuration for the optimization is given in Table 25. Remember that the baseline is from a fully loaded machine, and begins as the tube shown in Figure 67.

Table 25 – Baseline open-structure for optimization

	Value
Machine Definition	32 Carrier Maypole
Helix Angle (deg.)	45
Structure Height (mm)	279.3
Mandrel Diameter (mm)	44.45
Yarn Maximum Diameter (mm)	2.0
Target Volume Fraction	25%
Material Properties	{Retained from Table 12}
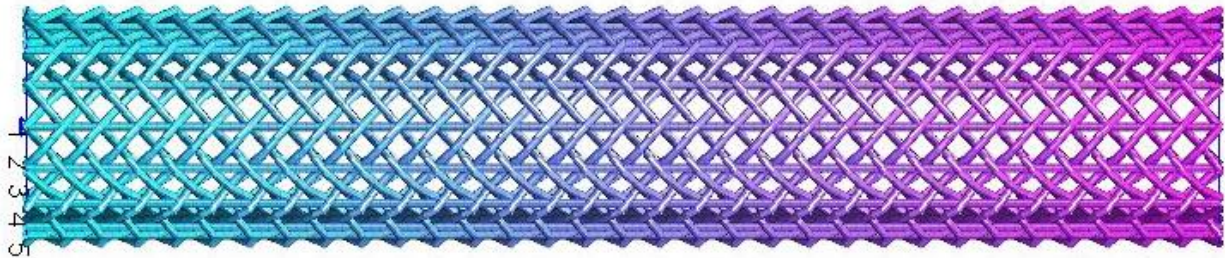
Figure 67 - Start of optimization: O-ACS tube from fully loaded machine

The final result is near the expected result of only axial reinforcement (Figure 68) as expected from the most basic structural optimization concepts (Michell, 1904). In fact, a reduction of the target volume to 23% would eliminate helical yarns entirely, and only 16 evenly sized axial yarns would remain. The results with the fine helical yarns are shown to illustrate the (more practical) intermediate solution. The axial yarns are all of equal size. A fine mesh of helical yarns helps contain them. By making the helical yarns as small as possible, not only is their weight decreased, but the axial yarns maintain straighter paths (less undulation) along the structure.
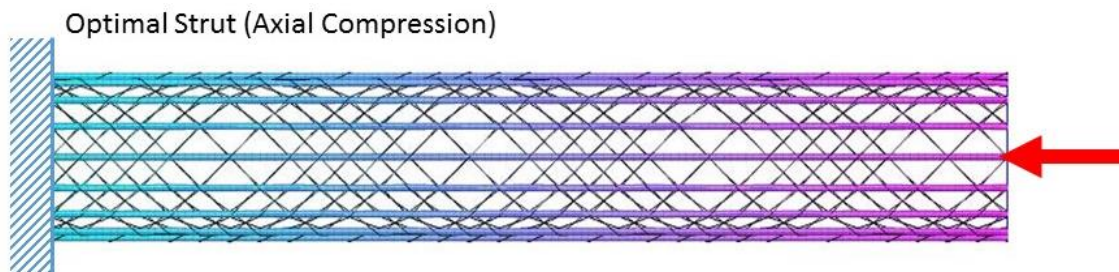
Figure 68 - Optimal Strut (Compression Load)

Optimal Driveshaft Design – Torsion

The ideal torsional shaft (Figure 69) is also mostly intuitive: helical yarns carry the load along their axis more efficiently than an interlaced structure. Again, all the final yarns are of equal diameter. The final helix angle of 44 degrees is easily explained by the Michell theory, which would say the yarns carry the torsion most efficiently along their axis. The effect of helix angle (alone) on specific stiffness for this tube with no axials is shown in Figure 70.
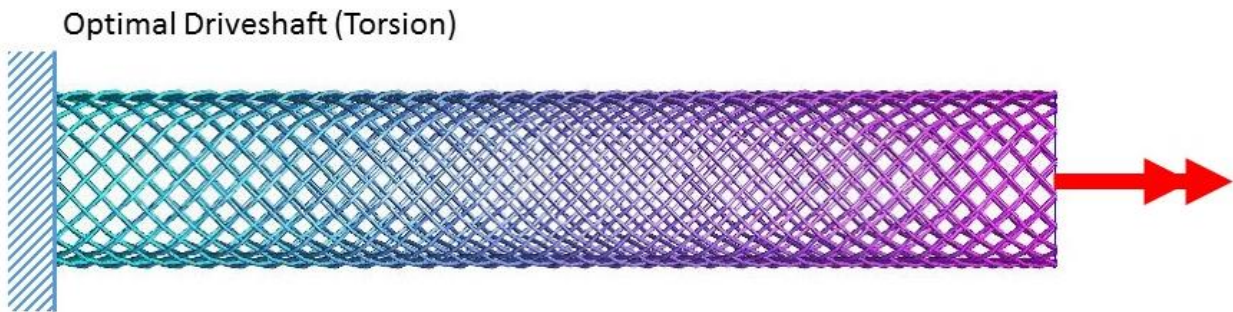
Figure 69 - Optimal Driveshaft (torsional load)
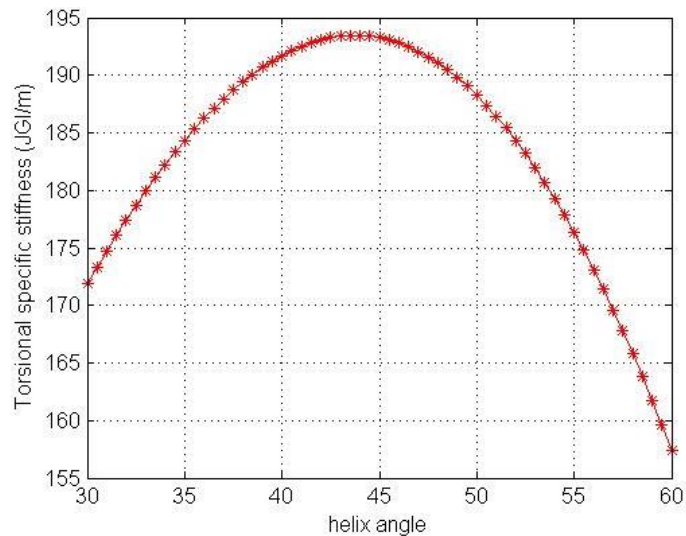
Figure 70 - Optimal Driveshaft: effect of helix angle

Optimal Boom Design – Cantilever Bending

Cantilever bending is the first structure from which the optimization results yields insight into design. First, the upper and lower axial yarns are maintained. While it is doubtful that the idea of area moment of inertia can be directly applied to a truss structure that lacks a solid cross section

(see Figure 29), the increase in diameter and distance of structural material from the structure centerline certainly increases the diameter. The real insight is that some helical yarns in the O-ACS must be maintained to carry shear loads and to put the upper and lower axials into tensile and compressive loads rather than bending. Traditional planar theory for bending trusses would suggest that the reinforcement between upper and lower should form equilateral triangles (such as in a Warren girder). We see the cantilever O-ACS is more efficient with a shallow helix angle, related to the ability to transfer the radial end-load into axial stresses in the upper and lower yarns (Figure 73). Another curious effect of the shallower angle is that the axials are more symmetric than in a case with steeper angle.
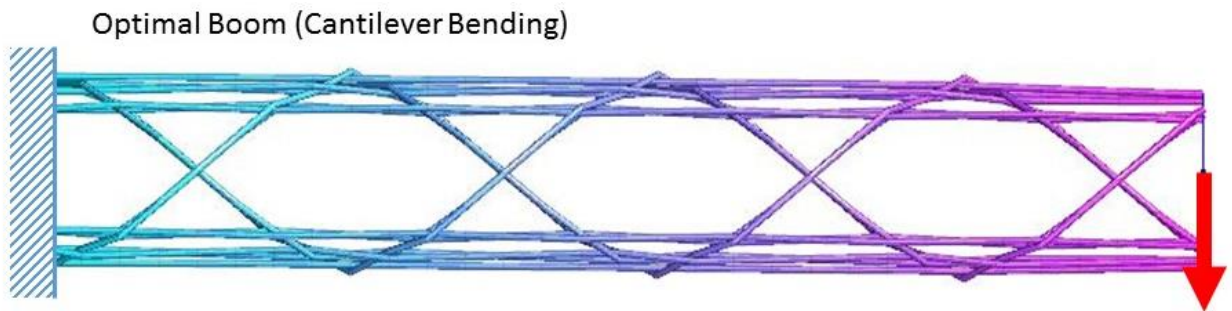
Figure 71 - Optimal Boom (cantilever bending load)
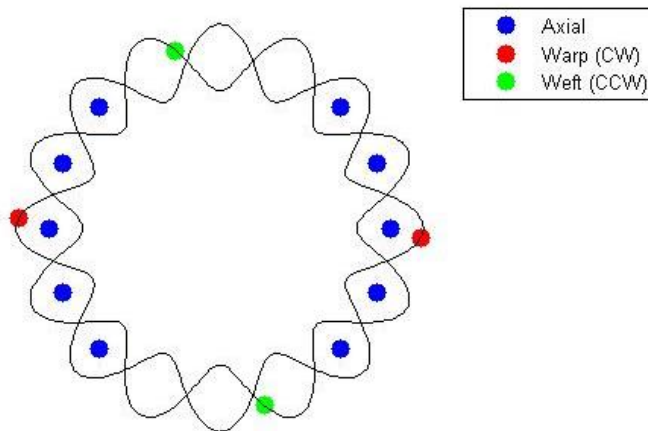
Figure 72 - Optimal Boom loading diagram

104
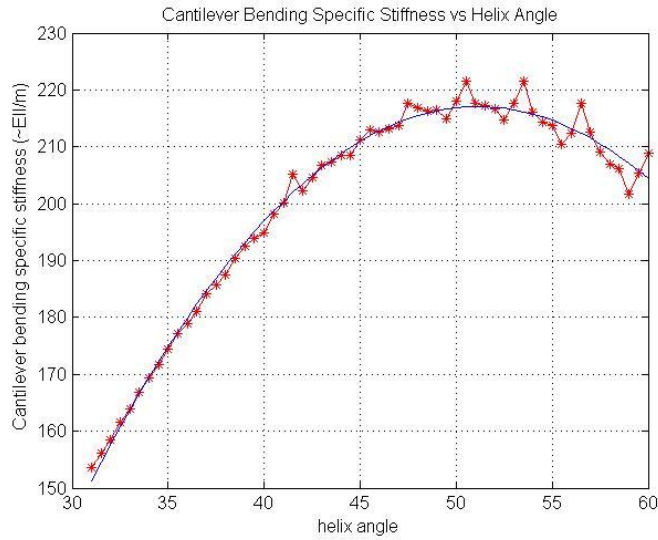
Figure 73 – Optimal Boom: effect of helix angle
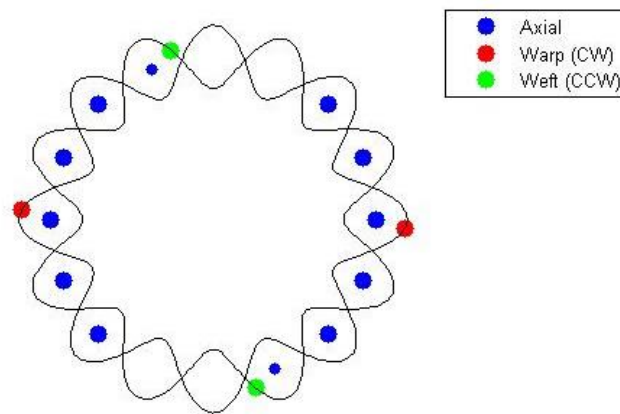
Figure 74 - Suboptimal Beam with less symmetric axial yarn placement

Optimal Bridge Design – Three-Point Bending

Finally, a three-point bending load is tested and the structure optimized (Figure 75). While the large upper and lower axials are maintained, there is a much higher reliance on the helical yarns to carry shear. This is simply a feature of the length of the beam used. A long beam would give a result closer to the boom bending results from before, as seen in Figure 77.
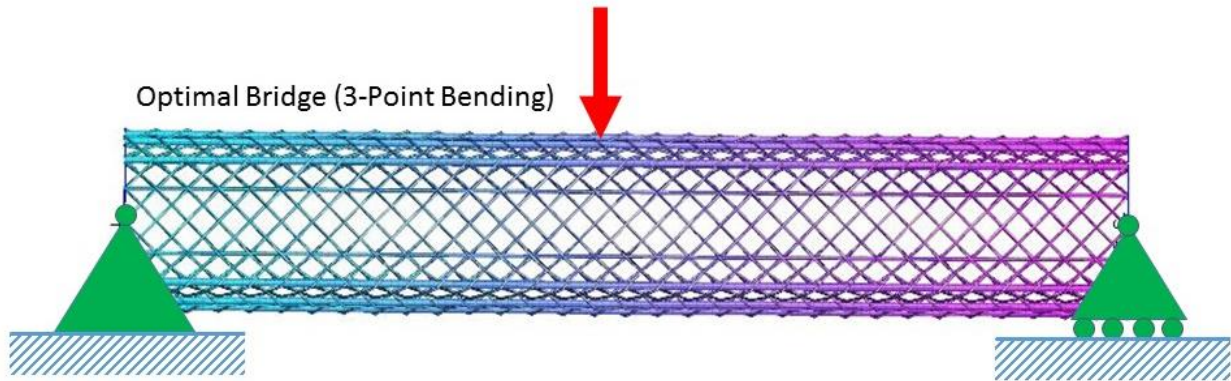
Figure 75 - Optimal Bridge (three-point bending load)
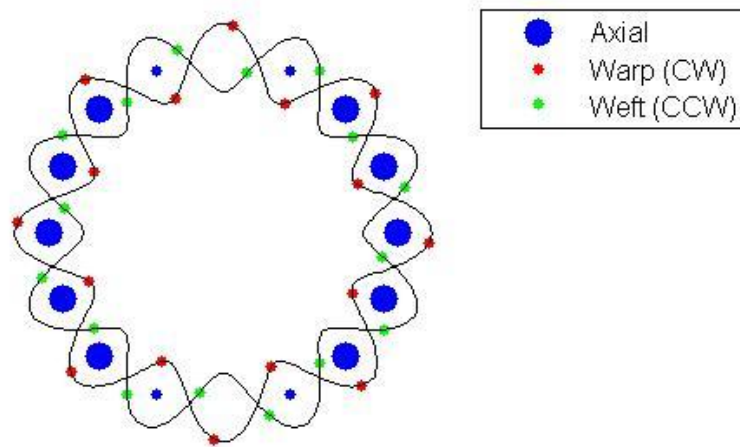
Figure 76 - Optimal Bridge loading diagram
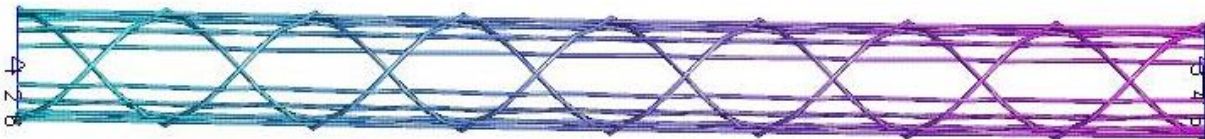
Figure 77 - Optimal Bridge on a longer span (where shear load is less meaningful)

Comparison to Suboptimal Designs and Commercial Products

Sources of Error

Most of the errors that may exist in the optimization are the same as those which apply in the Finite Element analysis. New errors are limited only to numeric precision. There are widely

106

varying scales of numbers in the geometry, finite element construction, finite element solution, and element load retrieval. These varied scales gradually decreases the numeric precision at each step in the simulation. This only causes issues when the sensitivities (Equation (51)) are calculated: A problem which is expected to yield a symmetric result may not do so because small errors in trigonometric functions cause (very small) differences in the sensitivities. When the multipliers are found (Equation (53)) any minute difference in the compliance values will force nearly symmetric problems into drastically asymmetric ones. This issue was solved by reformulating the geometry model to solve the compression and tension down to arbitrarily close precision. This accounted for the largest source of errors, and was resolved. Fortunately, in most cases where optimization is useful - bending, for instance – the sensitivities of the various yarns are vastly different, and the numeric precision does not come into any effect.

Conclusion

The optimization considers all the parameters of the structure as either constraints or design variables. The user of a design tool as presented here is typically designing within the constraints of a single braiding machine. Any given machine has a maximal loading capacity (maximum number of packages and uniaxial yarns) which creates a structure that bounds the upper limit on the total material present in the structure and thus bounds the limit of strength and stiffness. It may be found that loading fewer packages will create a structure with higher *specific* stiffness. Thus yarns are removed from the fully-loaded structure (in a mathematically sustainable manner) until the optimal structure is determined. Optimality Criteria optimization was used to determine the way individual yarns contribute to structure stiffness.

Several concepts of O-ACS design have proceeded from this work. First, diameter should always be increased to the limit of the application's space constraints. This both increases the distance of yarns from the neutral axis, and (for a given weight) will have less undulation between the yarns (as the ratio of mandrel diameter to yarn diameter increases). Helix angle is determined by parameter sweep or by Newton iteration. Yarn diameters are, as mentioned, determined using optimality. The results have proven insightful into the relationships among yarn locations. Axial reinforcement is helpful with any axial stress (whether due to axial or bending loads). The helical reinforcement is more varied in the way it assists the structure; sometimes it carries load itself, and other times it transfers load from one set of axials to another.

Because the optimal designs are often not directly intuitive, the optimization has achieved its goal of yielding insight into O-ACS design. A comparison between the optimized beams, samples from the test-matrix, and commercial competition are presented in the following review.

Review and Conclusion

The complete tool-set for the analysis and design of O-ACS structures has been developed. A geometry model was created starting with the kinematics of the braiding machine, compressing the structure against a mandrel, and tensioning the yarns in simulation. The individual yarns were discretized and given the structural properties of beams. A platform for applying loads and constraints to the open-structure was developed, allowing the computation of structure deformation and loads within the yarns and yarn intersections. The finite-element model was compared to physical samples, and found capable of accurately predicting torsional and bending stiffness. Finally, the model was used to create an optimization model capable of determining optimal yarn-placement for creating designed minimal-weight composite structures. All these simulations have been developed in ~2400 lines of MATLAB code. To be a practical design *tool*, the capabilities of the program must be made accessible to any engineer not familiar with the code or programming. To this end, a graphic user interface (GUI) was made for *fell_point* which allows easy setup and use of the tools (Figure 78).
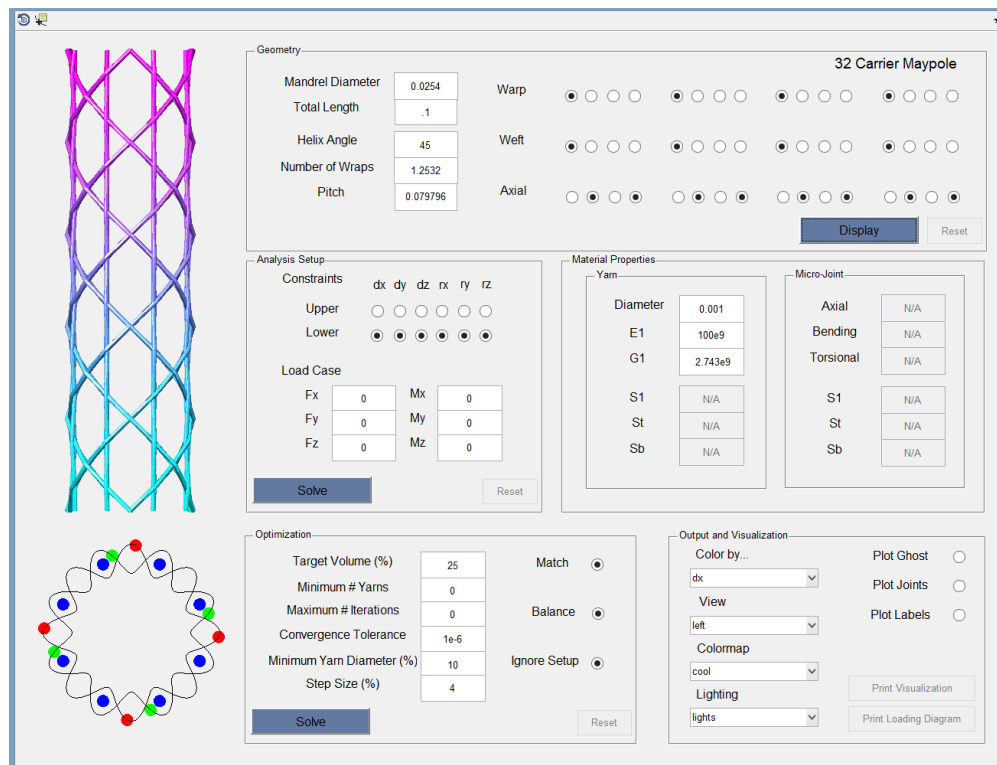
Figure 78 - The fell_point *graphic user interface*

The GUI allows the easy selection of carrier loading, and structure dimensions such as height, helix angle, and mandrel diameter (Figure 79). The machine definition (maximum number of carriers) is fixed based on the user's machine access and needs. The units are independent: the examples here use SI units (kg, m, s).
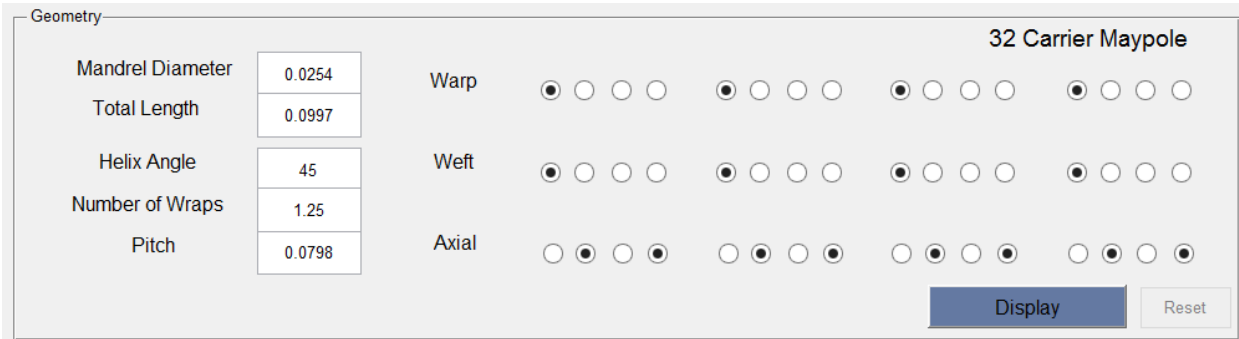
Figure 79 - Geometry Module control panel

The geometry is quickly displayed and a loading diagram for the structure is provided to show where the carriers would be loaded on the machine. In this way, a braider unfamiliar with braiding patterns can visualize the structure he expects to make, before committing to setting up the machine. This also allows the engineer to design a structure, and provide the braider with machine loading information (Figure 80).
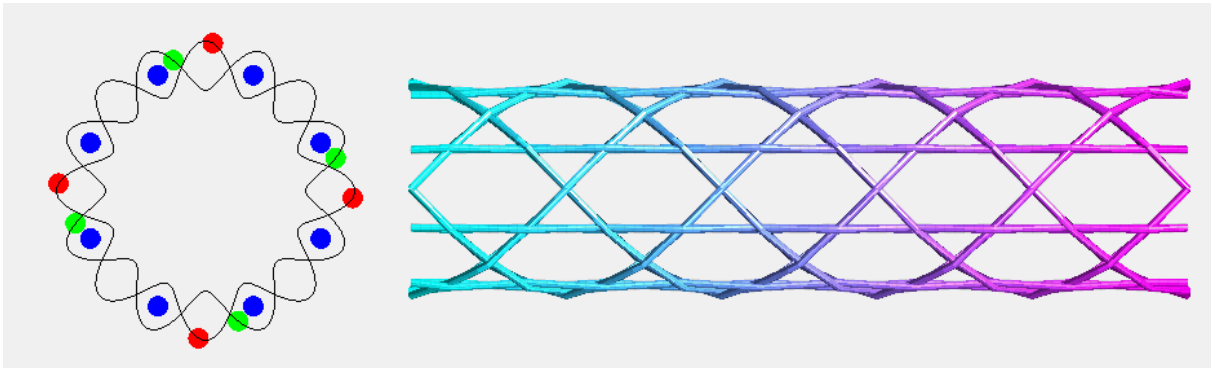
Figure 80 - Visualization window

The geometry can be immediate analyzed for deflection under a specified load case. Yarn properties (diameter and stiffness) can be entered and will update the geometry model if required. Constraints on the upper and lower yarn boundaries can be applied on the six degree of freedom at each end. A force, moment, or combination of both can be applied at the upper node (Figure 81).

110
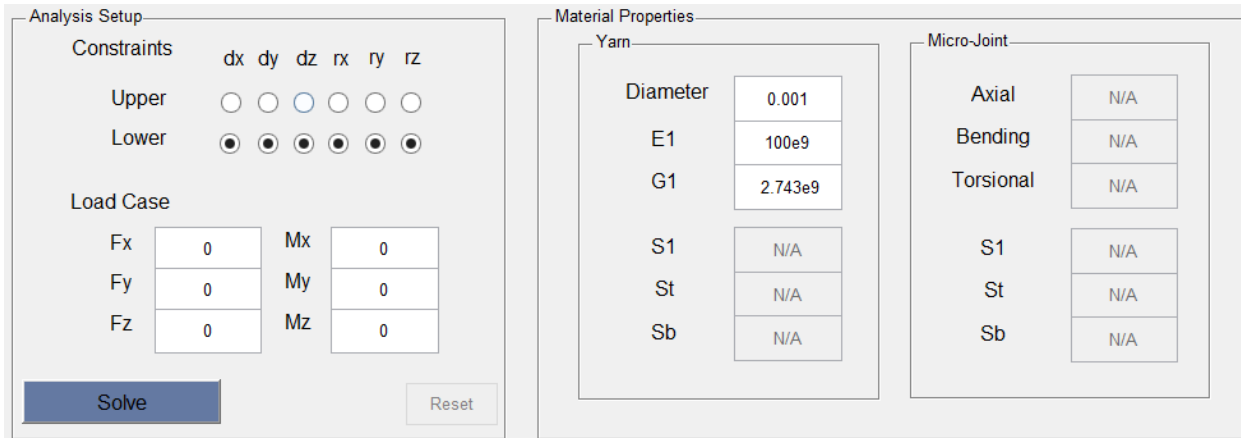
Figure 81 - Analysis setup and material model control panel

After initial analysis, the load and geometry can be used as the starting point for an optimization. The user simply specifies a final volume fraction and simple rules about when to end the optimization process. The matching and balancing constraints, as well as minimum yarn diameter, can also be imposed to drive the optimization toward results which can be realistically manufactured. Again, a loading diagram is generated for the final geometry such that the optimal design can be immediately taken to manufacturing.

Finally, the output visualization characteristics can be controlled. The view point, coloring, and shading are all accessible changes. This allows aesthetic control of the visualization, so that the images can be used for later reference or in a report, etc. (Figure 82).
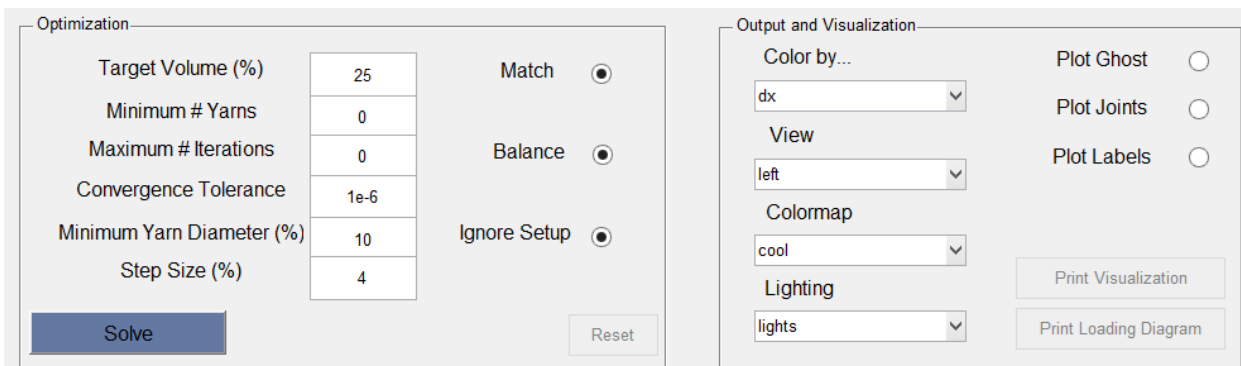
Figure 82 - Optimization and Visualization control panels

Lessons Learned and Extensions of the Present Work

The intent of the framework developed here is to create tools that will yield insight into O-ACS design. From each step of the design process (geometry, analysis, and optimization), there

are pieces of the code design which have been instructional in O-ACS design. There is always a limit where more detail in a simulation is not practical, and should no longer be added to a model. The author believes that the current model, for its present goals, is complete. Should future work wish to extend the objectives, some helpful guidance in that regard is presented here.

Much work was done in the construction of a geometry model based on concepts of braiding. The rule-based method for geometry was found to solve quickly and to arbitrary required precision. While the model appears to be a consistent representation of the physical geometry, the comparison was only made visually. By using an optical or Computational Tomography scanner, a 3-dimensional image of an actual structure could be directly compared to a model generated in *fell_point*. The discrepancies that I would expect could be found would be the following (which should serve as improvement goals for future development):

- The yarns are not circular in cross section. The model presented here assumes all yarns are truly circular for both geometry and strength computation
- The intersection of yarns is a flattening of two yarns. The model assumes this can be represented by the intrusion of yarns through each-other
- The real yarns may have enough bending stiffness to resist the shortest path assumption. In other words, there may be a curvature limit at yarn intersections. This is easily programmed, but requires significantly higher discretization than is currently used
- Axial yarn paths are not straight. This is a matter of manufacturing precision and the error should be eliminated as the O-ACS manufacturing process is better refined

Other than the concerns listed above, the geometry model should be a fair representation of physical geometry.

The finite element model guiding concept is the use of beam elements to represent yarns. As the yarns become better understood, the beam-element formulation used could be improved as well. This could include non-circular cross-sections, directional stiffness, and failure modes. The *fell_point* code has been organized such that incorporation of future element types is not complex. The joint intersections could also use a more detailed evaluation than was given here. Also, a major advantage of the O-ACS concept may be their resistance to buckling: no treatment of buckling stability was presented here. If it is more useful, the geometry from fell-point could be exported as key-points for use in a commercial finite element code. This would allow

extension to include solid elements rather than beams, and very detailed modeling of the yarn intersection and the resin joints.

The optimization is fundamentally sound. It could be extended to incorporate multiple constraints, or simply different constraints such as stress (once stress limits are known), or target deflections. The optimality criteria method used was selected for its easy extension to these and other goals. The beam element model was, as predicted, a good method for implementing the optimization due to the fast solution speed and inherent organization of yarn elements into groups. A problem that was not studied in detail is the manner in which the shifting yarns will force the optimization to local minima – or whether a global minima is actually present for all possible initial conditions. For practical purposes, the optimization gave results that were close to those that were expected. In axial tension and compression, axial yarns dominate the stiffness, and in torsion the helical yarns dominate – both of these are intuitive. In the various bending cases, the important revelation is the importance of retaining helical yarns for stability. While the axial yarns farthest from the neutral axis do contribute to the bending stiffness, it was found that certain patterns of helical reinforcement carry the load from upper to lower surface of the tube. Also, in short beams and cantilevers the helical yarns are actually better reinforcement than the axials. The optimal angle of the helical yarns is also very important to the stiffness, particularly for the torsional load case, where the result is not intuitive. When actual applications of the open-structure come to light, the optimization will be very useful in quickly establishing O-ACS solutions, and to see if optimized O-ACS tubes may have higher specific stiffness than commercial thin-wall tube equivalents.

Though not the direct focus of this work, much was discovered about the manufacturing and testing of O-ACS tubes. The manufacturing concerns have been described in detail in Appendix A. The primary result of the authors manufacturing experience has been to find that open-structures can, indeed, be manufactured using Wardwell-style carriers. The key is careful loading of the carriers and preparation of the pulleys and tensioning springs to account for the oversized, stiff, O-ACS yarn. The testing is known to be a problem and is current the focus of research elsewhere in the Auburn Advanced Braiding Lab. Particularly troublesome was the lack of rigidity in the compression test. Unless the samples are held in fixtures significantly more rigid than the structure itself, the test will be troubled. Perhaps an optical strain method could be

113

employed to eliminate the errors. Both the bending and torsion tests were successful, and match the Finite-Element model well.

Having created tools for their design, it is now possible to evaluate the effectiveness of O-ACS as a designed structure. They have many benefits over commercial tubes in their manufacturing range: Thin-walled tubes become impractical below a limit which is clearly seen in the range of available commercial tubes (Branscomb, Minimal Weight Composites Utilizing Advanced Manufacturing Techniques, 2012). The ability to increase the diameter (and thus bending and torsional stiffness) without increasing the mass of an open-structure is unique to its design. This work sought to find even better improvements by designing O-ACS tubes for their intended loading scenario. The results of the optimized tubes are presented in the following four figures. All tubes compared were chosen to have approximately equal weight per unit length (less than 1.5 g/cm). This limits the diameter of the commercial tubes to be about 2.5 mm, whereas the open-structures are all 4.375 mm diameter. This may initially sound like an unfair comparison (especially in bending and torsion); but that advantage is the entire key feature of the O-ACS: ability to increase diameter without a significant in mass. The Aluminum 6061 tube is the largest diameter, commercially available tube which weighs less than 1.5 g/cm; the stiffness' for that tube were computed using known material properties. The smooth-walled carbon fiber (CF) tube is also the largest diameter, commercially available tube which weighs less than 1.5 g/cm; the data for that tube was measured. It is a pulltruded tube with a woven exterior layer. All O-ACS tubes are computed using *fell_point*, which is has been validated well for torsion and bending, though not well for compression (see Chapter 6). In Figure 83, the axial stiffness of the tubes is compared. This is the least reliable of the charts, since the model was not well validated in compression, and the effect of buckling within the O-ACS tube is unknown. However, the results are appropriate as an initial estimate since the modulus of the carbon yarn is higher than that of the aluminum, and the volume fraction is typically higher than that of the CF tube (Branscomb, Minimal Weight Composites Utilizing Advanced Manufacturing Techniques, 2012). The second figure (Figure 84) shows the torsional results. The O-ACS tube is predicted to have 4 times that of the thin-walled carbon fiber tube. This is the dominance of diameter. Figure 85 and Figure 86 both show a large improvement over their commercial counterparts as well. In the cantilever load case the open-structure is over 14 times as rigid as the metal tube. All these

data confirm that designed tubes will dominate traditional thin-walled tubes in all loading conditions besides uniaxial compression; and perhaps there as well if buckling is considered.

Axial Specific Stiffness of Equal Weight-per-Length Round Tubes
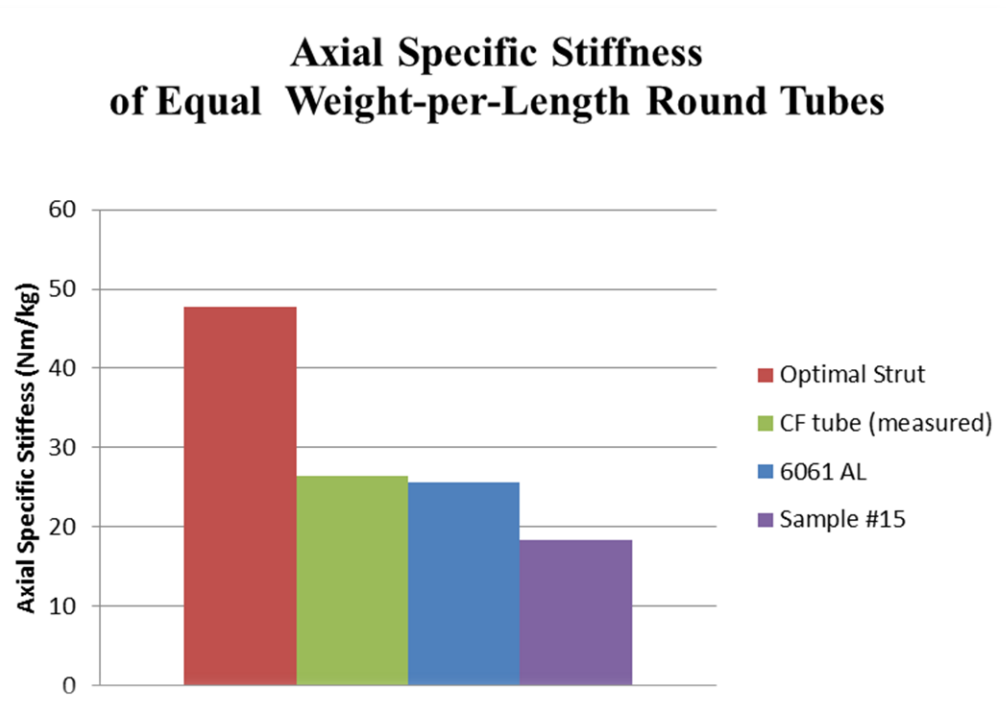
Figure 83- - O-ACS design axial stiffness comparison

Torsional Specific Stiffness of Equal Weight-per-Length Round Tubes
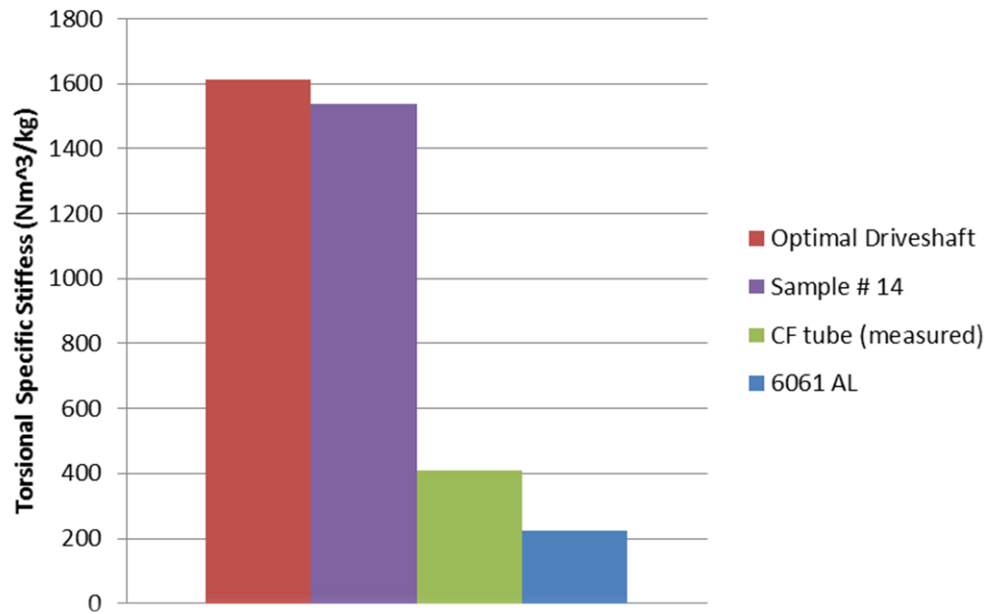
Figure 84 - O-ACS design torsional stiffness comparison

Bending Specific Stiffness of Equal Weight-per-Length Round Tubes
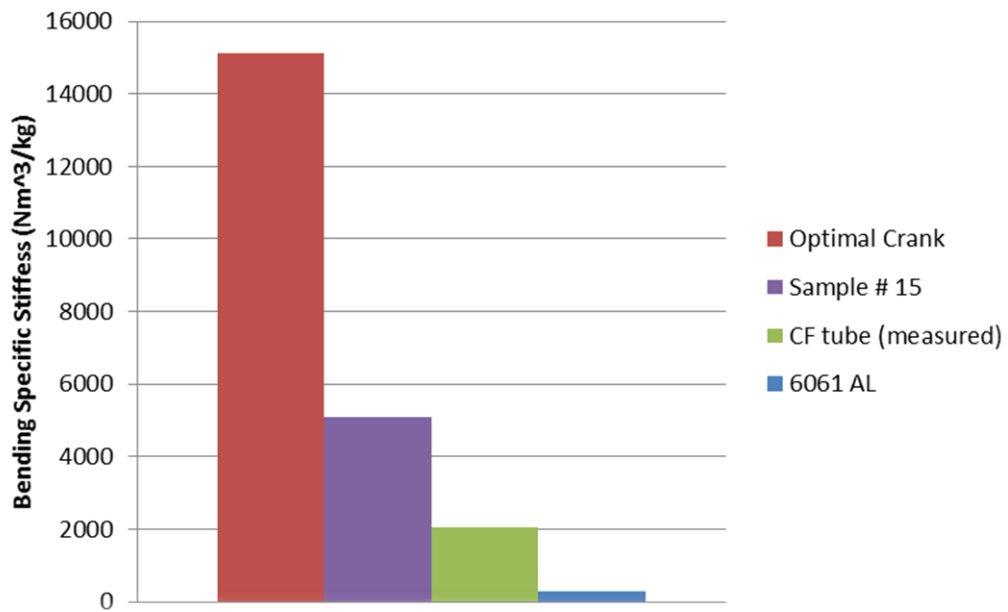
Figure 85 - O-ACS design bending stiffness comparison

116

3-Point Bending Specific Stiffness of Equal Weight-per-Length Round Tubes
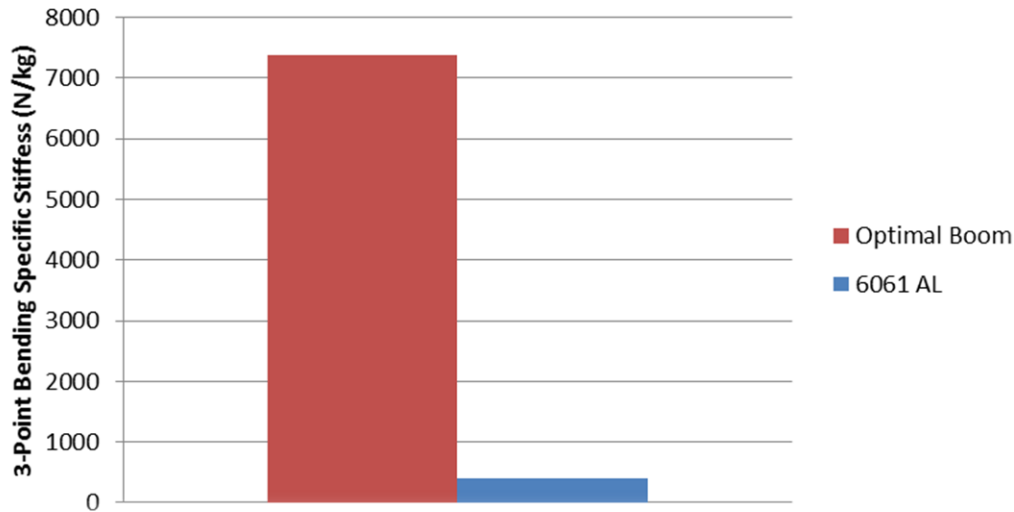
Figure 86 - O-ACS design 3-point bending comparison

As stated in the introduction, the objective of this thesis is:

To create design tools, useful to an engineer unfamiliar with the intricacies of O-ACS design, which compute optimal stiffness-to-weight O-ACS geometries – within constraints of design loads, a machine definition, and material properties.

The simulation tools from the very start have kept the constraints of Maypole braiding machines in their construction. The combination of a geometry simulation, FE analysis tools, and a topological optimization method have provided the tools. Proper techniques have been applied to accurately represent the composite yarns present in the structures. The simulation was validated against a very wide range of test samples, and found to be a fair prediction of actual O-ACS tube stiffness. Using a compliance based optimization method allows rapid establishment of the most efficient O-ACS geometries, without requiring detailed specification of design deflection or even of material strength. The design tools have been incorporated into a GUI which is accessible to any engineer, and will certainly improve the speed and accuracy with which open-structure tubes can be designed and manufactured.

117

References

Akkerman, R., & Rodriguez, B. (2008). *Braiding Simulation and Slip Evaluation for Arbitrary Mandrels.* Enschede: University of Twente.

Arora, J. (1989). *Introduction to Optimum Design.* New York: McGraw-Hill.

Bendsoe, M., & Sigmund, O. (2003). *Topology Optimization - theory, methods, and applications.* Berlin: Springer.

Branscomb, D. (2007). *A Machine Vision and Sensing System for Braid Defect Detection, Diagnosis, and PRevention During Manufacturing.* Auburn: Auburn University.

Branscomb, D. (2012). *Minimal Weight Composites Utilizing Advanced Manufacturing Techniques.* Auburn: Auburn University.

Broderick, T. E. (1985). Dependence of PET Molecular Weight and Process Conditions on 16 Mil Monofilament. *Textile Research Journal*, 277-284.

Cook, R., Malkus, D., Plesha, M., & Witt, R. (2002). *Concepts and Applications of Finite Element Analysis.* Madison: John Wiley and Sons.

Gilbert, J., Moler, C., & Schreiber, R. (1991). *Sparse Matrices in MATLAB: Design and Implementation.* Menlo Park: The Mathworks.

Haftka, R. T., Gurdel, Z., & Kamat, M. P. (1990). *Elements of Structural Optimization.* Boston: Kluwer Academic Publishers.

Jensen, M., Jensen, D., & Howcraft, A. (2010). Continuous Manufacturing of a Cylindrical Composite Lattice Structure. *Recent Advances in Textile Composites (Proceedings of the 10th International Conference on Textile Composites).* Lancester.

Ko, F., Pastore, C., & Had, A. (1989). *Atkins and Pierce Handbook of Industrial Braiding.* Covington: Atkins and Pierce.

Kothari, N. (2014). *Mechanical Characterization of the Braided Composite Yarn and Bond Strength Evaluation of the Joints of the Open-Architecture Composite Structure (O-ACS).* Auburn: Auburn University.

Logan, D. (2007). *A First Course in the Finite Element Method, 4th Edition.* Toronto: Thomson.

Lundstedt, T., Seifert, E., Abramo, L., Thelin, B., Nystrom, A., Pattersen, J., & Bergman, R. (1998). Experiment design and optimization. *Chemometrics and intelligent laboratory systems*, 3-40.

Maxwell, J. (1864). On the Calculation of the Equilibirum and the Stiffness of Frames. *Philosophical Magazine*, 294-299.

McDonnell Douglas Astronautics Company. (1973). *Isogrid Design Handbook.* Huntsville: NASA Marshall Space Flight Center.

Michell, A. (1904). The Limits of Economy of Material in Frame-structures. *Philosophical Magazine and Journal of Science*, 589-597.

Przemieniecki, J. (1968). *Theory of Matrix Structural Analysis.* New York: McGraw-Hill.

Rozvany, G. I. (2009). A critical review of established methods of structural topology optimization. *Structural Multidisciplinary Optimization*, 217-237.

Schneider, M., Pickett, A., & Wulfhorst, B. (2000). A NEW ROTARY BRAIDING MACHINE AND CAE PROCEDURES TO PRODUCE EFFICIENT 3D-BRAIED TEXTILES FOR COMPOSITES. *SAMPE symposium.* Long Beach.

Sigmund, O. (2001). A 99 line topology optimzation code written in MATLAB. *Structural Multidisciplinary Optimization*, 120-127.

Vanderplaats, G. N. (1984). *Numerical Optimization Techniques for Engineering Design.* New York: Mcgraw-Hill Book Company.

Vasiliev, V., & Gurdal, Z. (1999). Optimal Structural Design. In V. Vasiliev, & Z. Gurdal, *Optimal Design* (pp. 1-29). Lancaster: Technomic Publishing Company.

Weaver, W., & Gere, J. (1990). *Matrix Analysis of Framed Structures* (3 ed.). New York: Van Nostrand Reinhold.

Appendix

Guidelines for Manufacturing Open-Architecture Composite Structures

Using Conventional Maypole Braiding Equipment

Braided lattice composites show promise as a novel replacement in minimal weight structural applications. The concept provides two key advantages over existing minimal weight structures. First is their lightweight reinforcement due to special geometries and materials, which can be easily designed for specified loading constraints. Second, the braiding process ideally maintains low manufacturing costs due to high throughput, low material waste, and significant automation of the manufacturing process. It is this second concern which is addressed in this report.

To date, much experimentation in the design of Open-Architecture Composites Structures (O-ACS) is performed in the Auburn University Advanced Braiding Lab. The lab mainly utilizes two Maypole braiders; one 32-carrier and a second larger 64-carrier model. O-ACS fabrication involves large, tough yarns for which the traditional maypole braider using standard (#2BX) carriers is not well suited. While a larger machine (such as used for braiding steel cables) could be purchased, the use of specialized equipment severely restricts the cost-effective production of O-ACS. Thus, it is important to explore the abilities and limits of braiding lattices with traditional braiding equipment. Three main components of the fabrication process must be considered: yarn design, braider preparation, and mandrel treatment.

Yarn – Design for Manufacturing

While the O-ACS designer has certain weight and stiffness goals, it is important that the design be realizable using available equipment. Currently, yarns less than 30000 denier are braidable on a conventional Maypole braider with #2BX carriers. Some considerations when designing yarn are listed below.

I. Core
   a. The core of the yarn can be made in any size – 48K Carbon (approx. 23000 Den. dry) is the ideal size that allows braidable structures in the range from one inch to three inch mandrel diameter.

b. The jacket axial yarns can contribute to the yarn uni-axial strength and stiffness. However, because of the interlacing, they do not contribute as well as the perfectly aligned core fibers. Thus, fibers expected to provide strength and stiffness should be found primarily in the core.

II. Jacket Axials

    a. The number of axial yarns in the jacket (usually high strength fiber, 4 or 8 are utilized) significantly affects subsequent braidability of the O-ACS. Fewer is typically better, unless they be of such diameter that they cause the cross section to become 'square'.

    b. Fiberglass jacket axials are very smooth – this facilitates easier braiding of the O-ACS and also reduces the 'splinters' present in cured yarns with carbon jacket axials.

    c. Jacket axials should be pre-impregnated if structural fibers are used. This significantly affects micro-joint bonding the in the cured O-ACS structure.

    d. Jacket axials must be kept in tension during the braiding process. If they are not, there is a tendency for the jacket to 'slip' and expose a small length of core (.25 inches). This has been achieved with clamped eyelets behind the axial ports in the braider.

III. Jacket Braiders

    a. A true tri-axial geometry has very little inherent bending stiffness due to the interlacing (undulation) in the axial fibers. It is recommended that yarn jacket be true tri-axial braid

    b. Jacket helix angles between 30 and 40 degrees (from yarn axis) are braidable. The shallower angles allow faster production but slightly affect knotting

    c. Jacket braiders of textured nylon have (to date) proven very beneficial in promoting bonding between yarns in the micro-joints

An example of a very braidable yarn is given in Table 26. Here we reiterate the key characteristics of this yarn as they meet the points noted above: The total size is less than 30000 D which will allow the use of #2BX carriers. The main structure (and mass) is in the core. The helix angle is 30 degrees, which is the shallowest angle which prevents knotting during braiding.

The jacket braider yarns are nylon to help bonding, while the axials are glass for flexibility and low splintering. The resin used (UCF3330) is low-tack resin designed for braiding.

Table 26 - A braidable 48K CF core yarn specification

	Specification
Core	48K T700 Carbon (UCF3330 Pre-preg)
Jacket Braiders	4x500D Nylon warp, 4x500D Nylon weft
Jacket Axials	1500D S-glass (UCF3330 Pre-preg)
Helix Angle	30 degrees (from yarn axis)

Braider – Adjustment and Tuning for Use with O-ACS Yarns

The major limitation of the conventional braider is the carrier. Most of the modifications and preparatory actions required apply to every carrier which will be used. Nearly all parameters of the carrier configuration must be adjusted; pulley position, spring tension and retention, and bobbin winding all contribute to successful braiding. Proper procedure is described below in the order used during carrier loading and subsequent braiding.

First, the bobbins must be would properly. Usually the very fine yarns and fibers used on these braiding machines ensures that the yarn easily slips from the bobbin to the stationary carrier pulley. With the larger O-ACS yarns, the yarn will bind when being retrieved from the ends of the bobbin if not wound properly. Proper winding ensures that the winding tension is very high. The carbon yarns are not damaged by the tension and are not elastic so the high tension has no problematic effects. Proper winding also ensures that the yarn wraps neatly from one end of the carrier to the other. The pitch should be set so that the yarn wraps neatly and is compact. Any fall-off or build-up of the yarn on the bobbin ends will certainly cause binding. A clean bobbin (end-caps especially) helps smooth release when braiding. Make sure the yarn is not allowed to hang slack from the bobbin before loading, as the stiff yarn will attempt to uncoil itself and ruin the tight winding. Approximately 40 meters of the yarn in Table 26 will fit on a standard #2BX bobbin.

The bobbin is then loaded into a carrier. The carriers with rollers are superior for large yarns

(and wire, coincidentally), while the carriers with eyelets are best for fibers. Remaining notes consider only roller carriers. The stationary roller must be placed at such an angle that the yarn will be contained when the bobbin is completely full. The roller will appear to be set at an extreme outward angle. It is acceptable to leave it in this configuration even if the bobbin has little yarn. The sliding pulley should be bent such that it will not interfere with the stationary pulley even when fully extended. This position is usually farther 'inward' than the natural position, though proper setting typically requires observation and individual adjustment. Even after these adjustments, sometimes the upper pulley simply will not allow the catch to release. This can be solved by loosening the set screw and moving the pulley along the shaft away from the base. Only a small adjustment here should be needed.

The carrier springs are the next issue. A mismatch in tension between the axial and helical yarns is necessary. The helical yarns should be as tightly braided as possible (i.e. use the stiffest springs). The axial tension should then start low and be slowly increased until the helical tension cannot overcome the axials when braiding. This error will be seen as loose helical yarns in the O-ACS which do not lay down against the mandrel surface. For the yarn specified in Table 26, as many as 8 axials can be braided before the braider yarn tension will not overcome the drag, though this claim may be slightly dependent on mandrel diameter. Some preparation to the rest of the machine should be made. The carriers will bend under the tension of the heavy springs and all the friction present in the pre-impregnated yarns. They will often bend so far as to crash into the carriers that move in the opposite direction. This will cause a loud popping/snagging noise in the machine, and usually cannot be seen. The best solution is to put empty bobbins on the machine to act as 'bumpers' for the carriers that are actually braiding.

A last practical consideration is minimizing waste at the beginning of braid formation. This reduces waste and is often necessary with mandrels that are nearly the length of the structure needed. The first consideration is where the yarns are attached at the fell-point before the braiding is begun. The yarns should be taped to the mandrel as closely as practical to their proper place in the braid. This can be visualized by running the braider until the packages are at easily understood positions (12 o'clock, 3 o'clock, etc.) and pulling the yarns to the fell-point in the same visible arrangement. The helix angle should also be matched before the braiding is begun, as it can waste several wraps if allowed to settle itself without guidance. Run the traverse, watching for the yarn *on the side* of the mandrel to make the appropriate angle from fell-point to

124

uppermost carrier. Depending on the helix angle of the O-ACS tube, sometimes a forming ring must be used. This has been seen to actually help with yarn tensioning issues, and is usually not a problem. A six inch ring has been successfully used for tubes from one to three inches diameter.

This concludes the machine and carrier preparation requirements. The key aspects of carrier preparation are shown in Figure 87. While the forgoing offered specific advice, it is perhaps sufficient to suggest that *every effort be made to be neatly prepared*, any specifics follow from this simple rule and practice.
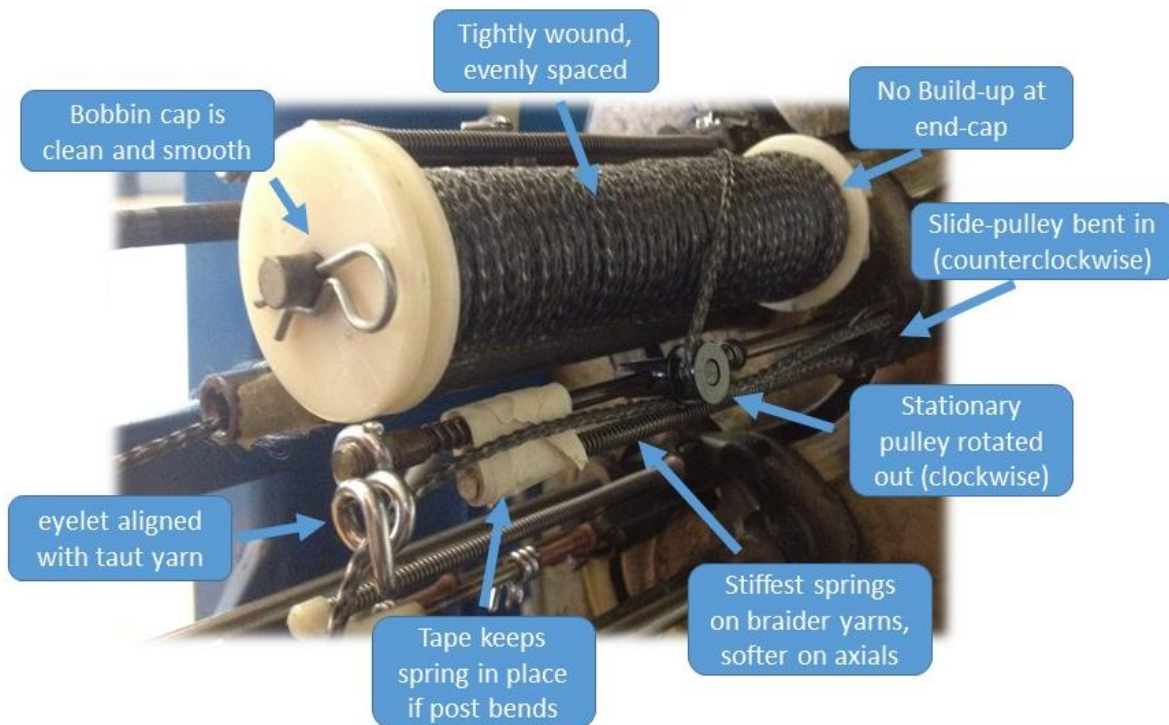

Figure 87 – Demonstration of proper carrier loading

Mandrel – Preparation for Removal of Cured Final Components

A mandrel shape is chosen based on the O-ACS geometry that is desired. Typically round and polygonal mandrels are all possible, so long as the cross-section is strictly convex. Usually the mandrels are metal: aluminum is a good compromise between rigidity and weight. Often a simple 'tube' is sufficient if properly prepared. The mandrel preparation involves two stages of surface prep, and a specific process for the starting and ending of O-ACS braiding. The mandrel

will be polished and the surface treated to allow easy removal of the structure and to prevent bonding of the laminating resin to the mandrel surface. When forming the O-ACS braid, consideration must be given that no obstruction be cured beneath the composite as this will cause difficulty in mandrel extraction.

First, the mandrel should be selected and inspected for imperfections. During the braiding process, the Open-Structure will be tightly formed against the mandrel surface. When using a circular mandrel, any deviation from round will cause the O-ACS to become locked to the mandrel. Care must be taken not to drop or otherwise impact and damage the mandrel. It is particularly important that only one end be used for clamping in the support brackets, as the clamping will damage the mandrel. Once the mandrel is selected and the clamping end marked, the remaining length of the mandrel should be polished.

With a given braider tension, it will be found that the smaller the mandrel the greater the pressure of the O-ACS against the mandrel surface when cured (and vice-versa). Thus, it is particularly important that smaller mandrels be polished well and cleaned regularly. Polygonal mandrels typically have lower pressure and require less prep (The use of vacuum bagged curing negates these comments). After polishing as required, the mandrel surface should be thoroughly cleaned using methylene chloride (commonly called Aircraft Remover) to remove all traces of contaminants. This is followed by rinsing with a solvent such as acetone. Finally, the surface should be treated with a mold release agent (Frekote 770NC is a good choice). This finalizes the static preparation of the mandrel. These steps should be repeated whenever the mandrel surface begins to foul due to excess resin or misuse.

Second, care must be taken when securing the yarns to the mandrel before braiding begins, and when encapsulating the ends of a length of braid before removal from the braiding machine. The chief goal is to ensure no materials are between the cured braid and the mandrel surface.

When setting the machine for braiding, yarns will be pulled down from the carriers to the mandrel. They are most easily attached at this point by wraps of tape (flash tape is a good choice). While the tape is sufficient to hold the yarns in place initially, it cannot resist the high tension of the actual braiding process. Thus, a clamp can be used over the tape to secure the yarns. Standard hose clamps work well for round mandrels and can be formed to almost any mandrel shape. After the yarns are securely clamped, the structure can now be braided.

After braiding is complete, the machine is stopped and the yarns still trail from the carriers down to the fell point. At this time, *both* ends of the braided structure should be wrapped with tape. On the farthest end, the yarns beyond the tape (which begin their accent to the carriers) can be cut using a razor. A sharp razor will not damage the mandrel surface significantly and allows for a clean cut. This leaves the end contained by one ring of tape. At the nearest (starting) end, the clamp should now be removed. The tape which was used in the initial setup of the machine (formerly under the clamp) should be pulled away, leaving only the secondary tape. This will leaves the ends of the structure free for a few inches: this excess can be timed away with the razor. The structure is now held in place by two rings of tape which are only on the outside of the braid, and the part is ready for curing. After curing, if all the steps have been followed carefully, the structures can be easily removed by pulling away the tape and sliding the structure off the end of the mandrel. The mandrel preparation procedure has been illustrated in Figure 88.
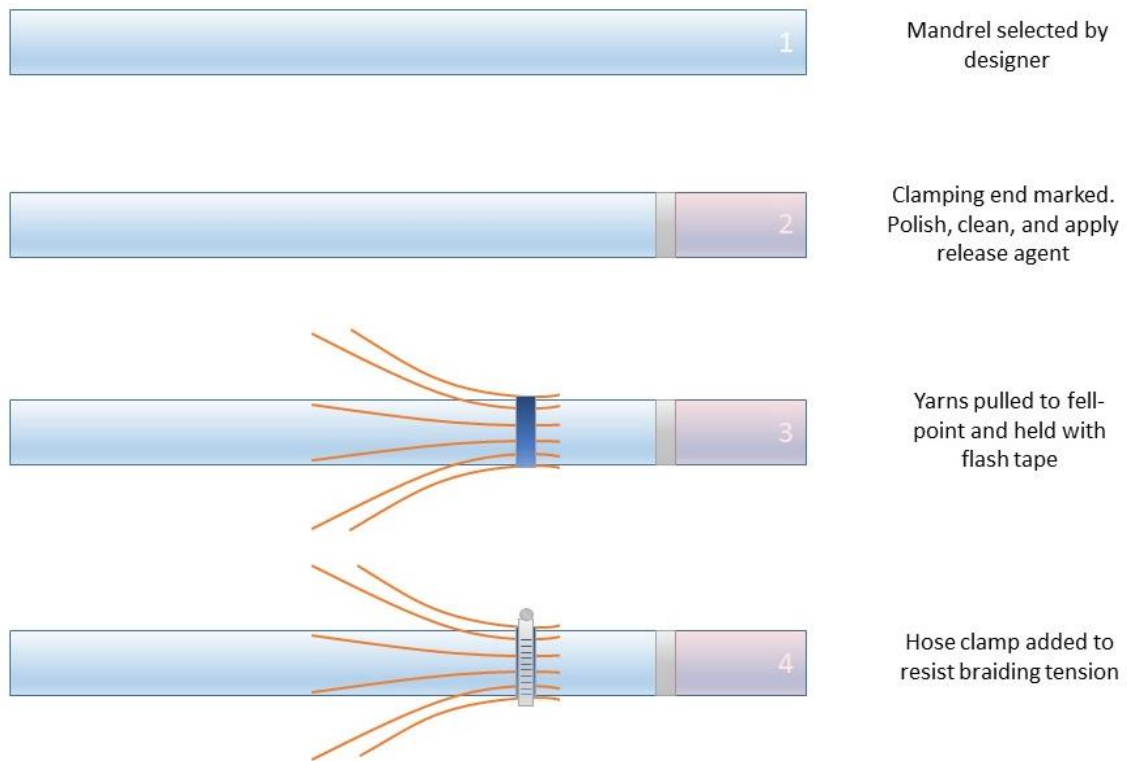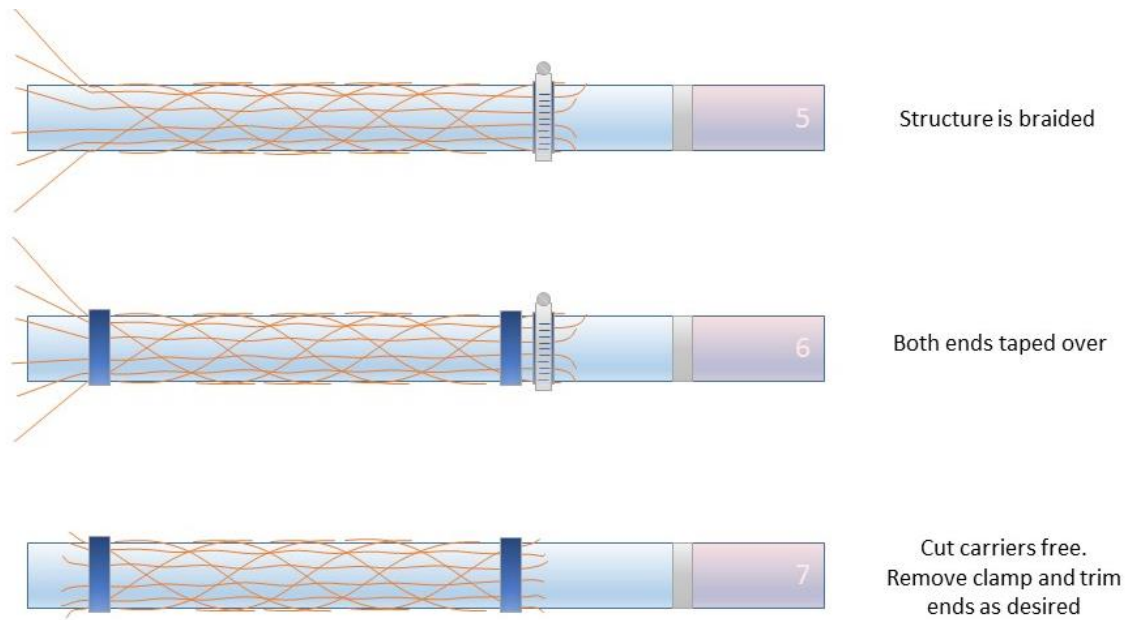
Figure 88 – Proper procedure to ensure mandrel can be removed after braiding

Speed Calculations

As a matter of practical interest within the Auburn Advanced Braiding Lab, equations for the calculation of traverse and braider speed relationships have been developed (Figure 89). These relate specifically to the Wardwell Composite Braider in the Auburn Lab. The model has been confirmed for multiple mandrel diameters. An example is shown in Figure 90. Typically a traverse speed of 24 inches per minute allows quick braiding while maintaining supervision over the machine.

calculator		Equation
Mandrel dia (in)	2.5	*input A*
Helix (deg)	60	*input B*
Traverse (in/min)	24	*input C*
Traverse Setting	864	C*36
Braider Setting	366	$\dfrac{207.5 * C}{A * \pi * \tan(\pi * (90 - B)/180)}$

Figure 89 – Calculations for braider and traverse speed

Figure 90 – Confirmation of braid speed and helix calculations